Detailed reconstructions of India–Somalia Plate motion, 60 Ma to present: implications for Somalia Plate absolute motion and India–Eurasia Plate motion

C. DeMets [1] and S. Merkouriev [2,3]

[1]*Department of Geoscience, University of Wisconsin-Madison, Madison, WI 53706, USA. E-mail: dcdemets@wisc.edu*
[2]*Pushkov Institute of Terrestrial Magnetism of the Russian Academy of Sciences, St Petersburg Filial. 1 Mendeleevskaya Liniya, St Petersburg 199034, Russia*
[3]*Saint Petersburg State University, Institute of Earth Sciences Universitetskaya nab., 7-9, St. Petersburg 199034, Russia*

SUMMARY

We estimate India–Somalia Plate motion at 45 times since 60 Ma from ∼9000 crossings of Carlsberg and northern Central Indian Ridge magnetic reversals C1–C26 and numerous fracture zone crossings. The new rotations reveal at least seven significant spreading rate changes since ∼60 Ma, some previously unknown. The largest changes occurred before 46 Ma, when the forces acting on the India Plate evolved rapidly due to the transition from subduction to continent–continent collision between India and Asia and the influence of the Reunion hotspot plume on the India Plate. The new rotations reveal a gradual ∼50 per cent decline in Carlsberg Ridge spreading rates from 57 to 52.7 Ma, but an end to the decline at ∼53 Ma, when spreading rates surged rapidly by up to 100 per cent. From 52 to 46.7 Ma, Carlsberg Ridge spreading rates collapsed by ∼90 per cent, possibly defining a protracted transition to continental collision between India and Asia. Significant kinematic events since 46.7 Ma have included a ∼25 per cent spreading rate recovery from 42 to 40 Ma, ultraslow spreading from 38.6 to 33.2 Ma, a gradual rate doubling from 33 to 18 Ma, a ∼50 per cent slowdown from 18 to 13 Ma, and apparently steady motion since 13 Ma. The new rotations successfully predict Carlsberg Ridge abyssal hill orientations for seafloor ages of 48 to 42 Ma and 20 to 0 Ma and Central Indian Ridge fracture zone traces for seafloor ages of 43–16 Ma, constituting useful tests of the rotation accuracies at these ages. When corrected for the movement of India relative to the Capricorn Plate since 16 Ma, the new rotations also successfully restore magnetic lineations C13, C18, C20 and C21, and fracture zone segments from the Capricorn Plate onto their Somalia Plate counterparts. This further confirms the accuracies of our new rotations back to C21n.1o (47.8 Ma), and validates a ∼16 Ma start date for India–Capricorn Plate motion and published correction for India–Capricorn motion. Anticorrelated changes in India–Somalia and Antarctic–Somalia seafloor spreading rates from 37 to 18 Ma may be evidence that Somalia Plate absolute motion changed during this period, possibly triggered by Somalia's post-30-Ma detachment from the Arabian Peninsula or the kinematic effects of the Afar and/or Reunion mantle plumes on the Somalia Plate. New India–Eurasia rotations that we estimate from an updated global plate circuit predict convergence rates from 53 to 47 Ma that are ∼30 per cent faster than previous estimates and that decline ∼75 per cent by ∼38 Ma. Changes in India–Somalia and India–Eurasia rates correspond closely with recently described Tibetan deformation pulses, consistent with linkages between all three. A joint inversion of Carlsberg and southern Central Indian ridge magnetic reversal and fracture zone data, including a correction for movement of the Capricorn Plate relative to India, satisfactorily realigns the reconstructed magnetic lineations and fracture zones back to C23n.1n (50.7 Ma), but misfits some data by 100 km or more at earlier times. The misfits may be evidence for deformation within the IndoCapricorn and/or Somalia plates before 48 Ma or a misinterpretation of magnetic reversal and/or fracture zone data from times before 48 Ma.

Key words: Plate motions; Indian Ocean; Africa.

1 INTRODUCTION

Reconstructions of seafloor spreading magnetic lineations and fracture zones along the Carlsberg and northern Central Indian ridges, which separate the India and Somalia plates (Fig. 1), are essential for efforts to understand the Cenozoic tectonics of the northern Indian Ocean and its surrounding continents. The rotations that describe past India–Somalia Plate motion not only link India to Eurasia via the extended global plate circuit between the two plates (Patriat & Achache 1984), but also indirectly record changes in Somalia–Nubia Plate motion across the widely studied East Africa rift system and changes in the Somalia Plate's absolute motion.

For the critical period from 70 to 40 Ma, when continental India and Eurasia first collided and the Reunion mantle plume arrived below the India Plate and migrated southward to its present position below the eastern Somalia Plate (Dyment 1998; Chenet *et al.* 2009), numerous authors have estimated rotations from the magnetic lineations and fracture zones created by the Carlsberg and Central Indian ridges (e.g. Fisher *et al.* 1971; Molnar *et al.* 1988; Patriat & Segoufin 1988; Royer *et al.* 2002; Cande *et al.* 2010; Eagles & Hoang 2014; Cande & Patriat 2015; Yatheesh *et al.* 2019). Those reconstructions reveal significant changes in the relative motions and geometries of both seafloor spreading centres between 70 and 40 Ma, including a major spreading rate slowdown and transition from north–south-dominated spreading to the NE–SW-directed opening that has continued to the present day.

Spanning the past 20 Ma, the seafloor spreading histories of the Carlsberg and Central Indian ridges have also been reconstructed in detail (DeMets *et al.* 2005; Merkouriev & DeMets 2006; Bull *et al.* 2010; DeMets *et al.* 2020). Those reconstructions, which indicate that India–Somalia seafloor spreading rates declined by 25–30 per cent from 20 to ∼12 Ma and have remained steady since, have been used to test hypotheses about the forces that elevated the Tibetan Plateau and gave rise to a new diffuse convergent oceanic boundary south of India (Molnar & Stock 2009; Iaffaldano *et al.* 2018). They have also been used as the basis for high resolution estimates of post-20 Ma India–Eurasia Plate motion (e.g. Molnar & Stock 2009; Iaffaldano *et al.* 2013; DeMets *et al.* 2020).

Less is known about the Carlsberg and Central Indian Ridge seafloor spreading histories from ≈40 to 20 Ma, when the Afar mantle plume arrived beneath eastern Africa (George *et al.* 1998; Hassan *et al.* 2020) and the Arabian Peninsula collided with Eurasia and detached from the rest of the Africa Plate (Bosworth *et al.* 2005; McQuarrie & van Hinsbergen 2013). For the Carlsberg Ridge, no well-documented reconstructions for 40–20 Ma have been published, possibly because slow-to-ultraslow seafloor spreading rates during this time (Mercuriev *et al.* 1995) make it difficult to identify its corresponding magnetic anomaly sequence (Chron 18 to 6). Along the Central Indian Ridge, where faster spreading rates from 40 to 20 Ma facilitate the identification of magnetic anomalies C18 to C6, Patriat & Segoufin (1988) estimate rotations for C18 (40 Ma), C13 (33.5 Ma) and C8 (26 Ma) from reversal identifications from Patriat (1987).

In this study, we estimate India–Somalia rotations at 45 distinct times during the past 60 Myr, including six times within the undersampled 40–20 Ma period. The new rotations are based on our interpretation of original magnetic and bathymetric data from the Arabian and Eastern Somali basins and the Central Indian Ridge north of the Vema Fracture Zone (Fig. 1), including Soviet-era magnetic data that superbly image 40–20-Myr-old magnetic lineations (red tracks in Fig. 2). The new rotations describe the relative movements of India and Somalia at high resolution throughout most of

the India Plate's collision with Eurasia, a key focus of many investigators. They also provide unprecedented kinematic detail during the 40–20 Ma period when a series of tectonic events fragmented the former Africa Plate into the modern Nubia and Somalia plates (see above). We use several types of independent observations to evaluate the accuracies of the new rotations. These include the orientations of Carlsberg Ridge abyssal hills, the traces of Central Indian Ridge fracture zones, and Central Indian Ridge magnetic lineations that predate the ∼16-Ma breakup of the IndoCapricorn Plate into distinct India and Capricorn plates.

Our new India–Somalia rotation sequence has numerous useful applications, of which we explore three. Motivated by Cande *et al.*'s (2010) discovery of anticorrelated changes in Africa–Antarctica and Africa–Capricorn seafloor spreading rates from 67 to 52 Ma and Cande & Stegman's (2011) interpretation of these changes as evidence that the Reunion hotspot plume affected the absolute motions of the India and Somalia plates, we use the new India-Somalia rotations in conjunction with detailed new rotations for the Somalia–Antarctic Plate pair (DeMets *et al.* 2021) to identify anticorrelated spreading rate changes after 52 Ma along the Somalia Plate's southern and northern boundaries. In particular, we examine whether a previously unknown but well-constrained anticorrelated change in Carlsberg Ridge and Southwest Indian Ridge spreading rates from 37 to 18 Ma signals that the Somalia Plate's absolute motion changed during this period.

We also use our newly estimated India–Somalia rotations and other up-to-date rotations from a global plate circuit to estimate India–Eurasia rotations for the past 60 Myr, partly to assist investigators who are working on problems related to the India–Eurasia collision and partly to re-examine an apparent correlation between a drop in India–Eurasia convergence rates after 52 Ma and a deformation pulse at ∼50 Ma indicated by chronologically detailed onshore records of magnetic inclinations and sediment accumulation rates from the Gonjo Basin of eastern Tibet (Li *et al.* 2020).

Finally, we investigate whether the Africa or IndoCapricorn Plate may have deformed internally between 60 and 16 Ma (Cande *et al.* 2010; Eagles & Hoang 2014; Cande & Patriat 2015), which is important for future improvements in the rotations that describe India–Eurasia Plate motion between 70 and ∼40 Ma. We first test whether our new India–Somalia rotations accurately reconstruct Central Indian Ridge magnetic lineations and fracture zones between Chrons 26 and 20 once the data are corrected for the post-16-Ma movement between the Capricorn and India plates. We then simultaneously invert C26-to-C20 Carlsberg and Central Indian Ridge data to test whether a single set of rotations satisfactorily fits some or all of the data and discuss the results as a basis for possible future work.

2 DATA

2.1 Magnetic anomalies: Carlsberg and northern Central Indian Ridges

We used original magnetic data from three sources (tracks depicted in red in Fig. 2). Our primary source is ≈320 000 km of Russian shipboard magnetics from a series of systematic regional surveys in the 1980s (Karasik *et al.* 1986; Glebovsky *et al.* 1995 Merkouriev & Sotchevanova 2003; Merkouriev & DeMets 2006). These are complemented by aeromagnetic data from the northern Central Indian Ridge (DeMets *et al*. 1994; DeMets *et al.* 2005), and all marine trackline data from the National Geophysical Data Center (blue and black lines in Fig. 2, respectively). Interested readers can
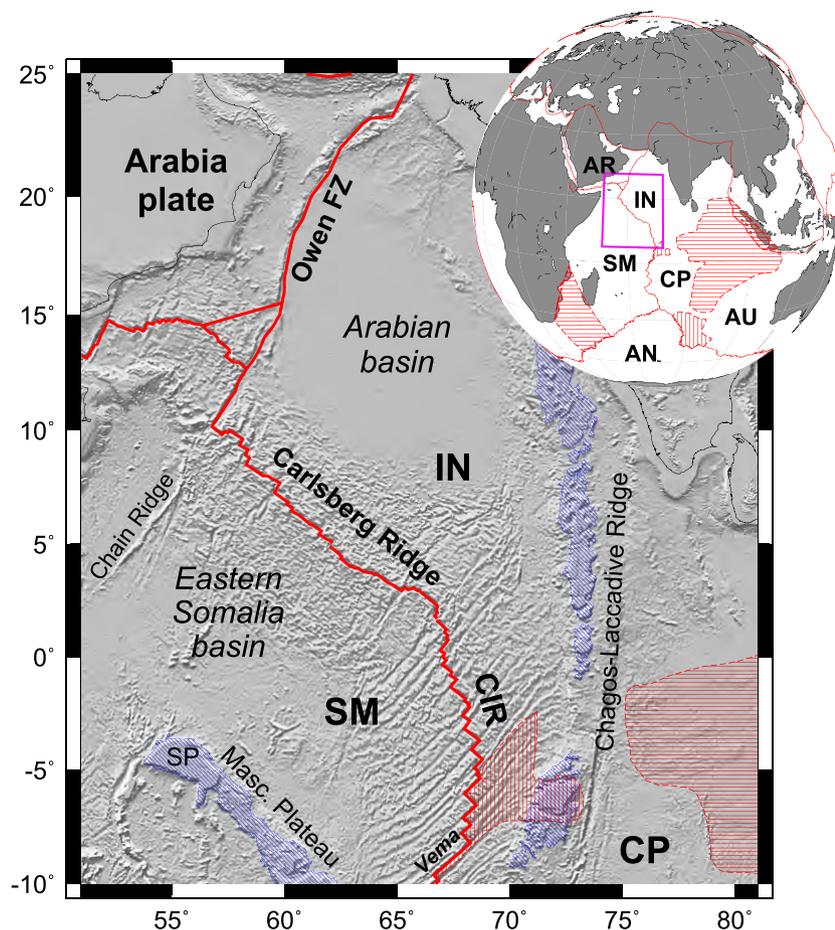
Figure 1. Study area map with bathymetry, plate boundaries, and major features mentioned in the text. Discrete and diffuse plate boundaries are shown by the red lines and red patterned areas, respectively. The blue patterned areas identify areas of the Seychelles Plateau (SP), Mascarene Plateau and Chagos-Laccadive Ridge with depths shallower than 2000 m. The abbreviations in the main map and inset are: AN, Antarctic Plate; AR, Arabia Plate; AU, Australia Plate; CIR, Central Indian Ridge; CP, Capricorn Plate; FZ, fracture zone; SM, Somalia Plate. The pink rectangle in the inset globe outlines the borders of Fig. 2. The plate boundaries are from DeMets *et al.* (2010).

view (at large scale) the original magnetic anomaly data without any interpretation in Fig. S2.

A magnetic anomaly grid of the above data (Fig. 3) clearly reveals the Vine-Mathews lineations created by seafloor spreading along the Carlsberg and northern Central Indian Ridges, particularly south of the ridge where closely spaced Russian track lines sample seafloor out to ages of ≈60 Ma. In previous studies, we used these data to identify 21 magnetic polarity reversals from Anomaly 1 (0.78 Ma) to the old edge of Anomaly 6 (19.7 Ma) (Merkouriev & DeMets 2006; DeMets *et al.* 2020). For this study, we identified 24 additional magnetic polarity reversals between and including Anomaly 6AAr.2 (21.7 Ma) and the old edge of Anomaly 26 (59.2 Ma). A synthetic magnetic profile for our study area displays the tie points for these 24 reversals (Fig. S3). The identifiers and GTS20 ages (Ogg 2020) for all 45 reversals are found in Table 1. We only interpreted the magnetic data from areas northwest of Fracture Zone H, the approximate northern limit of the diffuse India–Somalia–Capricorn triple junction (DeMets *et al.* 2005).

Previous investigators who interpreted magnetic anomalies C28–C20 throughout the Arabian basin and Eastern Somali basin (Dyment 1998; Chaubey *et al.* 2002) identified up to seven westward propagating rifts that systematically transferred seafloor from the Somalia to the India Plate between 59 and 49 Ma. The highly disrupted magnetic lineation sequences, particularly in the Arabian

basin, greatly shorten the length of the palaeospreading centre from which conjugate magnetic lineations are available to estimate finite rotations. Eagles & Hoang (2014) overcome this limitation by using a methodology that reconstructs magnetic lineations from both sides of the ridge in areas where conjugate lineations exist and also reconstructs magnetic lineations from just one side of the ridge subject to the assumption of symmetric palaeospreading rates. Chaubey *et al.* (2002) report that seafloor spreading half-rates from 64 to 46 Ma were 10–20 per cent faster in the Arabian basin than the Eastern Somali basin, in violation of the latter assumption. We thus elected to estimate rotations solely from conjugate palaeospreading segments that we identified on both sides of the ridge (Fig. 4).

The 8984 C1–C26 crossings that meet our criteria are well distributed along the Carlsberg and northern Central Indian Ridges (Figs 4 and S4). Most of these reversal crossings are from the DeMets *et al.* (2020) study of Chron 6-to-present India–Somalia motion (identified by the grey region in Fig. 4). Identifying reversals older than Chron 6 was challenging due to the low fidelity of the C18-to-C6AA reversal sequence, the sparser survey coverage of Arabian basin seafloor older than C6, and disruptions of the C26–C20 reversal sequence by pseudofaults in both basins. We nonetheless identified ≈2100 crossings of C6AA to C26, such that our C6AA to C26 best-fitting rotations are constrained by as many as 173 reversal crossings and no fewer than 41 (Table 1).
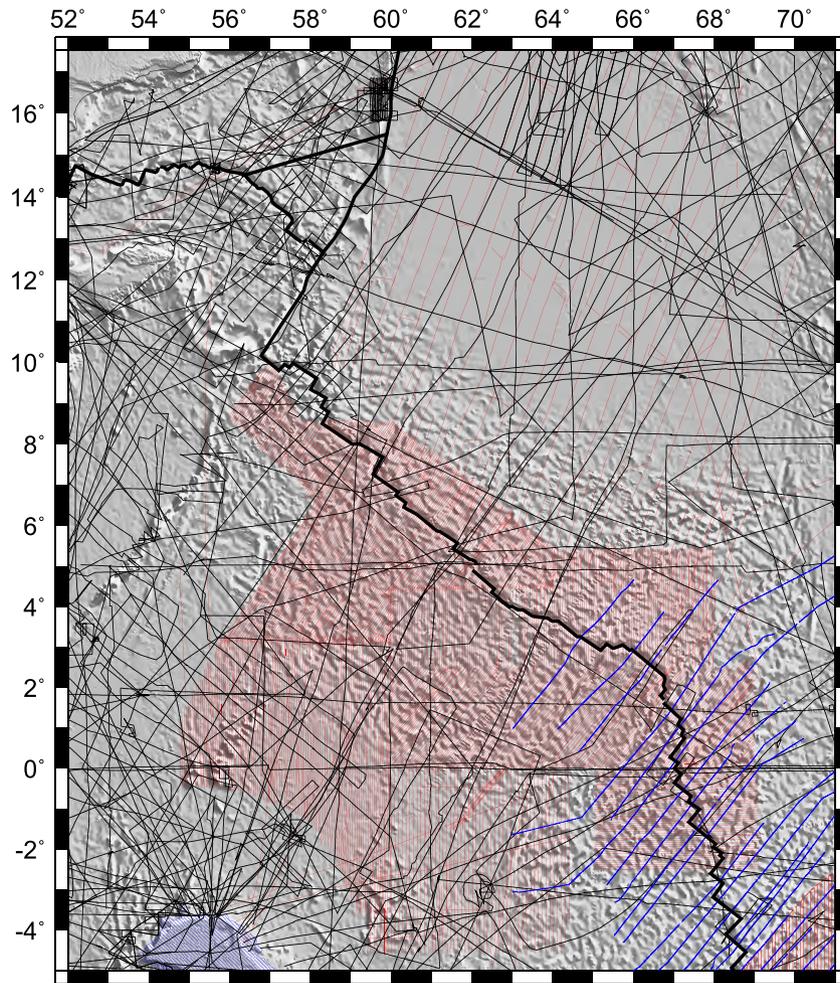
Figure 2. Ship and airplane magnetic profile tracks used for the analysis. The red, blue and black lines, respectively, locate tracks from Russian vessels (Merkouriev & DeMets 2006), from a 1990 aeromagnetic survey (DeMets *et al.* 1994), and all other sources. The bold line locates the active plate boundaries.

2.2 Magnetic anomalies: southern Central Indian Ridge

Prior to the breakup of the former IndoCapricorn Plate into distinct India and Capricorn plates at ∼20–16 Ma, the Carlsberg and Central Indian Ridges both accommodated India–Somalia Plate motion. Data from the Central Indian Ridge south of the Vema fracture zone (9–10°S) are thus used for some of the ensuing analysis, although none are used to estimate the new India–Somalia rotations featured in Section 3. The Central Indian Ridge data include identifications of C13 and C18n.2o from Cande *et al.* (2010), which are archived in the Global Magnetic Lineation Data Base (Seton *et al.* 2014). They also include ≈500 identifications of C20–C26 from the supplemental file of Yatheesh *et al.* (2019) and non-redundant crossings of the same reversals from Cande *et al.* (2010), Eagles & Hoang (2014) and Cande & Patriat (2015) from the Global Magnetic Lineation Data Base. Our southern Central Indian Ridge kinematic data also include Boussole and Mauritius fracture zone flow lines that we digitized from bathymetric data.

2.3 Transform faults and fracture zone flow lines

The youngest rotation that we estimated, that for Chron 1n, is constrained partly by the traces of the transform faults that offset fracture zones B, E, F and G (Fig. 5b). We digitized the 15-km-long FZ

B transform fault from multibeam coverage reported by Kamesh Raju *et al.* (2008). The transform faults at fracture zones E, F and G, which offset the ridge axis by respective distances of 70, 30 and 50 km, were digitized from a 3-km bathymetric grid (Fig. S5) that we created from depth measurements along the ship tracks in Fig. 2. Other Central Indian Ridge transform faults between 3° and 9°S have been surveyed with multibeam systems (Drolia & DeMets 2005; Kamesh Raju *et al.* 2012) but do not record India–Somalia Plate motion due to diffuse India–Capricorn deformation east of the ridge at these latitudes (DeMets *et al.* 2005; Drolia & DeMets 2005).

Two groups of fracture zone flow lines constrain our rotations. For the reconstructions from 42.2 Ma (C20n.1n) to the present, the rotations are estimated from the traces of Fracture Zones A through G. The traces of these fracture zones are generally simple for seafloor ages younger than 30–25 Ma, but curve significantly at their northeastern and southwestern ends before they terminate against older, morphologically smoother seafloor that accreted at faster seafloor spreading rates (Figs 4, 5b, 6, 7 and S5).

For reconstructions older than 42.2 Ma, we evaluated two geographically distinct sets of flow lines to constrain our rotations, one at the eastern end of the Carlsberg Ridge near the palaeocentre of the
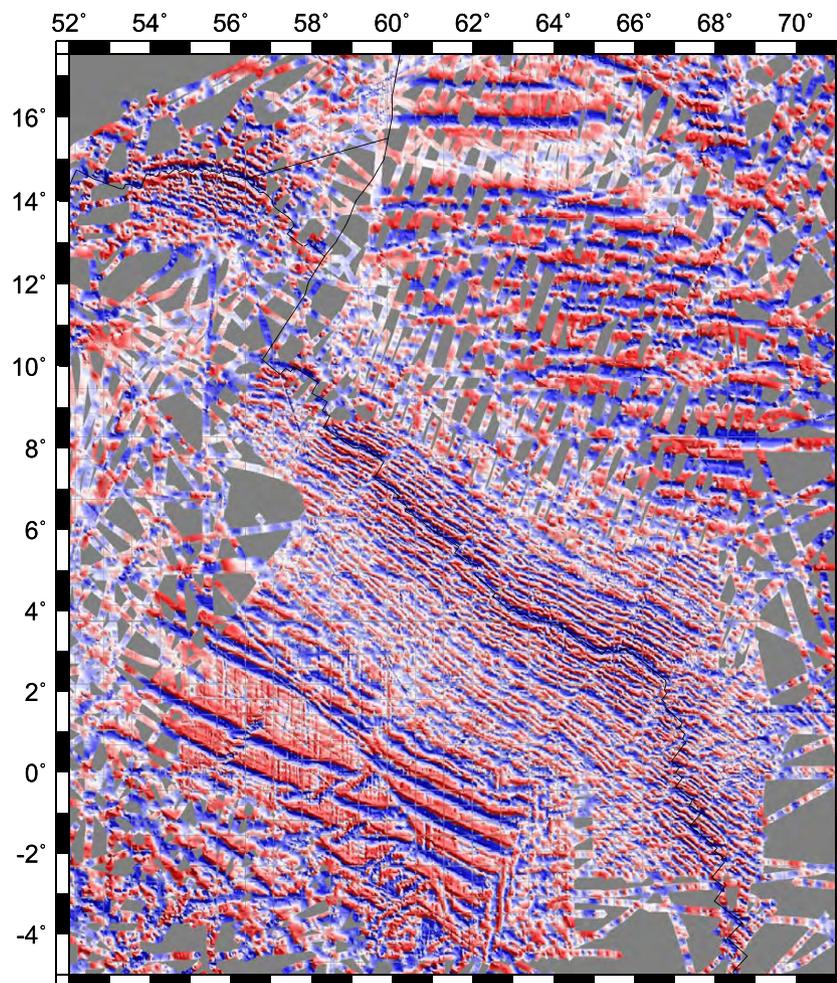
Figure 3. Magnetic anomaly grid derived from dense Russian and other magnetic data in our study area. The magnetic track line locations are shown in Fig. 2. Reds and blues indicate areas of positive and negative magnetic anomalies, respectively.

India–Somalia Plate boundary at the time of C20, and the other at the western end of the Carlsberg Ridge near the Owen Fracture Zone. At the east end of the Carlsberg Ridge, magnetic lineations older than C20 are offset on both sides of the ridge by the Rudra fracture zone and an unnamed fracture zone that we refer to hereafter as the Maldive fracture zone (Figs 4 and 5b). Both of these fracture zones are clearly defined by the vertical derivative of the regional gravity field (Fig. 5a). At the west end of the Carlsberg Ridge, the vertical gravity gradient clearly reveals two parallel fracture zones south of the ridge axis and 100–200 km east of the Chain Ridge, adjacent to seafloor with ages between C26 and C20 (Figs 4, 5a and b). Following Royer *et al.* (2002), we refer to these two fracture zones collectively as the Chain Fracture Zone. In Section 1 of our Supporting Information, models that variously use one or both groups of these fracture zones to constrain the India–Somalia C26-to-C20 rotations are compared.

The Chain, Maldive and Rudra fracture zones were all abandoned during a reconfiguration of the palaeoridge at the time of C20 (43–42 Ma), when the palaeo-opening direction rotated ≈40° clockwise. In order to constrain our kinematic model during this poorly understood transition, we experimented with several Central Indian Ridge fracture zones that appear to bridge the change in the palaeoridge geometry. Via a series of trial inversions, we identified one flow line (within the rectangular region in Figs 5a and b) that is

consistent with the magnetic reversal and other flow line constraints. In Section 4.3.3, we show that the rotation sequence derived with this flow line successfully matches the traces of other Central Indian Ridge fracture zones that were excluded from our inversion.

The fracture zones described above were digitized in GeoMapApp (Carbotte *et al.* 2004 and www.marine-geo.org) from observations that include satellite gravity field version 29 and its vertical gradient (ftp//topex.ucsd.edu/pub/global_grav_1min; Sandwell *et al.* 2014), an author-produced bathymetric grid in Fig. S5, and the bathymetric data native to GeoMapApp. Later in the analysis, we also use data from a transit multibeam sonar track (Charles 2007; located by the green line in Fig. 5b) in order to evaluate the accuracy of our newly determined rotations (Section 4.3.4).

3 METHODS

The methods and fitting functions we use to estimate best-fitting are summarized below and described in detail by Merkouriev & DeMets (2014a). The magnetic reversal, transform fault and fracture zone crossings are inverted simultaneously in order to estimate the sequence of finite rotations that minimizes the cumulative weighted least-squares data misfit. Magnetic reversal crossings are fit using the great-circle fitting criteria of Hellinger (1981); fracture zone

Table 1. Data summary.

Magnetic reversal	Age (Ma)	India-Somalia† # data : WRMS (km)	
		Anom	FZ
1no	0.773	337 : 1.84	99 : 0.33
2ny	1.775	344 : 1.28	85 : 0.43
2An.1y	2.595	409 : 1.49	114 : 0.62
2An.3o	3.596	365 : 1.57	76 : 0.87
3n.1y	4.187	386 : 1.52	149 : 0.99
3n.4o	5.235	330 : 1.53	96 : 1.34
3An.1y	6.023	274 : 1.72	78 : 2.24
3An.2o	6.727	272 : 1.62	77 : 2.79
4n.1y	7.537	239 : 1.63	70 : 3.18
4n.2o	8.125	280 : 1.56	106 : 3.33
4Ao	9.105	305 : 1.50	69 : 3.73
5n.1y	9.786	366 : 1.75	139 : 3.61
5n.2o	11.056	443 : 1.87	174 : 3.62
5An.2o	12.474	367 : 1.66	140 : 3.34
5ACy	13.739	328 : 2.13	117 : 3.30
5ADo	14.609	292 : 1.97	173 : 3.19
5Cn.1y	15.974	351 : 1.85	171 : 3.65
5Dy	17.235	339 : 1.75	128 : 4.28
5Ey	18.007	289 : 1.86	104 : 3.94
6ny	18.636	264 : 2.23	104 : 4.03
6no	19.535	276 : 2.17	180 : 4.85
6AAr.2o	21.691	173 : 2.57	171 : 6.74
8n.1y	25.099	147 : 2.83	161 : 8.46
11n.1y	29.183	151 : 2.17	105 : 10.79
13ny	33.214	124 : 2.76	196 : 1.09
18n.1y	38.398	97 : 2.96	43 : 0.71
18n.2o	40.073	120 : 2.31	28 : 0.60
19ny	41.030	98 : 2.55	17 : 0.93
20n.1y	42.196	125 : 2.69	57 : 0.61
20n.1o	43.450	98 : 2.84	91 : 0.67
21n.1y	46.235	117 : 2.86	94 : 1.23
21n.1o	47.760	67 : 2.66	94 : 6.50
22n.1y	48.878	57 : 2.60	45 : 8.56
22n.1o	49.666	52 : 3.47	80 : 7.32
23n.1y	50.767	86 : 2.32	21 : 4.51
23n.2y	51.047	53 : 2.91	39 : 5.16
23n.2o	51.724	52 : 2.61	40 : 4.10
24n.1y	52.540	41 : 3.81	10 : 3.37
24n.1o	52.930	44 : 3.84	1 : 4.92
24n.3y	53.250	61 : 2.79	10 : 2.41
24n.3o	53.900	74 : 2.86	70 : 0.84
25ny	57.101	82 : 2.84	29 : 1.28
25no	57.656	76 : 2.96	68 : 0.92
26ny	58.959	69 : 1.41	25 : 1.66
26no	59.237	64 : 1.66	37 : 0.89

Chron designators followed by a 'y' or 'o', respectively indicate the young or old edge of the chron. The ages for all the reversals are from the astronomically tuned GTS20 timescale of Ogg (2020). Anom and FZ, respectively indicate the number of magnetic anomaly and fracture zone crossings that were used to estimate the finite rotations in Table 2. Ages estimated for the fracture zone crossings are approximated based on their position along their respective flow lines, but are not used for the inversion. Instead, each fracture zone crossing contributes information to the finite rotation estimates for all ages. WRMS is the weighted RMS misfit in km of a best-fitting rotation adjusted for the number of parameters that were estimated to fit the data.

crossings are fit using the Shaw & Cande (1990) flow line methodology; transform fault crossings are fit using the small-circle fitting function of Merkouriev & DeMets (2014a). An *a priori* correction is applied to every best-fitting rotation to compensate for outward

displacement of the magnetic reversal boundaries, a systematic error that largely impacts estimates of seafloor spreading rates for Chrons 1 and 2 (DeMets & Wilson 2008).

We use weighted root-mean-square (WRMS) misfits to the individual data types as our primary means for describing and comparing data misfits. The WRMS misfits account for the assigned data uncertainties and the number of parameters that were adjusted to fit the data for a given time and/or type of data.

The rotation covariances are estimated using methods described by Chang (1988), whereby the covariances depend on the assigned data uncertainties and the geometry and distribution of the reconstructed data. Due to the heterogeneity of the data for the 45 times that are represented in our data set, we did not estimate alternative rotation covariances via the bootstrap method that is outlined by DeMets & Merkouriev (2019). The rotation covariances in Table 2 are tied to the Somalia Plate and thus describe the uncertainties in the locations of points that are rotated from the Somalia onto the India Plate. For reader convenience, rotations and covariances that can be used to reconstruct the positions and uncertainties of India Plate points onto the Somalia Plate are listed in Table S1.

Stage rotations that describe plate motion from time t_2 to t_1 were determined using the standard method, that is given finite rotations $\hat{A}_{t_2}^{B \to A}$ and $\hat{A}_{t_1}^{B \to A}$ that reconstruct Plate B onto Plate A for times t_2 and t_1, the stage rotation $\hat{A}_{t_2 \to t_1}^{B \to A}$ that reconstructs the motion of Plate B relative to Plate A from t_2 to t_1 is given by $\hat{A}_{t_1}^T \hat{A}_{t_2}$. Angular velocities that are suitable for describing India Plate movement in a frame of reference tied to the Somalia Plate are found in Table 3. Angular velocities that describe Somalia Plate motion in a frame of reference tied to the India Plate are provided for reader convenience in Table S2.

The stage spreading rates for our own and all previously published rotations that are used below are normalized to magnetic reversal ages from the astronomically tuned GTS20 timescale (Ogg 2020) unless otherwise noted. Later in the analysis, we also use reversal ages from the GTS12 (Ogg 2012) and MQSD20 (Malinverno *et al.* 2020) geomagnetic reversal timescales in order to evaluate the robustness of our results.

4 RESULTS: INDIA–SOMALIA PLATE MOTION

4.1 Preferred rotations and reconstructions: reversal and flow line fits and misfits

The plate kinematic observations that constrain our preferred rotations consist of the following: (1) The magnetic reversal identifications that are described in Section 2 and displayed in Fig. 4. (2) Four transform faults. (3) For the C1–C21 rotations, flow lines for fracture zone A on the India Plate, fracture zones B–G from each of the India and Somalia plates, and the Somalia Plate flow line at 7–8°S. (4) For rotations older than C20n.1n, the Rudra and Maldive fracture zone flow lines at the eastern end of the Carlsberg Ridge.

Our reasons for selecting the Rudra and Maldive fracture zones to constrain the rotations for times before C20n.1n are described in Section 1 of the Supporting Information. Alternative rotations that instead best fit the Chain fracture zone flow lines at the western end of the Carlsberg Ridge predict C20n.1n–C26 flow lines that differ in location by up to ±50 km from the flow lines estimated with the preferred rotations. The ambiguity about the flow lines that best record India–Somalia Plate motion before Chron 20 is an important limitation of our analysis.
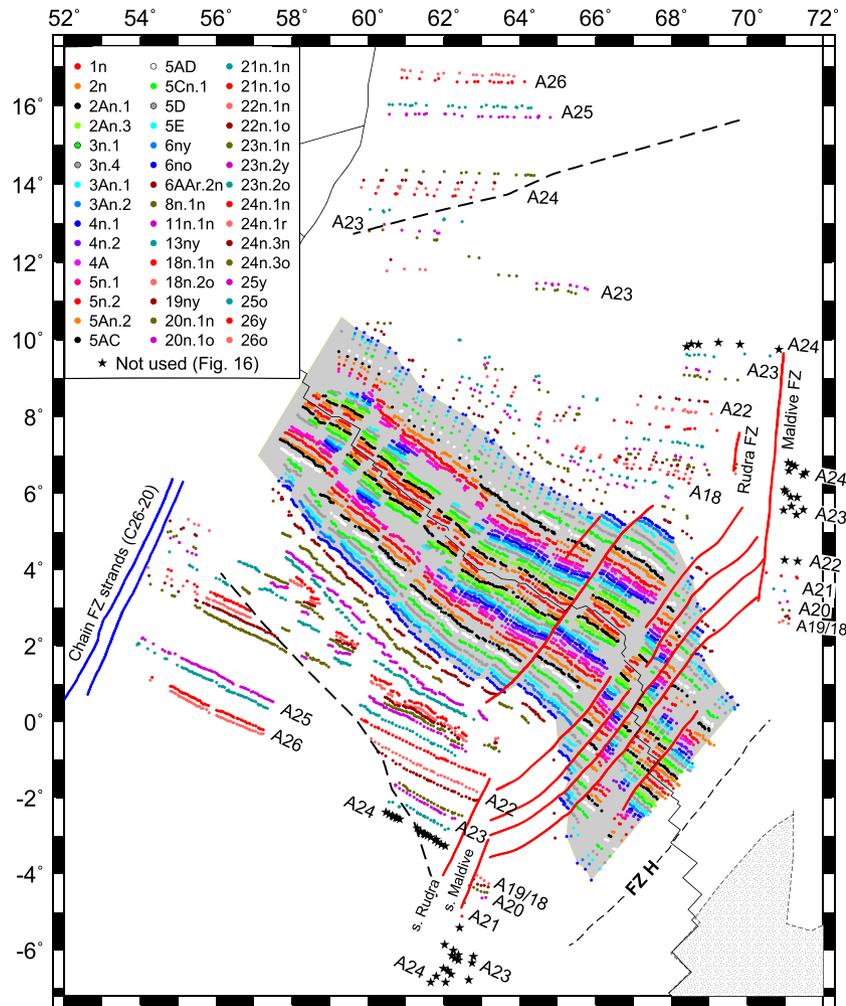
Figure 4. All 8984 identifications of magnetic anomalies 1n through the old edge of anomaly 26 that were inverted to estimate India–Somalia rotations for the past 59 Myr (identified by the coloured circles in the legend). Stars show other reversal identifications used in the analysis but excluded from the rotation estimation. Selected anomalies are labelled. Red lines show the transform fault traces and all but one of the fracture zone flow lines that constrain the Table 2 rotations. Blue lines show traces of the Chain fracture zone that are also used for the analysis. The reversal tie points and original magnetic anomaly data used for our identifications are shown in Figs S1 and S3, respectively. Most of the crossings of magnetic anomalies A1–A6 that are located within the grey-shaded area were previously used for reconstructions by Merkouriev & DeMets (2006) and DeMets *et al.* (2020). All the other reversal identifications were made for this study from the data shown in Figs S1 and S3.

Table 2 lists the best-fitting rotations and covariances from our inversion of all 8984 crossings of C1n–C26, 101 transform fault crossings and 3981 fracture zone crossings. Reconstructions of the palaeo-plate boundary with the best-fitting rotations clearly reveal a major transition in the orientation and segmentation of the palaeo-spreading centre between C21 and C18 (Fig. 6). Details of the best fitting reconstructions are displayed at much larger scale in Fig. S4, which also displays the seafloor bathymetry and track-line magnetic data.

The weighted root-mean-square (WRMS) misfits of the Table 2 rotations to the numerous reversal crossings range from 1.5 to 3 km (red circles in Fig. 7) and generally increase with reversal age. The misfits are similar to those reported for reconstructions of the Mid-Atlantic Ridge spreading centres and Southwest Indian Ridge (Merkouriev & DeMets 2014a, b; DeMets *et al.* 2015a; DeMets & Merkouriev 2019; DeMets *et al.* 2021), but are several times smaller than the 7.8 km WRMS misfit reported by Eagles & Hoang (2014) for their reconstructions of C5–C34 from the Carlsberg Ridge. The least-squares misfit normalized by the degrees of freedom (i.e. χ^2_ν),

is 1.00 for the 8984 reversal crossings. The ±1.6 to ±3.5 km uncertainties we assigned to the reversal crossings thus closely approximate the random component of their location errors.

The conjugate magnetic lineations are well fit everywhere except for the spreading segment that is located immediately east of the Maldive Fracture Zone (located by the black stars in Fig. 4). For this spreading segment, the conjugate reversal crossings for C18n.2o through C21n.1o are well fit by our best fitting rotations (Fig. 8), but the conjugate magnetic lineations older than Chron 21 are systematically overrotated (Fig. 8). The overrotations average 20–30 km for C22n.1n through C23n.2o and increase to 86 km and 97 km for C24n.1n and 24n.1r, respectively (also see Fig. S4). Given these large misfits, we elected not to use the C22 and older reversal crossings from this spreading segment to estimate the best fitting rotations. The overrotations of C22-and-older magnetic lineations resemble overrotations of the same magnetic lineations farther south along the Central Indian Ridge (Section 4.3.4), possibly indicating that the Maldive/Rudra fracture zones were part of an active oceanic plate boundary until the time of C21.
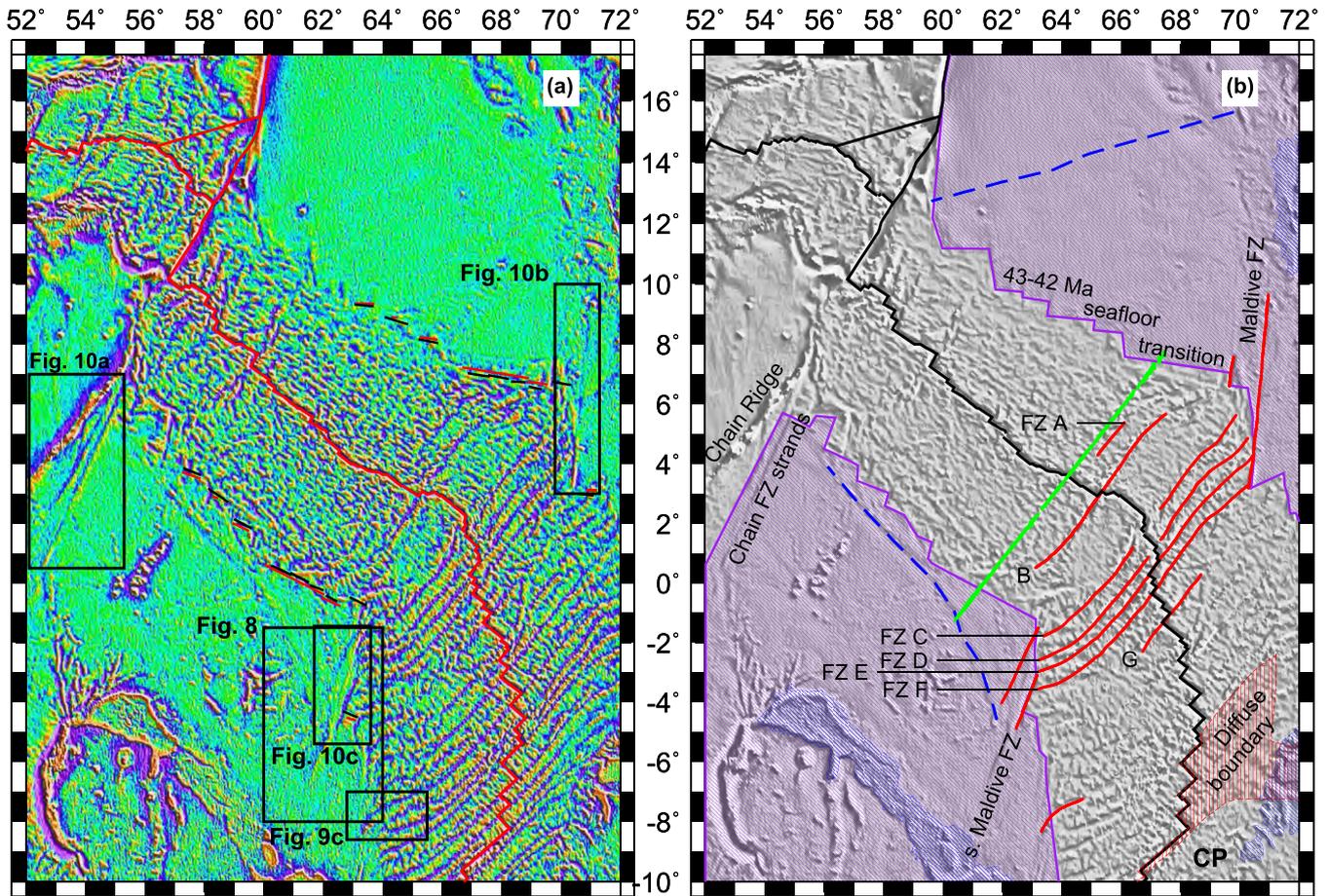
Figure 5. Satellite-derived seafloor gravity in our study area (Version 29 from ftp//topex.ucsd.edu/pub/global_grav_1min - Sandwell *et al.* 2014). Panel (a) shows the vertical gravity gradient with plate boundary (red line). The transition from smooth to rough seafloor morphology occurs during Anomaly 20, whose old (43.4 Ma) and young (42.3 Ma) edges are reconstructed with the red and black lines, respectively, on both sides of the ridge. Panel (b) displays the free-air gravity anomalies. The green line locates the KNOX10RR multibeam sonar track that we use to evaluate the accuracy of our newly derived rotations later in the analysis. The red lines show the fracture zone flow lines that are used to estimate all the India-Somalia rotations in this analysis. The purple shading demarcates India–Somalia seafloor older than 43.4 Ma (Chron 20n.1o). CP, Capricorn Plate.

The WRMS misfits for the fracture zone flow lines in seafloor younger than 40 Ma increase from 0.5 km for the youngest portions of each flow line to ∼11 km at 29 Ma (blue circles in Fig. 7). These are the same as or slightly larger than WRMS misfits of 0.5– 8 km for reconstructions of Nubia–South America and Southwest Indian Ridge fracture zones over similar time periods (DeMets & Merkouriev 2019; DeMets *et al.* 2021). The largest flow line misfits, which range from 10 to 32 km, occur along the Somalia Plate segments of Fracture Zones C and D at seafloor ages older than ∼21 Ma (Fig. 9b), where we may have misinterpreted how the geometries of both fracture zones evolved after 42 Ma (C20).

The Rudra and Maldive flow lines, which abut seafloor older than C20, are generally well fit (Figs 10b, c and S4). North of the ridge on the India Plate, the misfits to both flow lines are less than 5 km along 90 per cent of their lengths and never larger than 6.5 km (Figs 9b and S4). South of the ridge, the misfits range from 5 to 15 km along most of the two flow lines (Figs 9d and S4).

χ^2_ν is 2.2 for the 3981 fracture zone crossings, indicating that the average flow line misfits are 50 per cent larger than the assigned flow line uncertainties, which range from ±0.3 to ±16 km. Increasing the weighting of the flow line data in order to improve their fits degrades the fits to the more reliable magnetic reversal crossings, an undesirable tradeoff. We thus left the flow line uncertainties

unchanged. As a consequence, the rotation covariances in Tables 2 and 3 may underestimate the true uncertainties in the reconstructed flow lines and palaeo-slip directions by as much as 50 per cent.

4.2 India–Somalia Plate motion since 59 Ma

4.2.1 Finite opening poles and stage poles

From C26 (59 Ma) to C6 (19.7 Ma), India–Somalia finite opening poles migrated anticlockwise along a path near the central Red Sea (Fig. 11b). Since C6, the finite pole has migrated several angular degrees farther southwards to a position near the MORVEL 3-Myr-average opening pole (black star in Fig. 11b). The C5n.2-to-present opening pole (Table 2) is located four angular degrees southeast of the C6no-to-C5n.2 stage pole estimated from our Table 2 rotations (27.7°N, 28.9°E). This agrees with previous evidence for a modest southeastward migration of the opening pole since 20 Ma (Merkouriev & DeMets 2006; DeMets *et al.* 2020).

The kinematic data that we used to estimate the Table 2 rotations typically span arc distances of 14 arc degrees or less, insufficient to define the stage pole locations with much accuracy. The India–Somalia stage poles and their elliptical confidence regions are therefore spread out from NW to SE (Fig.
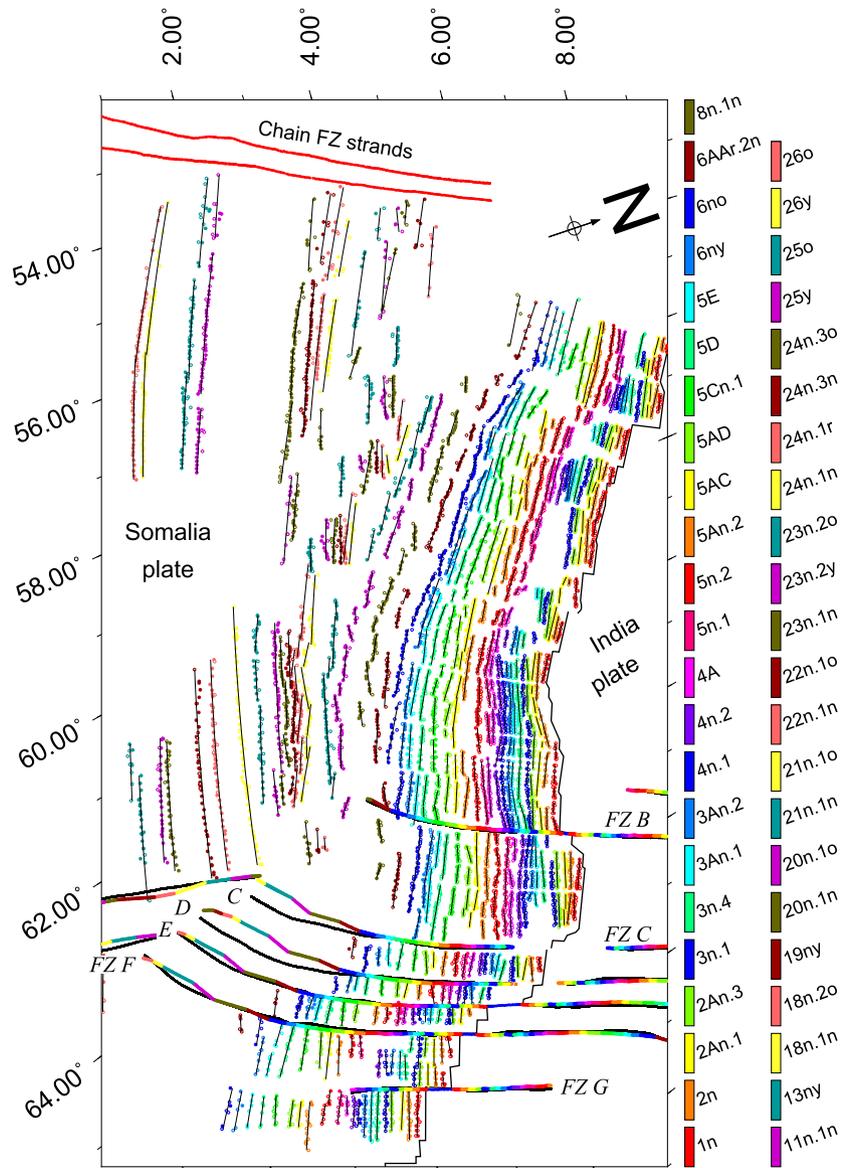
Figure 6. Reconstructions of India Plate reversal crossings onto the Somalia Plate with the best-fitting rotations from Table 2. The reconstructed flow lines for fracture zones B–G (coloured circles) are compared to the digitized flow lines (black circles). Black lines show the great circle segments that best fit each segment of reconstructed reversal crossings. The solid and open symbols show reversal crossings in their original and rotated positions, respectively. The oblique Mercator projection is centred on 35°N, 24.4°W. Fig. S3 shows the same reconstructions and original magnetic anomaly data in greater detail. Fig. 8 shows reconstructions of C18n.2o and older reversal crossings from east of the Maldive Fracture Zone.

12). The problem is the most acute for the rotations for C24 and older reversals, whose opening angles are constrained by reversal crossings entirely from the westernmost Carlsberg Ridge (Figs 4 and 6).

The stage poles are grouped by age within three roughly lunate regions (identified by the purple, blue and red shaded areas in Fig. 12). The stage poles for C26 to C20n.1o (59.2–43.4 Ma) generally sweep through central northern Africa (purple region in Fig. 12), consistent with the NNE-trending flow lines that constrain the rotations for times before C20n.1n. The stage poles for C20n.1n to C6AA (42.2–21.7 Ma) are located 1000–3000 km farther northeast (red poles in Fig. 12), consistent with the more clockwise trends of the flow lines for this period (e.g. Fig. 6). Most of the stage poles for times since C5 are clustered randomly around the Red Sea, consistent with the fixity of the pole since at least 10 Ma.

Based on the above, the noisy stage poles appear to define at least three distinct phases in India–Somalia Plate motion since 60 Ma. The transition between the oldest two phases coincided with the 43–42 Ma palaeoridge reconfiguration clearly displayed in data interpretations from Karasik *et al.* (1986), Dyment (1998), Chaubey *et al.* (2002) and Royer *et al.* (2002) (also see Figs 3 and 4).

4.2.2 Total opening distance and spreading rate histories

The numerous reversal crossings that constrain our India–Somalia rotations yield precise estimates of the history of seafloor opening between the two plates since 60 Ma (Fig. 11a). Along a flow line near the centre of the plate boundary, where the reconstructed opening distances are the best constrained, the 1σ opening distance uncertainties that are propagated from the Table 2 rotation covari-
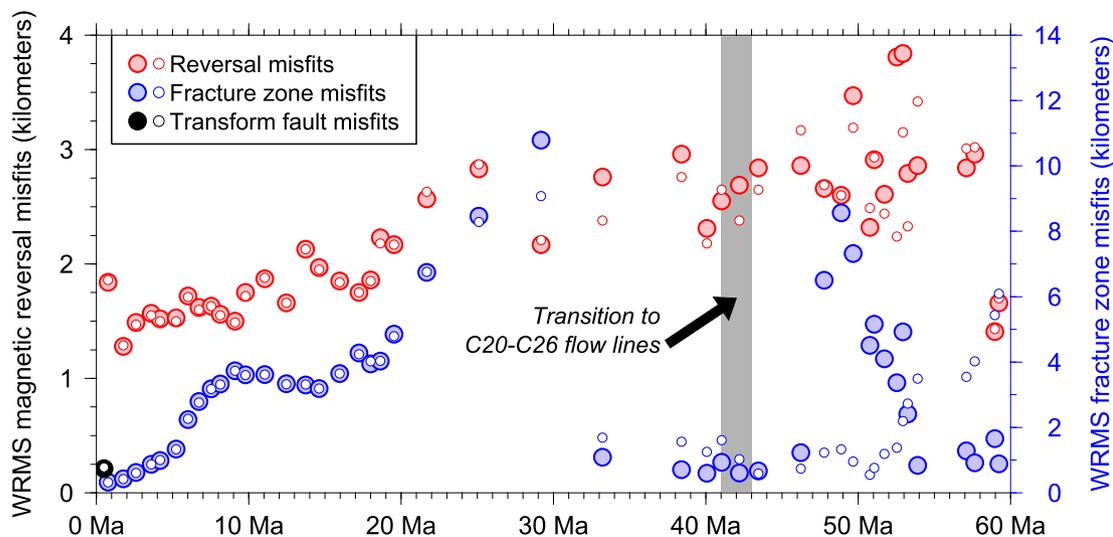
Figure 7. Weighted root-mean-square (WRMS) misfits to the magnetic reversal, fracture zone, and transform fault crossings for the preferred India–Somalia rotations in Table 2 (large filled circles) and alternative rotations in Table S3 (small open circles). The ages of the fracture zone crossings are approximated from the age of their nearest neighbouring flow-line point assuming symmetric seafloor spreading. CIR, Central Indian Ridge.

ances are only ± 0.16–0.70 km for C1n to C23 and ± 1.3–4.2 km for times before C23. Consequently, the opening distance history (Fig. 11a) and its derivative seafloor spreading rate history (Fig. 13) are sensitive indicators of past changes in India–Somalia Plate motion.

A simple examination of the time progression of India-Somalia opening distances that are estimated with our Table 2 rotations is instructive (Fig. 11a). For times older than 50 Ma, the most prominent change occurred at 53 Ma, when the slope of the reconstructed opening distances steepened suddenly, demarcating a sudden spreading rate increase. From ≈ 52 Ma until 45 Ma, a progressive shallowing of the age-versus-distance slope indicates a gradual rather than instantaneous decrease in India–Somalia spreading rates. Along with other lesser slope changes that are marked in Fig. 11a, the reconstructed opening distances define at least six discrete slope changes and at least one and possibly two periods of continuous slope change (indicated by the pink-shaded region in Fig. 11a). During the past 13–14 Myr, new seafloor has accreted at a steady rate about a stationary or nearly stationary pole, as previously concluded by DeMets *et al.* (2020).

From 59.2 to at least 57.1 Ma (C26o to C25ny), India-Somalia seafloor spreading rates declined rapidly by 50 per cent or more (Fig. 13a). This slowdown may have ended as early as 57.1 Ma (the young edge of C25) or as late as 53.9 Ma (the old edge of C24n.3. After 53.9 Ma, the spreading rate may have doubled from 80–90 ± 20 mm yr^{-1} (95 per cent uncertainty) to 181 ± 10 mm yr^{-1} between 52.5 and 51.7 Ma (C24n.1n–C23n.2o). In Section 4.3.1, we examine in more detail the evidence for this previously unrecognized spreading rate pulse.

After 51.7 Ma (C23n.2o), India–Somalia seafloor spreading rates slowed rapidly to only 28 ± 1.2 mm yr^{-1} at 46.2–43.4 Ma, consistent with a continuous slowdown for nearly 6 Myr (Fig. 13a). No change in the plate slip direction occurred during this slowdown—the slip direction instead began rotating rapidly clockwise 3–4 Myr after the slowdown ceased (Fig. 13b). The rapid, $\sim 40°$ clockwise change in the plate slip direction that began at 43 Ma coincided with a reconfiguration of the ancestral Carlsberg and Central Indian Ridges to geometries that are similar to their modern geometries (e.g. Fig. 5).

After 46.2 Ma, a short 25–30 per cent spreading rate recovery occurred from 42.2 to 40.1 Ma (Fig. 13a). Two independent lines of evidence support the existence of this brief, relatively small spreading rate pulse. First, it is robust with respect to reversal ages for three recent timescales (Fig. S6). Secondly, it overlapped a similar-magnitude spreading rate slowdown along the Southwest Indian Ridge (Section 5.1). After 40.1 Ma, India–Somalia spreading rates slowed by a further 50 per cent, from 29 ± 1.4 mm yr^{-1} during 42.2–40.1 Ma to only 16.2 ± 0.3 mm yr^{-1} at 38.4–33.2 Ma (Fig. 13a). Due to the low fidelity of the magnetic anomalies between C18n.1n (38.4 Ma) and C13ny (33.2 Ma), we did not attempt to identify additional magnetic reversals with intermediate ages. Any changes in spreading rates during the long period of slow-to-ultraslow spreading after ~ 38.4 Ma are thus unresolved by our analysis.

Between 38.4 and 17.2 Ma (C5Dy), the spreading rates increased during all eight time intervals that are sampled by our reconstructions, from a low of 16.2 ± 0.3 mm yr^{-1} at 38.4–33.2 Ma to 21.4 ± 0.5 mm yr^{-1} at 25.1–21.7 Ma and 44.1 ± 1.4 mm yr^{-1} at 18.0–17.2 Ma (Fig. 13a). During the same period, the plate slip direction rotated gradually $\approx 20°$ anticlockwise (Fig. 13b). In Section 5.1, we discuss this long-lasting spreading rate acceleration in the broader context of the Somalia Plate's absolute motion.

From 17.2 to 13 Ma, seafloor spreading rates declined by a third from 44 ± 1.4 to 26.5 ± 0.8 mm yr^{-1}. This highly significant spreading rate slowdown coincided with a period of slow southward pole migration and gradual anticlockwise rotation of the plate slip direction (Figs 12 and 13b). The most recent spreading phase has been characterized by steady motion since 13 ± 1 Ma, including a stationary pole (Fig. 12), steady plate slip directions (Fig. 13b) and steady spreading rates (Fig. 13a).

4.3 Tests for accuracy and robustness

4.3.1 Robustness and significance of the 52.5–51.7 Ma spreading rate pulse

Geodynamic modeling of the effects of the Reunion hotspot plume and India Plate subduction on Indian Plate motion from 80 to 20 Ma (e.g. van Hinsbergen *et al.* 2011; Pusok & Stegman 2020) suggests

Table 2. India–Somalia best-fitting finite rotations.

Chron	DOF	Lat.	Long.	Ω	Rotation covariances*					
		(°N)	(°E)	(degrees)	a	b	c	d	e	f
1n	482	23.39	32.50	0.318	6.6	12.8	1.1	25.4	2.0	0.3
2n	386	23.91	34.01	0.730	6.4	12.6	1.0	25.5	2.0	0.4
2An.1	460	23.37	33.35	1.064	6.5	12.6	0.9	25.1	1.9	0.3
2An.3	394	21.33	37.06	1.631	7.3	14.1	0.9	28.4	2.0	0.4
3n.1	474	23.63	31.27	1.693	6.9	13.4	0.9	26.6	1.8	0.3
3n.4	383	22.69	34.14	2.231	7.6	14.6	0.7	29.3	1.8	0.6
3An.1	309	23.72	31.15	2.399	13.4	25.1	0.5	50.3	2.5	1.3
3An.2	310	23.05	32.94	2.757	11.4	21.5	0.3	44.1	2.2	1.4
4n.1	268	23.27	32.36	3.024	15.3	29.7	0.6	61.3	2.9	1.5
4n.2	345	22.85	32.44	3.312	12.4	24.3	0.5	50.0	2.2	1.0
4A	325	23.70	30.97	3.607	10.9	20.7	0.9	42.5	3.4	1.4
5n.1	452	23.12	31.42	3.928	12.6	23.7	1.3	47.2	3.3	0.9
5n.2	564	23.51	31.55	4.438	10.5	19.9	1.4	39.8	3.5	0.9
5An.2	456	24.13	29.73	4.858	13.4	24.9	1.1	48.6	2.9	0.9
5AC	398	23.05	32.27	5.653	18.2	35.0	1.7	70.2	4.2	1.0
5AD	416	24.39	29.96	5.800	14.9	29.2	1.4	60.0	3.4	0.9
5Cn.1	467	24.74	29.83	6.410	15.2	30.4	1.3	63.7	3.6	0.9
5D	422	24.52	30.87	7.195	14.3	26.7	0.6	54.5	2.8	1.2
5E	354	24.98	30.59	7.611	20.1	38.6	1.1	80.4	4.7	1.8
6ny	325	24.91	31.19	8.091	31.7	61.3	3.1	125.7	8.3	2.2
6no	415	25.41	30.47	8.405	26.0	50.2	2.7	102.4	6.5	1.5
6AAr.2n	309	26.61	29.29	8.971	9.9	18.1	1.3	36.5	4.2	1.5
8n.1n	277	27.54	30.30	9.992	27.9	53.9	5.8	108.0	13.2	3.1
11n.1n	229	24.20	37.13	13.122	47.0	88.3	7.8	170.6	17.4	3.7
13ny	297	24.31	39.55	14.828	30.1	55.5	5.4	102.4	9.6	1.6
18n.1n	119	22.74	42.86	17.970	174.2	305.7	9.4	537.3	15.9	1.2
18n.2o	121	22.82	43.08	18.608	31.0	53.7	1.2	93.5	1.9	0.4
19ny	96	23.05	42.72	18.918	151.9	258.2	−11.2	439.6	−19.5	1.2
20n.1n	161	23.40	42.34	19.221	17.9	30.2	−0.5	51.5	−1.3	0.4
20n.1o	174	22.72	42.71	20.126	15.7	24.2	−0.9	38.1	−1.8	0.3
21n.1n	192	21.97	42.42	21.365	12.5	18.7	−1.2	28.8	−2.1	0.3
21n.1o	154	21.96	40.93	21.919	27.6	48.8	0.5	88.7	1.1	0.6
22n.1n	95	19.88	41.63	24.571	37.5	63.6	−0.8	111.1	−0.8	1.0
22n.1o	125	19.35	41.39	25.678	23.4	39.4	1.1	70.2	2.0	0.7
23n.1n	92	19.67	39.35	26.352	26.8	45.1	2.3	79.7	6.0	2.4
23n.2y	81	19.25	39.52	27.186	32.5	52.7	2.5	91.7	4.8	1.4
23n.2o	81	19.19	38.31	27.835	31.8	55.7	5.3	103.7	10.8	2.3
24n.1n	44	17.57	38.99	31.503	1240.2	2006.7	293.0	3256.0	480.2	75.4
24n.1r	38	17.78	38.54	31.855	1364.2	2273.0	322.3	3581.6	581.0	83.2
24n.3n	64	18.67	36.90	30.509	634.5	1003.7	135.3	1595.1	219.6	35.2
24n.3o	133	18.45	36.34	30.980	690.7	1140.1	140.0	1886.9	232.7	29.5
25y	102	21.99	26.32	28.021	177.1	298.9	57.0	507.7	98.0	20.4
25o	135	21.58	26.36	28.840	235.9	391.9	73.7	653.7	123.4	24.0
26y	87	20.94	25.92	30.750	322.5	546.9	113.2	931.2	194.4	42.3
26o	94	20.63	26.11	31.444	665.0	1141.5	230.5	1963.5	397.6	81.7

Notes: These finite rotations reconstruct the Somalia Plate onto the India Plate and include corrections for 3.5 km of outward displacement described in the text. The rotation angles Ω are positive CCW. DOF, the degrees of freedom, equals the total number of anomaly, transform fault, and fracture zone flow-line crossings used to estimate the rotation for a given time reduced by the number of estimated parameters. The weighted RMS misfits for these rotations are given in Table 1 and displayed in Fig. 7. The rotation covariances are propagated from the data uncertainties and geometric distribution of the observations using the method of Chang (1988). The Cartesian covariances, which have units of 10^{-8} rad^2, were calculated in a Somalia-fixed reference frame and thus describe the uncertainties in the locations of points that are rotated from Somalia onto India. Elements *a*, *d*, and *f* are the variances of the (0°N, 0°E), (0°N, 90°E), and 90°N components of the rotation. The covariance matrices are reconstructed as follows: $\begin{pmatrix} a & b & c \\ b & d & e \\ c & e & f \end{pmatrix}$.

that both contributed significantly to speedups and slowdowns in Indian Plate motion during this period. Our new evidence for a possible doubling of the India–Somalia seafloor spreading rate from 52.5 to 51.7 Ma thus warrants careful scrutiny, particularly in light of evidence that a possible earlier India Plate spreading rate pulse at 67–64 Ma may instead be an artefact of inaccurate ages for one or both of C29 and C28 (Perez-Diaz *et al.* 2020). Below we evaluate the

robustness of the possible spreading rate pulse at 52.5–51.7 Ma with respect to magnetic reversal ages from the C33-to-C13 MQSD20 reversal timescale and GTS12 (Ogg 2012) and via synthetic modelling of closely spaced Russian magnetic anomaly profiles from 55- to 50-Myr-old seafloor on both sides of the Carlsberg Ridge.

Malinverno *et al.* (2020) estimate revised ages for magnetic reversals between Chron 33 and Chron 13 based on minimizing the

Table 3. India-Somalia stage angular velocities.

Interval	Lat.	Long.	$\dot{\omega}$	Covariances					
	(°N)	(°E)	(° Myr^{-1})	a	b	c	d	e	f
1n-0	23.39	32.50	0.412	0.11	0.21	0.02	0.43	0.03	0.00
2n-1n	24.30	35.19	0.411	0.13	0.25	0.02	0.51	0.04	0.01
2An.1-2n	22.18	31.90	0.407	0.20	0.38	0.03	0.75	0.05	0.01
2An.3-2An.1	17.26	43.64	0.574	0.14	0.27	0.02	0.53	0.04	0.01
3n.1-2An.3	29.08	315.62	0.305	0.42	0.79	0.05	1.57	0.10	0.02
3n.4-3n.1	19.30	42.75	0.521	0.14	0.26	0.01	0.51	0.03	0.01
3An.1-3n.4	31.12	353.83	0.261	0.35	0.64	0.01	1.27	0.06	0.03
3An.2-3An.1	17.96	44.19	0.522	0.52	0.95	0.00	1.89	0.07	0.05
4n.1-3An.2	25.56	26.31	0.331	0.42	0.79	0.00	1.59	0.06	0.04
4n.2-4n.1	18.48	33.08	0.492	0.84	1.59	0.01	3.19	0.10	0.07
4A-4n.2	32.33	14.01	0.316	0.26	0.48	0.01	0.95	0.04	0.02
5n.1-4A	16.35	35.90	0.476	0.53	0.97	0.03	1.92	0.11	0.04
5n.2-5n.1	26.52	32.73	0.402	0.15	0.28	0.01	0.53	0.03	0.01
5An.2-5n.2	29.74	10.47	0.313	0.13	0.23	0.01	0.43	0.02	0.01
5AC-5An.2	15.29	46.12	0.655	0.21	0.38	0.01	0.73	0.03	0.01
5AD-5AC	41.26	321.81	0.334	0.48	0.87	0.01	1.68	0.05	0.02
5Cn.1-5AD	28.18	28.78	0.448	0.18	0.33	0.00	0.65	0.02	0.01
5D-5Cn.1	21.99	38.98	0.629	0.21	0.37	0.00	0.72	0.01	0.01
5E-5D	33.09	26.05	0.546	0.63	1.13	0.00	2.21	0.06	0.05
6ny-5E	22.84	40.30	0.771	1.43	2.60	0.03	5.10	0.18	0.09
6no-6ny	37.70	11.49	0.374	0.81	1.45	0.01	2.73	0.07	0.04
6AAr.2n-6no	43.18	10.92	0.285	0.09	0.16	0.00	0.28	0.00	0.01
8n.1n-6AAr.2n	34.51	40.55	0.306	0.04	0.06	0.00	0.12	0.01	0.00
11n.1n-8n.1n	10.99	54.00	0.839	0.05	0.09	0.01	0.16	0.01	0.00
13ny-11n.1n	21.87	57.17	0.444	0.06	0.10	0.00	0.16	0.01	0.00
18n.1n-13ny	12.92	55.57	0.634	0.08	0.14	0.00	0.23	0.01	0.00
18n.2o-18n.1n	23.95	49.35	0.383	1.03	1.41	−0.06	1.95	−0.08	0.01
19ny-18n.2o	37.43	22.44	0.350	2.16	3.47	−0.17	5.65	−0.27	0.02
20n.1n-19ny	45.00	19.89	0.296	1.87	2.33	−0.29	2.95	−0.37	0.06
20n.1o-20n.1n	7.62	47.00	0.750	0.28	0.37	−0.03	0.50	−0.04	0.01
21n.1n-20n.1o	10.96	36.09	0.457	0.05	0.06	−0.01	0.07	−0.01	0.00
21n.1o-21n.1n	22.72	354.81	0.498	0.20	0.30	−0.01	0.47	−0.01	0.01
22n.1n-21n.1o	2.68	43.11	2.499	0.66	0.95	−0.06	1.46	−0.07	0.02
22n.1o-22n.1n	9.15	34.07	1.440	1.36	1.78	−0.15	2.52	−0.16	0.05
23n.1n-22n.1o	29.27	343.17	1.005	0.53	0.74	−0.03	1.11	−0.01	0.03
23n.2y-23n.1n	5.46	41.06	3.072	9.59	13.19	−0.33	19.93	0.02	0.37
23n.2o-23n.2y	21.55	356.40	1.248	1.82	2.51	−0.03	3.83	0.06	0.09
24n.1n-23n.2o	4.80	40.26	4.625	19.41	31.10	4.31	50.16	7.10	1.15
24n.3n-24n.1n	18.49	253.63	2.209	50.43	64.48	1.08	84.38	2.54	0.81
24n.3o-24n.3n	12.03	3.60	0.858	39.48	53.36	1.96	75.00	4.05	0.83
25y-24n.3o	17.23	259.11	1.842	1.29	1.54	−0.12	1.89	−0.10	0.05
25o-25y	8.21	24.03	1.519	17.11	23.90	1.49	34.55	2.97	0.89
26y-25o	13.23	17.50	1.496	4.21	5.86	0.39	8.52	0.83	0.29
26o-26y	5.91	29.57	2.586	156.00	229.74	22.08	350.84	42.52	11.54

Notes: These angular velocities specify India relative to Somalia Plate motion from the old to the young limits of the specified interval. The angular rotation rates $\dot{\omega}$, which are positive anticlockwise, are normalized to the GTS20 magnetic reversal ages in Table 1. The angular velocities and Cartesian covariances, which are tied to the Somalia Plate, are derived from the Table 2 finite rotations, which have covariances that are also tied to the Somalia Plate. The covariances have units of 10^{-6} rad^2 Myr^{-2}. The Table 2 footnotes give further information about the covariances. Angular velocities that are suitable for calculating Somalia Plate motion in an India Plate frame of reference are found in Table S2.

variability of C33–C13 spreading rates that they estimate from 154 magnetic profiles in the Atlantic, Indian Ocean and Pacific basins. Fig. 13(a) compares the spreading rate histories that we estimated with reversal ages from the MQSD20 and GTS20 timescales. The spreading rate pulse from 52.5 to 51.7 Ma, which has a 181 ± 10 mm yr^{-1} peak opening rate for the GTS20 reversal ages, has a smaller peak rate of 158 ± 9 mm yr^{-1} when we use MQSD20 reversal ages (Fig. 13a). The estimated spreading rate for the 53.9–52.5 Ma interval immediately before the spreading rate pulse is however also reduced, such that the magnitude of the spreading rate increase remains relatively unchanged. Substituting GTS12 reversal ages from

Ogg (2012) increases the peak spreading rate to 187 ± 10 mm yr^{-1} (Fig. S6). The GTS12, MQSD20 and GTS20 reversal timescales thus all support the existence of the apparent spreading rate pulse.

The only magnetic profiles in our study area that cross magnetic lineations C24n.3o to C23n.1n, which bracket the period during which the short-lived spreading rate pulse occurred, are located along the western Carlsberg Ridge (Fig. 14). We compared those profiles to two synthetic magnetic profiles. One was created assuming that the spreading rate remained constant from 53.9 to 50.8 Ma (blue synthetic profiles in Fig. 14) whereas the other was created using variable spreading rates for 53.9–50.8 Ma (red synthetic
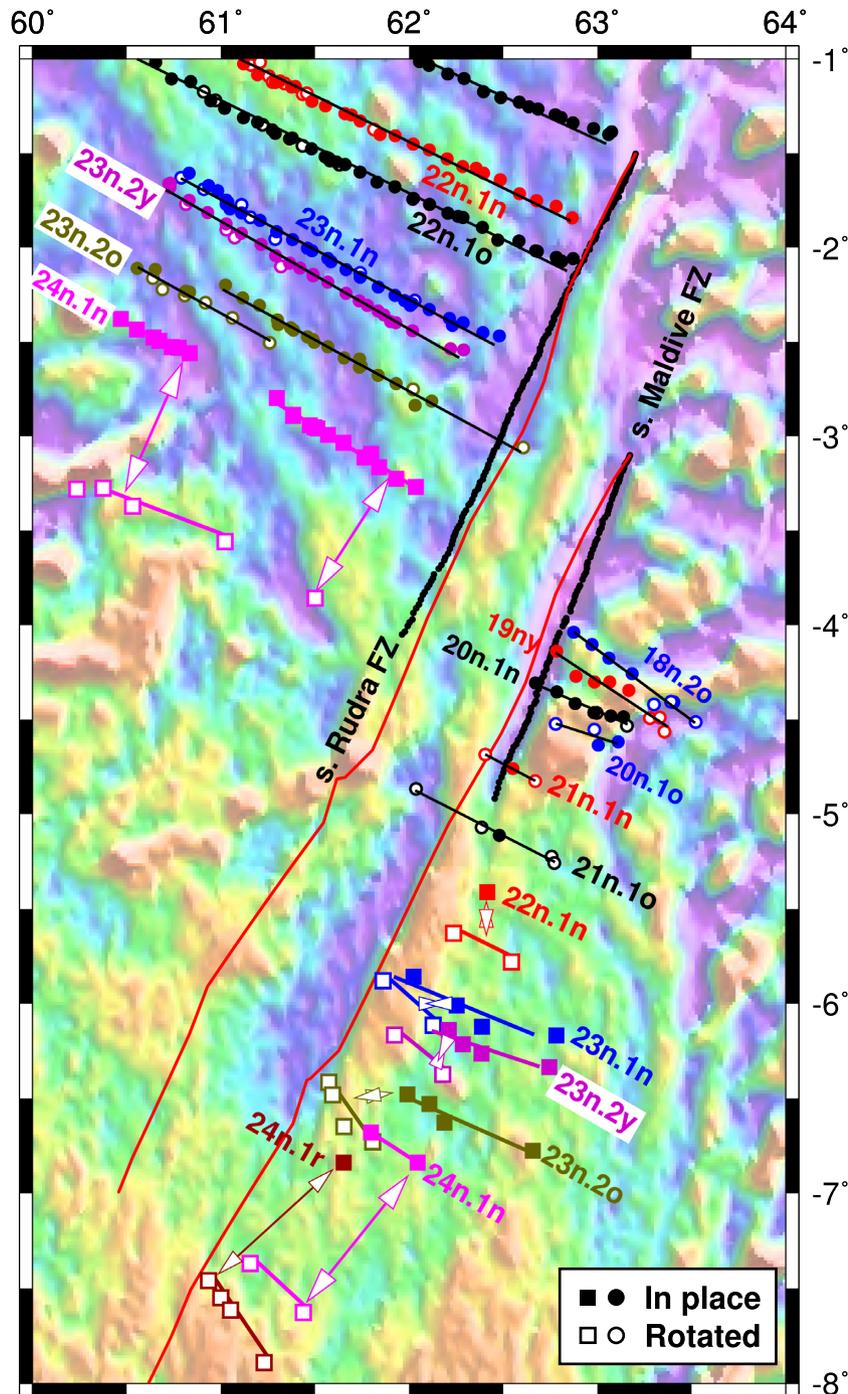
Figure 8. Reconstructions of India Plate magnetic reversal crossings for Chrons 18n.2 to 24n.1r and the southern Maldive and Rudra fracture zone flow lines on the Somalia Plate with the Table 2 rotations. The reversal crossings shown with circles were used to estimate the Table 2 rotations whereas the reversal crossings identified by the squares were excluded (see text). The reconstructed positions of the latter reversal crossings are predicted with rotations estimated from C22 to 24 reversal crossings farther west along the Carlsberg Ridge. The black and red lines, respectively, show the interpreted traces of the southern Maldive and Rudra fracture zone traces and their fitted flow lines. As is shown in the figure, the crossings of Chrons 22 and 23 east of the Maldive FZ are systematically overrotated by 20–30 km and the C24n.1n and C24n.1r reversal crossings by 107 km. The misfits are consistent with similar overrotations of the C22–C24 reversal crossings farther south along the Central Indian Ridge (see text). The map location is identified in Fig. 5(a). The underlying grid shows gravity anomalies (see Fig. 5 for reference).

profiles in Fig. 14). The former constant-spreading-rate synthetic profile clearly underestimates the amount of new seafloor in the Arabian basin from C24n.1n to C23n.2o (Fig. 14b). In contrast, the observed Arabian basin profiles are well matched by a synthetic profile with a faster half-spreading rate (66 mm yr^{-1}) from 52.5 to

51.7 Ma and slower half-spreading rates (45-57 mm yr^{-1}) before and after this period. In the Eastern Somali basin, the observed magnetic profiles are also better matched by a synthetic profile that was created with a faster (~15 per cent faster) C24n.1n-to-C23n.2o half-spreading rate than for the adjacent intervals (Fig. 14a).
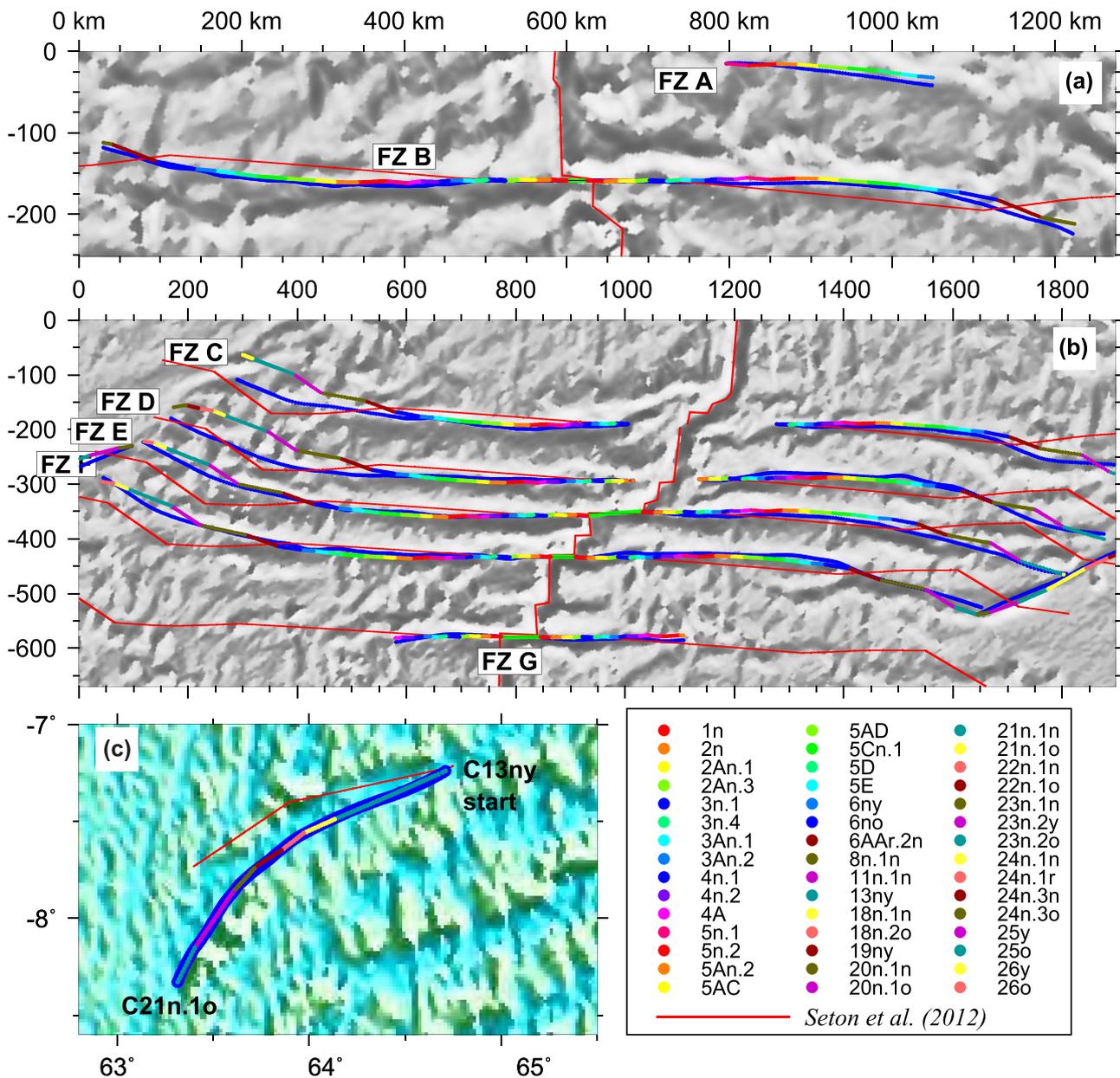
Figure 9. Fits to the fracture zone flow lines and transform faults that constrain the best-fitting rotations for Chrons 1 to 21 in Table 2. The blue and green lines show the digitized flow line and transform fault traces, respectively. The coloured circles show the flow lines predicted by our best-fitting rotations (Table 2), with ages coded to the colours in the figure legend (lower right). The red flow lines are predicted with India–Somalia rotations from Seton *et al.* (2012). Panels (a) and (b) are oblique Mercator projections centred on the C5n.2 India–Somalia pole. The area depicted in panel (c) is identified in Fig. 5(a). Fits to the flow lines that constrain the C20–C26 Table 2 rotations are shown in Figs 10(b) and (d). The flow line fits in (a) and (b) are displayed at larger scale in Fig. S3. The underlying grids show gravity anomalies (see Fig. 5 for reference).

Our synthetic modelling is thus consistent with the existence of the 52.5–51.7 Ma spreading rate pulse, although the ≈20 per cent spreading rate acceleration that is indicated by our qualitative synthetic modeling is smaller than is suggested by our angular velocities and is contingent on the accuracies of the GTS20 magnetic reversal ages that were used to create the synthetic magnetic profiles.

In Section 2 of our Supporting Information, we evaluate whether 60–40 Ma seafloor spreading rates across the southernmost Central Indian Ridge, which also recorded Africa–India Plate motion during this period, reveal any evidence for the 52.5–51.7 Ma spread-

ing rate pulse. Spreading rates that we estimated with the rotations that best fit the well mapped crossings of 15 magnetic reversals from C26o to C20n.1n (described in Section 2.2) are ≈20 per cent faster from 53 to 49.7 Ma than before 53 Ma (Fig. S7b). This is consistent with, but smaller than the larger spreading rate pulse along the Carlsberg Ridge. In Section 5.2.2, we similarly find that Carlberg Ridge opening rates that are estimated using results from previous studies are consistent with the existence of a period of rapid spreading at 52 Ma, but with a lower peak rate than we estimate.
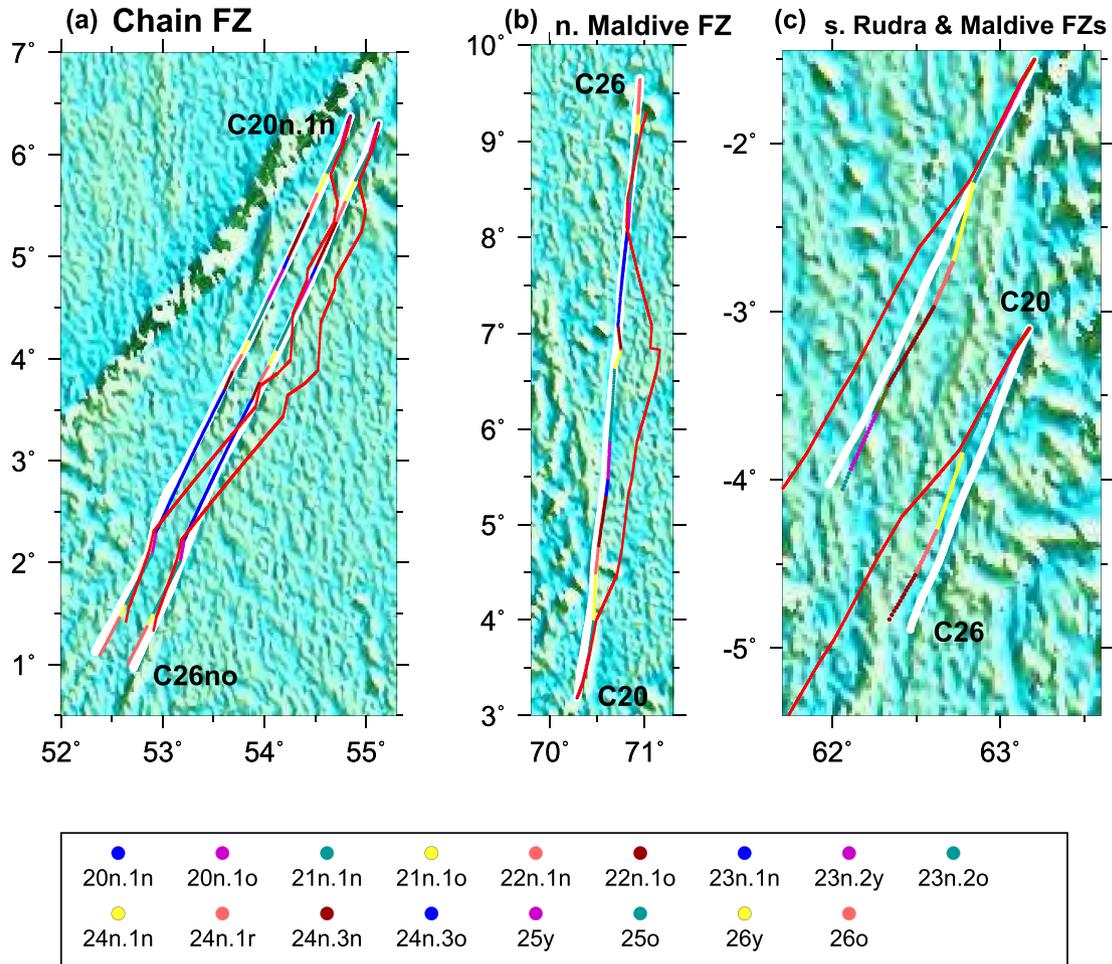
Figure 10. Fracture zone (FZ) flow line fits and predictions for Chron 20n.1n (42.2 Ma) to Chron 26no (59.2 Ma), as follows: (a) Chain FZ strands: The coloured circles show the fits of rotations in Table S3, which were estimated in part from the two Chain FZ strands. The red flow lines are predicted by the Table 2 rotations, which were derived in part from the Maldive and Rudra FZ flow lines in panels (b) and (c) (Fig. 4). (b) The coloured circles show the Table 2 rotation fits to the Maldive FZ on the India Plate. The red flow line is predicted with rotations from Table S3. (c) The coloured circles show the Table 2 rotation fits to the Maldive and Rudra FZs on the Somalia Plate. The red flow line is predicted with rotations from Table S3. The locations of the areas in panels (a)–(c) are indicated in Fig. 5(a). The underlying grids show gravity anomalies (see Fig. 5 for reference).

4.3.2 Central Indian Ridge fracture zone fits and evolution: 5°S to 14°S

Along the Central Indian Ridge south of ≈5°S, the fracture zones on the Somalia Plate that predate the ∼20–16 Ma onset of movement between the India and Capricorn plates (Bull *et al.* 2010) record India–Somalia Plate motion and can thus be used to test our Table 2 India–Somalia rotations for times before 16 Ma. The flow lines that are predicted with the Table 2 rotations should match the traces of these Central Indian Ridge fracture zone traces in seafloor older than 16 Ma if the Table 2 rotations are accurate and if the offsets and/or traces of the fracture zones have not been altered by palaeo-ridge jumps, propagating rifts or asymmetric spreading. A close match between the predicted and observed fracture zone traces constitutes evidence that the Table 2 rotations are accurate. Poor matches are less easily interpreted since they can be caused by rotation inaccuracies or any of the factors listed in the previous sentence.

Based on where the C5Cn.1 (16.0 Ma) magnetic lineations intersect the Central Indian Ridge fracture zones, we used the Table 2 rotations to reconstruct two flow lines for each fracture zone south

of ≈5°S. One of the flow lines originates at the northwest intersection of the C5Cn.1 magnetic lineation with the fracture zone and the other originates at the southeast intersection (Fig. 15). The predicted flow line pairs for most of the fracture zones closely follow their corresponding fracture zone traces back to the time of C20n.1n (Fig. 15). For example, the predicted traces for the Vityaz fracture zone differ from the observed traces by less than ±5 km on both sides of the fracture zone valley at most times since C18n.2o (Fig. 15). The flow lines estimated for Fracture Zones L, O and P and the southern side of the Vema fracture zone valley also closely follow their corresponding fracture zone valley walls. These close matches are evidence for the accuracy of the Table 2 C5Cn.1–C20 rotations.

The abandonment at ≈42 Ma (C20n.1y) of the long-offset Rudra and Maldive fracture zones as the primary India–Africa transform faults for the right-stepping transform faults that define the staircase geometry of the modern Central Indian Ridge coincided with a 40–50° clockwise rotation of the plate slip direction that continued until at least 40 Ma and possibly until 33 Ma (Fig. 13b). West of the present Central Indian Ridge, the progressive clockwise rotation of the plate slip direction after 42 Ma would have increased the
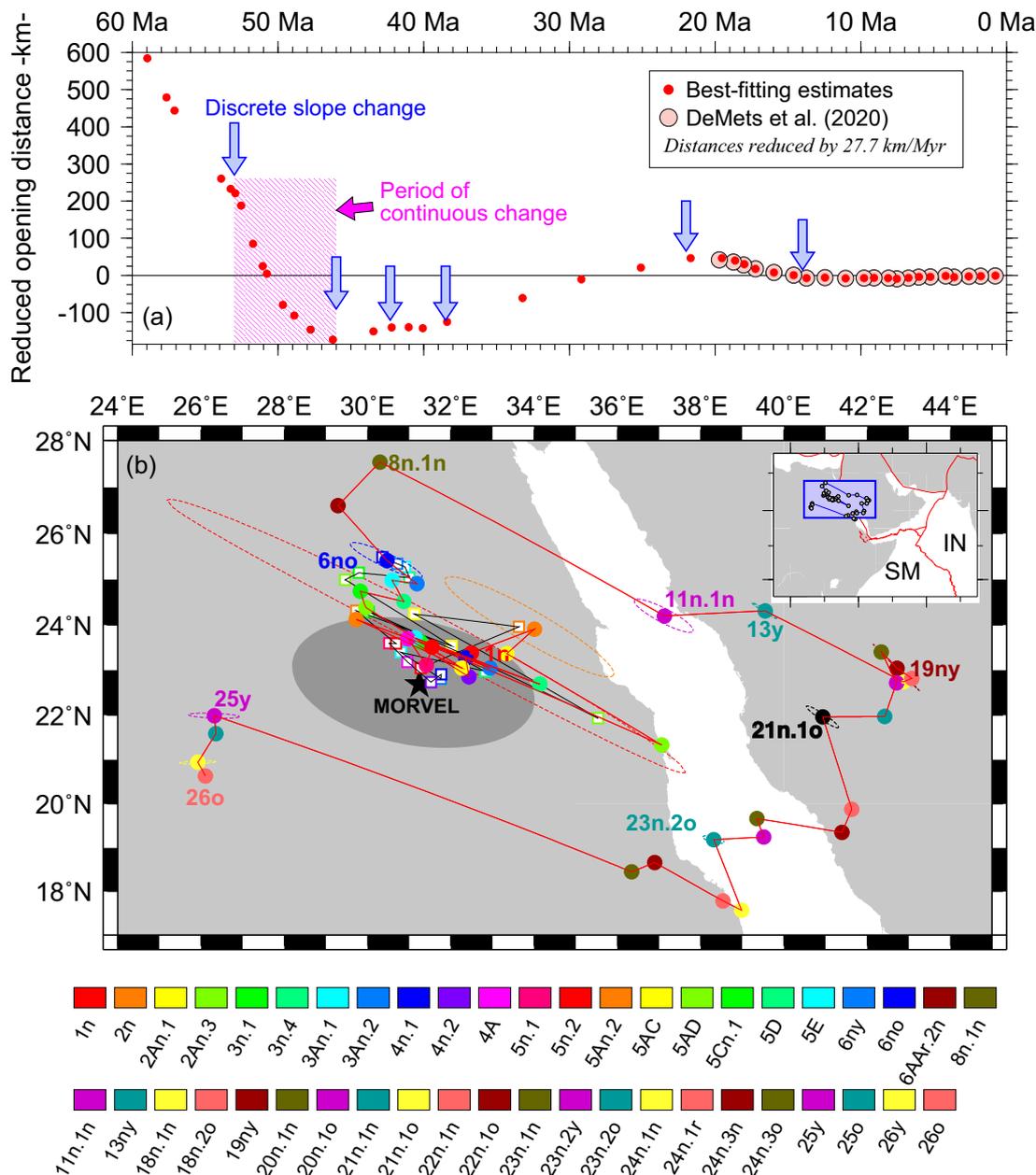
Figure 11. India–Somalia residual opening distances (a) and finite opening poles (b). In (a) the red circles show opening distances determined with the Table 2 finite rotations and reduced by 27.7 km Myr^{-1}, the average spreading rate since 13 Ma. The opening distances are calculated for a flow line that originates at 3.6°N, 64.2°E. The reduced distances shown by the pink circles were estimated using India–Somalia rotations from DeMets *et al.* (2020). (b) C1n–C26 finite opening poles from Table 2 (circles) and C1n–C6 poles from table 2 of DeMets *et al.* (2020) (open squares). For clarity, Panel (b) displays only selected 2-D 95 per cent pole confidence ellipses. The blue rectangle in the inset map locates the main map in relation to the regional plate boundaries (red lines). IN, India; SM, Somalia.

component of fault-normal divergence across the right-stepping, NE-striking transform faults, possibly widening the palaeotransform fault valleys via the emplacement of volcanics, the rearrangement of faults within their transform valleys and the development of intratransform spreading centres (Hekinian *et al.* 1992; Pockalny *et al.* 1997; Lodolo *et al.* 2013; Maia 2019).

The Central Indian Ridge gravity field is consistent with some widening of the palaeotransform fault valleys (Fig. 15). Within the Vema fracture zone valley on the Somalia Plate, we identified four ENE-striking linear gravity features (located by the black dashed lines in Fig. 15) that may be relict intratransform fault segments

that developed within the palaeotransform fault valley in response to the change in slip direction. Small circles around our Chron 18n.1n–13ny stage pole for a Somalia Plate frame of reference closely match the orientations of all four of the lineations (Fig. 15), constituting strong evidence that these features accommodated India–Somalia slip during this period.

Along other fracture zones that are located north and south of the Vema fracture zone, elongate gravity lows that are consistent with crustal thinning are located between the walls of most of the fracture zone valleys at seafloor ages of ≈40–30 Ma (Fig. 15). These gravity lows become narrower from southwest to northeast,
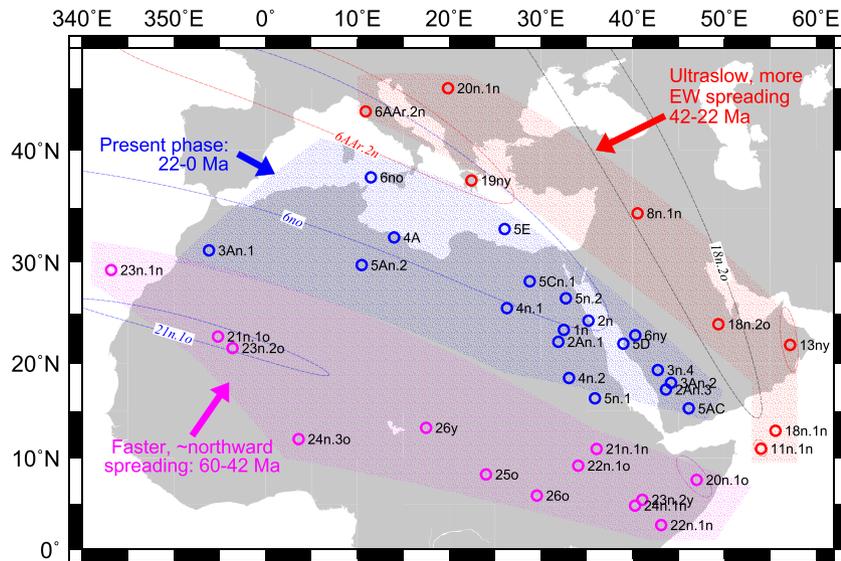
Figure 12. India–Somalia stage poles in a Somalia Plate frame of reference (Table 3). For clarity, each stage pole is labelled only by its oldest bracketing reversal. For example the stage poles that are labeled '5An.2' and '6no' refer to the respective intervals C5An.2 to C5n.2 and C6no to C5E. Ninety-five per cent confidence regions are displayed only for selected stage poles and are identified with the same convention as for the poles. The red, blue and purple patterned regions (and poles) identify stage pole clusters that define three distinct opening phases for the Carlsberg Ridge.

which may reflect the gradual anticlockwise rotation of the plate slip direction after ≈30 Ma and corresponding gradual reduction in the magnitude of the fault-normal divergent component of motion (Fig. 13b).

4.3.3 Comparison to abyssal hill and magnetic lineation azimuths

If the orientations of abyssal hills are determined by the average state of stress near the ridge, as is proposed by Cormier & Sloan (2018), then changes over time in plate slip directions along a seafloor spreading centre should give rise to similar changes in the azimuths of same-aged abyssal hills (and magnetic lineations) provided that the obliquity of the seafloor spreading remains the same or changes more slowly than the plate slip direction. We therefore tested the accuracy of our new rotations by comparing the slip direction history that we estimated with our new Table 2 rotations to the directions orthogonal to abyssal hills and reconstructed magnetic lineations.

Fig. 16 compares India–Somalia slip directions that we estimated with the angular velocities in Tables 3 and S2 to the azimuths of 213 abyssal hills imaged by a continuous multibeam sonar track across the Carlsberg Ridge (Charles 2007, located by the blue line in the Fig. 16a map inset) and ∼1200 Carlsberg Ridge magnetic lineation azimuths (green circles in Fig. 16). The slip directions we estimated in India and Somalia Plate frames of reference (Figs 16a and b, respectively) agree with the abyssal hill and magnetic lineation azimuths to within ±5° at most times during the past 20 Myr and before 42.2 Ma (C20n.1n). For example, the directions that are orthogonal to the abyssal hills and magnetic lineations from 48-to-44 Myr-old Somalia Plate seafloor average N25.5–N27°E and N25–26°E, respectively. These agree with each other within their uncertainties and differ by less than 2° from the N24–25°E India–Somalia slip direction from 47.8 to 43.4 Ma (Fig. 16b). These close agreements argue strongly for the accuracy of our C1-to-C6 and C21-to-C20 angular velocities and finite rotation poles.

The azimuths of the magnetic lineations and abyssal hills that are located on 42.2-Myr-to-20-Myr-old seafloor, when ultraslow-to-slow seafloor spreading occurred, are 10–40° anticlockwise from

their expected orientations based on the angular velocities for this period (Fig. 16). We interpret this as evidence for oblique spreading during 42–20 Ma given the strong association between slow seafloor spreading rates and oblique seafloor spreading (see for example fig. 1 of Zhang *et al.* 2018). Notably, the plate slip directions and directions of the abyssal hill and magnetic lineations all rotate clockwise by 20–25° between 40 and 20 Ma (Fig. 16). The similarities between the observed and predicted 40-to-20-Ma directional changes suggest that the Table 2 rotations for this period are also accurate.

4.3.4 Fits and misfits to southern Central Indian Ridge magnetic lineations and flow lines

Tests of the accuracies of our India-Somalia rotations using magnetic lineations and fracture zones from the southern third of the Central Indian Ridge (Fig. 17), where Capricorn–Somalia Plate motion has been accommodated for the past ∼16 Ma, requires a correction to account for the movement of the Capricorn Plate relative to India. From marine seismic and plate kinematic evidence that are presented by Bull *et al.* (2010), we assume that movement between the India and Capricorn plates began at 16 Ma (see fig. 2 in their paper) and use their Capricorn–India rotation for C5Cn.1 (16.0 Ma) to correct for the integrated movement between the two plates. This correction is denoted below by $\hat{A}_{C5Cn.1}^{CP \rightarrow IN}$.

As a test, we rotated magnetic reversals and conjugate fracture zone segments from the Capricorn Plate east of the ridge onto the Somalia Plate using the Table 2 India–Somalia rotations without any correction for Capricorn–India movement (Fig. 18a). The reconstructed conjugate fracture zone segments are all misaligned by 40–80 km with respect to their Somalia Plate counterparts (compare the solid and dashed lines in Fig. 18a). The reconstructed reversal crossings are also misaligned with their conjugate crossings. For example, the rotated crossings of C13 underrotate the Somalia Plate C13 crossings by 45–75 km.

We repeated the same reconstruction after correcting our India–Somalia rotations $\hat{A}^{IN \rightarrow SM}$ for Capricorn–India Plate motion as follows: $\hat{A}^{IN \rightarrow SM}\hat{A}_{C5Cn.1}^{CP \rightarrow IN}$. With these corrections, the reconstructed
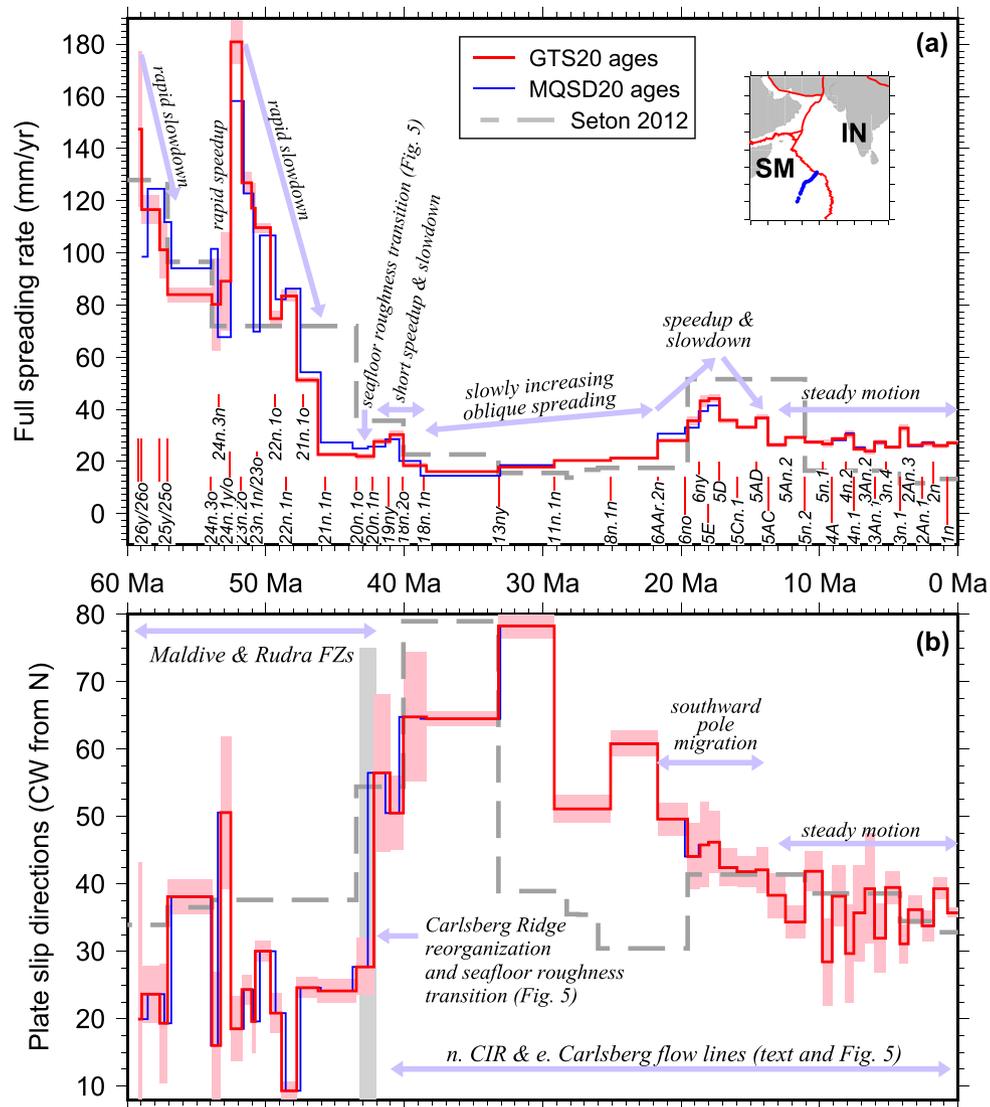
Figure 13. India relative to Somalia stage velocities estimated with angular velocities derived from the Table 2 best-fitting finite rotations and reversal ages from GTS2020 (red line) and Malinverno *et al.* (2020) (MQSD20 label and blue line). The grey dashed line shows stage velocities estimated with rotations from Seton *et al.* (2012) and normalized to GTS2020. The stage velocities are estimated along the Somalia Plate flow line indicated in the inset map. (a) Stage spreading rates and interpretive text. The pink-shaded area shows the 95 per cent uncertainties propagated from the angular velocity covariances. All rates are corrected for outward displacement. (b) Stage plate slip directions. CIR, Central Indian Ridge; IN, India; SM, Somalia; MQSD20, Malinverno *et al.* (2020).

fracture zone segments from east of the Central Indian Ridge are closely aligned with their Somalia Plate conjugate segments (Fig. 18b). For example, restoring the two ≈E–W-oriented fracture zone segments that offset C13 and C18 northeast of the ridge (indicated by the solid and dashed red lines in Fig. 18b) to their positions on the Somalia Plate at the time of Chron 13 aligns the rotated and in-place conjugate fracture zone segments to within 1–3 km, less than the uncertainties in locating these fracture zones. The reconstructed crossings of C13, C18.2o, C20n.1n, C20n.1o and C21n.1n are also closely aligned with their counterparts (Fig. 18b). For example, the reconstructed C13 reversal crossings, which were previously misaligned with their conjugate crossings by 45–75 km (Fig. 18a), are located only 0–10 km from their conjugate crossings. The reconstructed crossings of C18n.2o differ indistinguishably from their conjugate counterparts and the reconstructed crossings of C21n.1n and C21n.1o are, respectively, located within 10 and 20 km of their Somalia Plate conjugate crossings.

The close realignments of the conjugate fracture zone segments and magnetic lineations with C13–C21 India–Somalia rotations that have been corrected for Capricorn–India Plate motion jointly imply the following: (1) our Table 2 rotations for C13 through C21n.1o are accurate. (2) The Bull *et al.* (2010) C5Cn.1 Capricorn–India rotation is accurate. (3) Movement between the India and Capricorn plates began at ∼16 Ma. (4) Our India–Somalia rotations and the Bull *et al.* (2010) C5Cn.1 Capricorn–India rotation can be used to reconstruct the seafloor spreading history of the southern Central Indian Ridge with approximate accuracies of 5–10 km back to 46.2 Ma and 20 km back to 47.8 Ma.

Similar reconstructions of C22 and older reversals with India–Somalia rotations that are adjusted for Capricorn–Indian Plate motion are less successful. For example, the reconstructed crossings of C22n.1n, C23n.2o and C24n.3o are overrotated by respective distances of 40, 80 and 150 km (Fig. 18a), similar to the overrotations of these same reversals directly east of the southern Maldive fracture
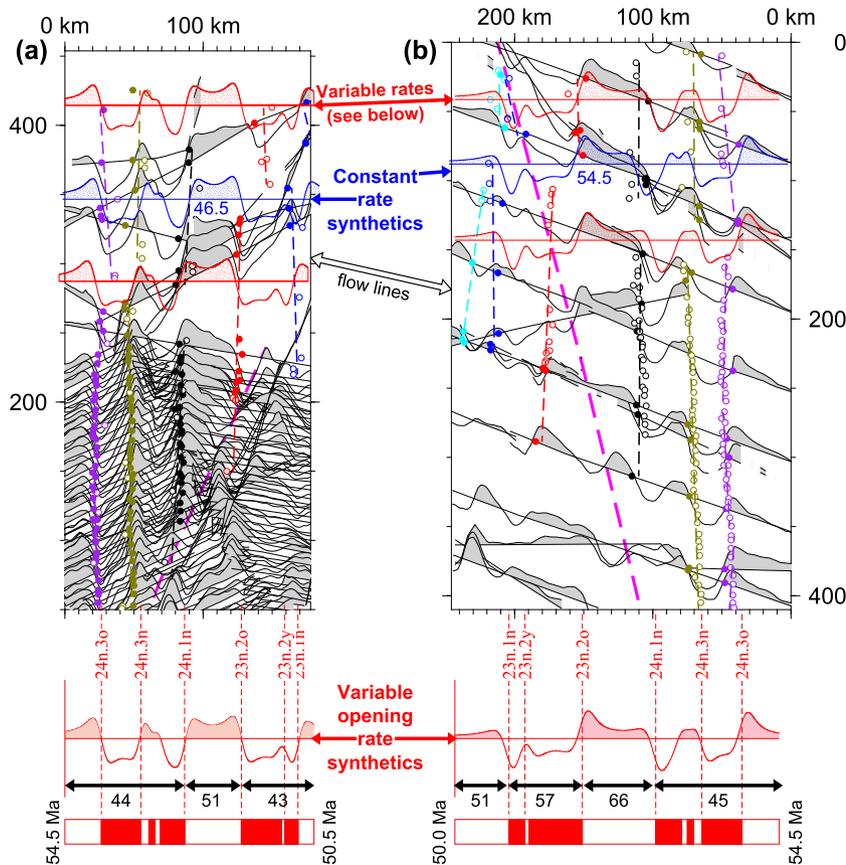
Figure 14. Comparison of observed (black/grey) to synthetic (red and blue) magnetic profiles that span magnetic reversals C23 and C24 on the Somalia (panel a) and India (panel b) plates. The maps, whose locations are shown in Fig. 17, are oblique Mercator projections centred on oblique equatorial poles that lie along the great circle that connects the centre of each map to the C23n.2y-to-24n.3n stage pole for the Somalia Plate (a) and India Plate (b) frames of reference. The black numerals below each synthetic profile specify the half-opening-rates that were used to generate the red synthetic profiles (units of mm yr^{-1}). The red synthetic profiles within and below each map are identical. Constant half-opening rates of 46.5 mm yr^{-1} (panel a) and 49 mm yr^{-1} (panel b) were used to create the blue-shaded synthetic profiles on the maps. Circles show the magnetic reversal crossings at their original locations (solid symbols) and rotated onto the opposite plate (open symbols) with the Table 2 rotations. Reversal ages are from GTS20 (Table 1).

zone ~2000 km farther north (Fig. 8). In contrast to the large over-rotations for C22 through C24, the crossings of C25ny and C26ny from the Capricorn Plate are, respectively, underrotated by 60 and 15 km relative to their Somalia Plate conjugate crossings (Fig. 18b). The magnitudes and senses of the misfits for the C26 through C22 reversals thus vary unpredictably. In Section 5.4, we consider whether these larger misfits are due to greater-than-expected errors in the rotations for these times or possible deformation within the India Plate and/or Somalia Plate before C21.

5 APPLICATIONS TO RELATED TOPICS

5.1 Somalia Plate absolute motion

Due to the Africa Plate's abundance of hotspot trails and central location within the global plate circuit, accurate estimates of its absolute motion are essential for regional and global models of absolute plate motions and tests of hotspot fixity (e.g. Doubrovine *et al.* 2012; Maher *et al.* 2015). At least three tectonic events that affected the Somalia portion of the Africa Plate during the past 40 Ma are likely to have impacted its absolute motion. The initiation of continental extension between 33.9 and 28.4 Ma within the former AfroArabian Plate at the location of the present Gulf of Aden (Bosworth *et al.* 2005) marked the start of the Arabian Peninsula's detachment from

the wider Africa Plate. At 31±1 Ma, the eruption of voluminous flood basalts in northern Ethiopia (Hofmann *et al.* 1997) signaled the arrival of the Afar mantle plume beneath the region, where it migrated from areas farther south (Hassan *et al.* 2020). At ~27 Ma, the Arabian Peninsula collided with Eurasia (McQuarrie & van Hinsbergen 2013). All three events may have altered the forces acting on eastern Africa at and after ~30 Ma. From ≈24 to 20 Ma, widespread volcanic diking, rift-normal faulting, and marine sedimentation along the borders of the Red Sea and rapid subsidence and uplift of the Red Sea rift shoulders (Bosworth *et al.* 2005) marked the Arabia Plate's separation from Nubia. The 31–18 Ma detachment of Arabia from Africa, including associated ≈E–W extension across the East Africa Rift, was completed by the initiation of seafloor spreading in the eastern Gulf of Aden at 19.7 Ma (C6no) and in the central Gulf of Aden at 17.6 Ma (C5D, Fournier *et al.* 2010; d'Acremont *et al.* 2006).

Any changes in the absolute motion of the Somalia Plate during the reconfiguration of its boundaries between 31 and 18 Ma should have altered its motion relative to all its neighbouring plates. We thus compared India–Somalia, Antarctic–Somalia and Capricorn–Somalia seafloor spreading histories at central locations along their respective boundaries (Fig. 19) based on India–Somalia angular velocities in Table 3, Antarctic–Somalia angular velocities from table 10 of DeMets *et al.* (2021) and Capricorn–Somalia angular velocities derived from finite rotations in Table S4. Several interesting
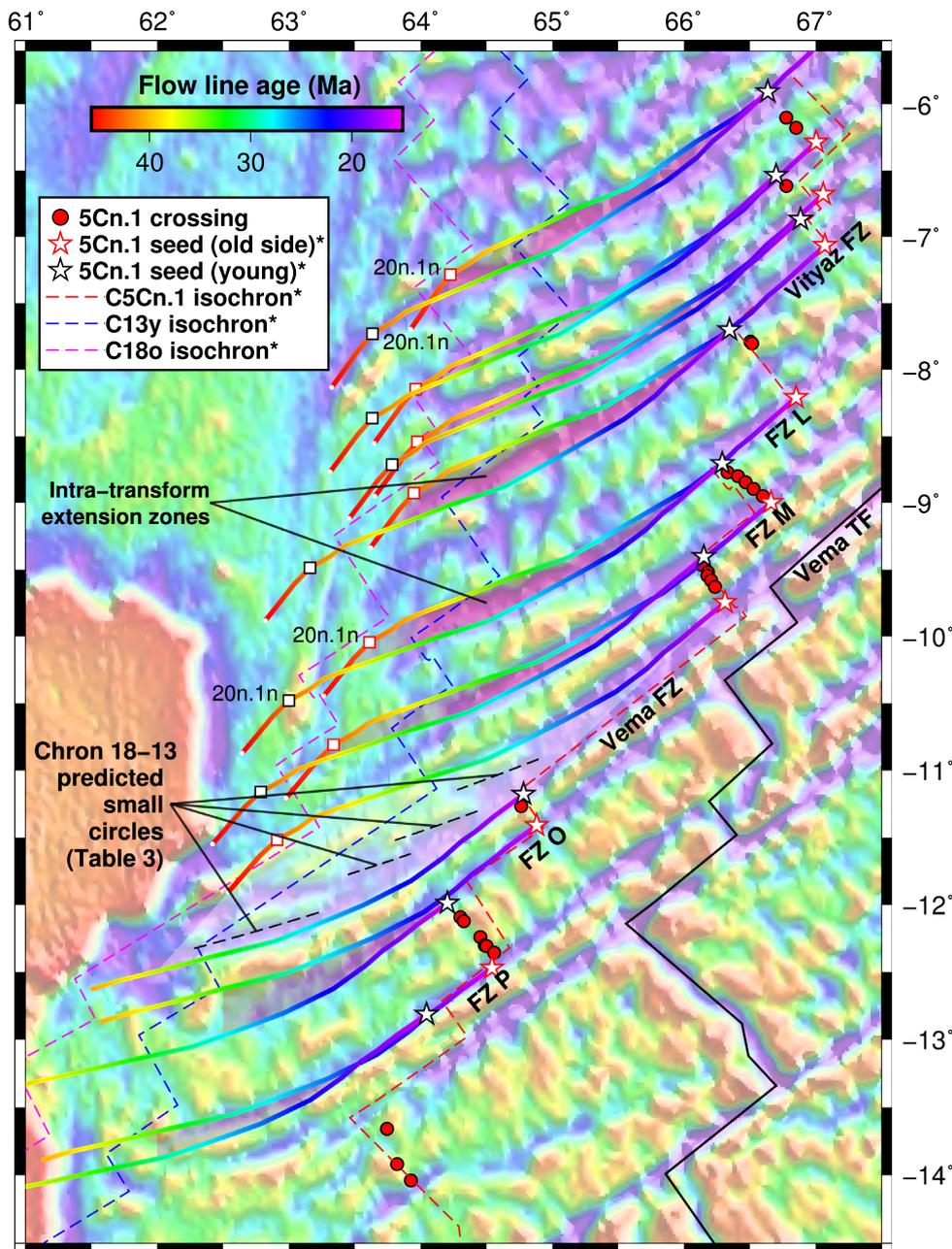
Figure 15. Test of Table 2 rotations via reconstructions of Somalia Plate Central Indian Ridge (CIR) fracture zones older than Chron 5Cn.1 (see text). Per fracture zone, one flow line originates at the northeast palaeo-ridge-transform intersection (RTI) (red stars) and the other at the southwest palaeo-RTI. Red, blue and magenta dashed lines show the present CIR restored to its location at the times of C5Cn.1, C13ny and C18n.2o, respectively, with Table 2 half-rotations corrected for India–Capricorn motion for C5Cn.1 to the present (see text). For reference, the open squares locate the flow line at the time of C20n.1n (42.3 Ma). Rapid CW rotation of the palaeoslip direction at 42–40 Ma (Fig. 13) introduced extension across the then NNE-to-NE-trending fracture zones. Areas of thinned crust bounded by the fracture zone flow-line pairs are evident in the gravity field (Fig. 5), consistent with the predicted extension. The long-offset Vema FZ developed four apparent intratransform segments, whose azimuths are well predicted by small circles (black dashed lines) around the Somalia-side C18-to-C13 stage pole from Table 3.

patterns emerge from the comparison. The estimated changes in India–Somalia and Capricorn–Somalia occur simultaneously and include rapid declines from 52 to 46 Ma, brief recoveries from 43 to 39 Ma, steady or slow increases from 39 to 19 Ma, 25 per cent slow-downs from 19 to ∼15 Ma and steady motion since 14 Ma. Both also record rapid clockwise rotations of their plate slip directions from 44 to 40 Ma, slow anticlockwise rotations from ∼30 to 17 Ma and steady plate slip directions thereafter. The close agreement between

the India–Somalia and Capricorn–Somalia opening histories suggests that both of these independently derived rotation sequences are accurate and further implies that the India and Capricorn plates have moved as a single plate or have been strongly coupled since at least 52 Ma.

Along the Somalia–Antarctic Plate boundary, a rapid clockwise change of direction at ≈40 Ma and gradual anticlockwise change of the slip direction since ∼35 Ma coincided with
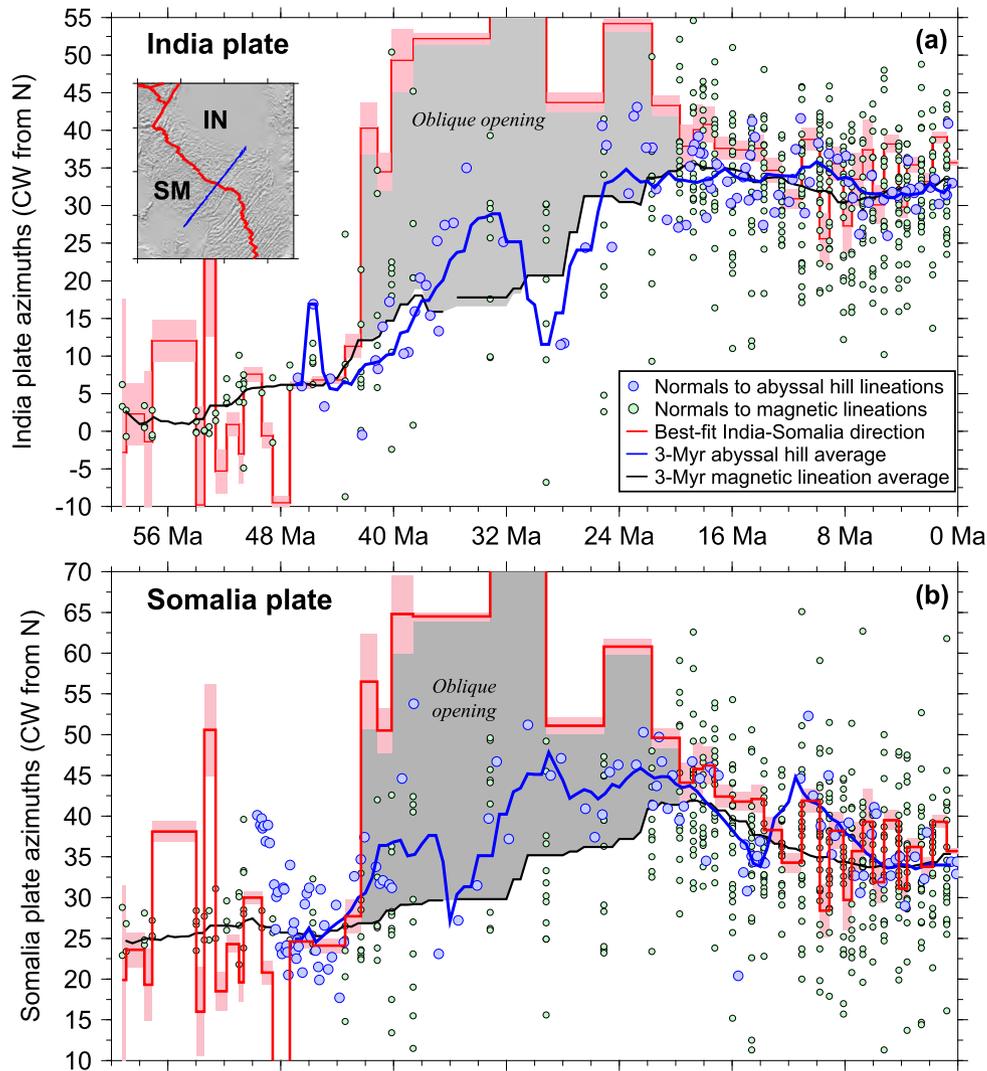
Figure 16. Azimuths predicted by India–Somalia stage rotations (red lines) compared to the normals to azimuths of reconstructed magnetic lineations (grey circles and black lines) (e.g. Fig. S3) and the normals to abyssal hill lineation azimuths (blue lines and blue circles) imaged by the multibeam track located in the inset map (blue). The abyssal hill lineation ages were estimated by comparing each lineation's distance from the ridge axis to distances estimated with the Table 2 rotations assuming symmetric spreading. The plate slip directions were estimated with angular velocities from Tables 3 and S2 for abyssal hills and magnetic lineations from the Somalia Plate (panel b) and India Plate (panel a), respectively. The period of oblique opening (grey area) coincides closely with the 38–22 Ma period of ultraslow-to-slow spreading (Fig. 13). IN, India; SM, Somalia.

similar-sense changes in India–Somalia and Capricorn–Somalia directions (Fig. 19b). In contrast, the changes in Somalia–Antarctic spreading rates are mostly anticorrelated with spreading rate changes along the other two spreading centres (Fig. 19a). Somalia–Antarctic spreading rates increased 25–50 per cent from 52 to 45 Ma, opposite the slowdowns along the other two spreading centres. From 42 to 37 Ma, Somalia-Antarctic spreading rates dropped ∼50 per cent but then recovered, similar to but opposite in sign from the 43–39 Ma spreading rate pulses along the other two spreading centres. A sustained 50 per cent slowdown of Somalia–Antarctic spreading rates from 31 Ma until 18–17 Ma coincided with sustained speedups along the other two spreading centres. Since 18 Ma, the changes in the Somalia–Antarctic spreading velocities have been uncorrelated with changes along the other two ridges.

We hypothesize that changes in the Somalia Plate's absolute motion are responsible for some and possibly all the similarities described above. We tested our hypothesis by focusing on the largest magnitude and hence most robustly determined change, namely the

anticorrelated spreading rate changes from ∼33 to 18 Ma. Specifically, given angular velocities $\omega_{t_4 \to t_3}^{IN \to SM}$ and $\omega_{t_2 \to t_1}^{IN \to SM}$ that describe the motions of the India Plate relative to Somalia for the intervals t_4 to t_3 and t_2 to t_1, the angular velocity that specifies the net change in India–Somalia motion from time t_3 to t_2 $\Delta\omega_{t_3 \to t_2}^{IN \to SM}$ is given by $\omega_{t_4 \to t_3}^{IN \to SM} - \omega_{t_2 \to t_1}^{IN \to SM}$. This angular velocity of change $\Delta\omega_{t_3 \to t_2}^{IN \to SM}$ is easily related to the changes in the absolute motions of the India and Somalia plates during the same period as follows:

$$\Delta\omega_{t_3 \to t_2}^{IN \to SM} = \Delta\omega_{t_3 \to t_2}^{IN \to HS} - \Delta\omega_{t_3 \to t_2}^{SM \to HS}, \tag{1}$$

where 'HS' indicates a hotspot/mantle frame of reference. Similar equations apply for the changes in the Antarctic–Somalia and Capricorn–Somalia Plate motions from times t_3 to t_2, namely,

$$\Delta\omega_{t_3 \to t_2}^{AN \to SM} = \Delta\omega_{t_3 \to t_2}^{AN \to HS} - \Delta\omega_{t_3 \to t_2}^{SM \to HS} \tag{2}$$

$$\Delta\omega_{t_3 \to t_2}^{CP \to SM} = \Delta\omega_{t_3 \to t_2}^{CP \to HS} - \Delta\omega_{t_3 \to t_2}^{SM \to HS}. \tag{3}$$
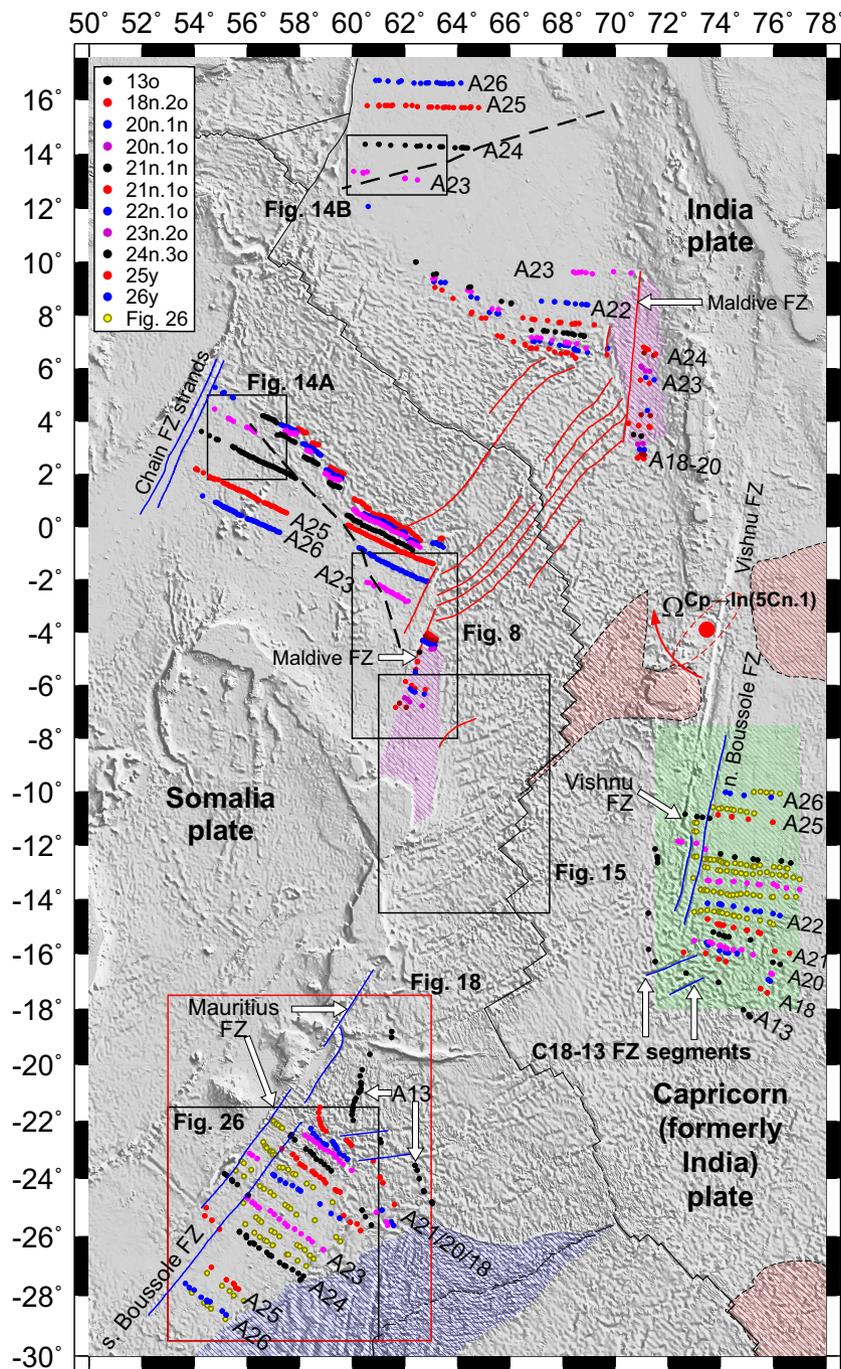
Figure 17. Magnetic anomalies 13o to 26 from this study, Cande *et al.* (2010), Eagles & Hoang (2014), Cande & Patriat (2015) and Yahteesh *et al.* (2019) that are reconstructed in Figs 8, 18 and 26. The red flow lines identify the fracture zones that constrain the Table 2 India–Somalia rotations. The blue flow lines identify C26-to-C20 fracture zones that are used to test for deformation within the India and/or Somalia plates before ∼20 Ma. The red circle and arrow identify the pole and sense of rotation that restores all motion of the Capricorn Plate relative to India (Bull *et al.* 2010) assuming that the motion began at ∼16 Ma (C5Cn.1). The red and blue patterned regions, respectively approximate the diffuse Capricorn Plate boundaries and region of seafloor created along the Southwest Indian Ridge. The data within the purple- and green-shaded regions on the Capricorn and India plates are rotated onto the Somalia Plate in Figs 8 and 18, respectively. The grid shows seafloor bathymetry.

Eqs (1)–(3) relate the net angular velocity changes for three plate pairs to the net angular velocity changes in the absolute motions of all three plates from time t_3 to t_2. If the only constraints/observations are the three angular velocities of change in the relative plate motions, then the equations are underdetermined with respect to solving for the angular velocity of change in the Somalia Plate's absolute motion. Solving uniquely for $\Delta\omega_{t_3 \to t_2}^{SM \to HS}$ either requires additional

information about the changes in the absolute motions of one or more of the Antarctic, Capricorn or India Plate or other simplifying assumptions.

We approximated $\omega_{t_4 \to t_3}^{IN \to SM}$ and $\omega_{t_2 \to t_1}^{IN \to SM}$ using stage angular velocities that span C18n.1y to C13y (38.4–33.2 Ma) and C6ny to C5AC (18.6–13.7 Ma), respectively. These angular velocities approximate India–Somalia Plate motions immediately before 33
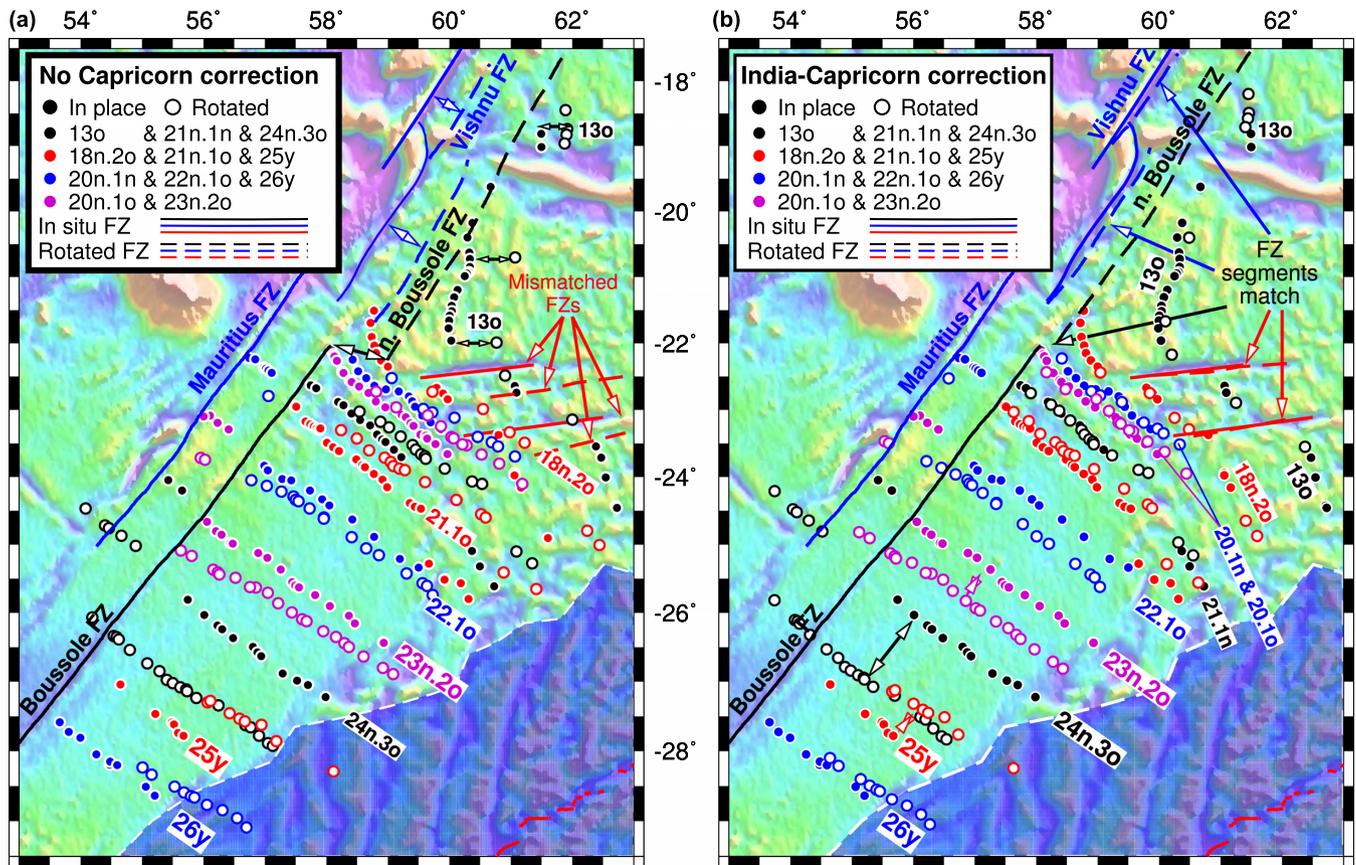
Figure 18. Reconstructions of C13–C26 reversal crossings and fracture zone segments without (panel a) and with (panel b) a correction for the rotation of the Capricorn Plate relative to India. In (a), all the rotated reversal crossings (open circles) are reconstructed onto the Somalia Plate from their locations east of the Central Indian Ridge (Fig. 17) using the Table 2 $\hat{A}^{India \rightarrow Somalia}$ rotations. The same points are rotated in panel (b) using $\hat{A}^{India \rightarrow Somalia} \hat{A}^{Capricorn \rightarrow India}$, where the latter rotation accounts for all Capricorn–India Plate motion since the postulated initiation of movement between the two plates at the time of Chron 5Cn.1 (16 Ma) (Bull *et al.* 2010). The Table 2 C13ny rotation angle was increased by the ratio of the C13o to C13ny reversal ages in order to rotate the C13o crossings in both panels. Rotated and in-place fracture zone segments are shown with dashed and solid lines, respectively. In both panels, segments of the Vishnu and Boussole fracture zones from the Capricorn Plate (dashed lines) have been restored to their positions at the time of Chron 20n.1o and two fracture zone segments of approximate age C18-to-C13 (red dashed lines oriented ∼E–W) have been rotated from their Capricorn Plate locations shown in Fig. 17 to their positions at the time of Chron 13. The grids show seafloor gravity (Fig. 5).

Ma and after 19 Ma and span long enough time intervals to average down the noise. Differencing these two angular velocities yields an India–Somalia differential angular velocity $\Delta \omega_{t_3 \rightarrow t_2}^{IN \rightarrow SM}$ that spans 33.2–18.6 Ma, the desired interval. We similarly estimated Capricorn–Somalia and Antarctic–Somalia angular velocities for the periods immediately before ∼31 Ma and after ∼19 Ma and determined the differential angular velocities $\Delta \omega_{t_3 \rightarrow t_2}^{CP \rightarrow SM}$ and $\Delta \omega_{t_3 \rightarrow t_2}^{AN \rightarrow SM}$. These span respective intervals of 33.7–18.0 Ma (C13no–C5E) and 31.0–18.0 Ma (C12no–C5E) for the Capricorn–Somalia and Antarctic–Somalia Plate pairs. Section 3 of the Supporting Information documents these and other calculations that are related to the material below.

If the absolute motions of the Antarctic, Capricorn and India plates changed little or not at all from 33 to Ma (i.e. the first terms on the right-hand sides of eqs 1–3 were zero or nearly zero), then the differential angular velocities for all three plate pairs would independently give the angular velocity of change for the Somalia Plate's absolute motion. Interestingly, the poles for all three differential angular velocities are located directly east of the Somalia Plate (Fig. 20a) and therefore predict that the velocity of the Somalia Plate increased in a dominantly southward direction between 31 and 18 Ma relative to each of the Antarctic, Capricorn and India

plates (Fig. 20b). The 10–25 mm yr^{-1} magnitudes of the estimated velocity changes (Fig. 20b) agree with the spreading rate changes that are illustrated in Fig. 19. The directions and rates of the 31–18 Ma velocity changes for all three plate pairs are encouragingly consistent given that they are derived from independent sets of plate kinematic data.

The similarities of the 31–18 Ma changes in the relative motions for all three plate pairs suggest a common underlying cause, namely a 31-to-18 Ma change in the absolute motion of the Somalia Plate. We tested this possibility by deriving $\Delta \omega_{31 \rightarrow 18Ma}^{SM \rightarrow HS}$ from Africa Plate absolute motion rotations from Table S2 of Maher *et al.* (2015), which Maher *et al.* determined from seamount ages and the tracks of three hot spot trails in the Atlantic Basin beneath the present Nubia Plate and one below the present Somalia Plate (the Reunion hot spot trail). The details of our calculations of $\Delta \omega_{31 \rightarrow 18Ma}^{SM \rightarrow HS}$ are found in Section 3 of the Supporting Information.

Along the Carlsberg Ridge between India and Somalia, $\Delta \omega_{31 \rightarrow 18Ma}^{SM \rightarrow HS}$ predicts that the Somalia Plate's absolute motion changed at right angles to the direction of seafloor spreading from 31 to 18 Ma (black arrows in Fig. 20c), in disagreement with our evidence for a 20–25 mm yr^{-1} spreading rate speedup between ∼33
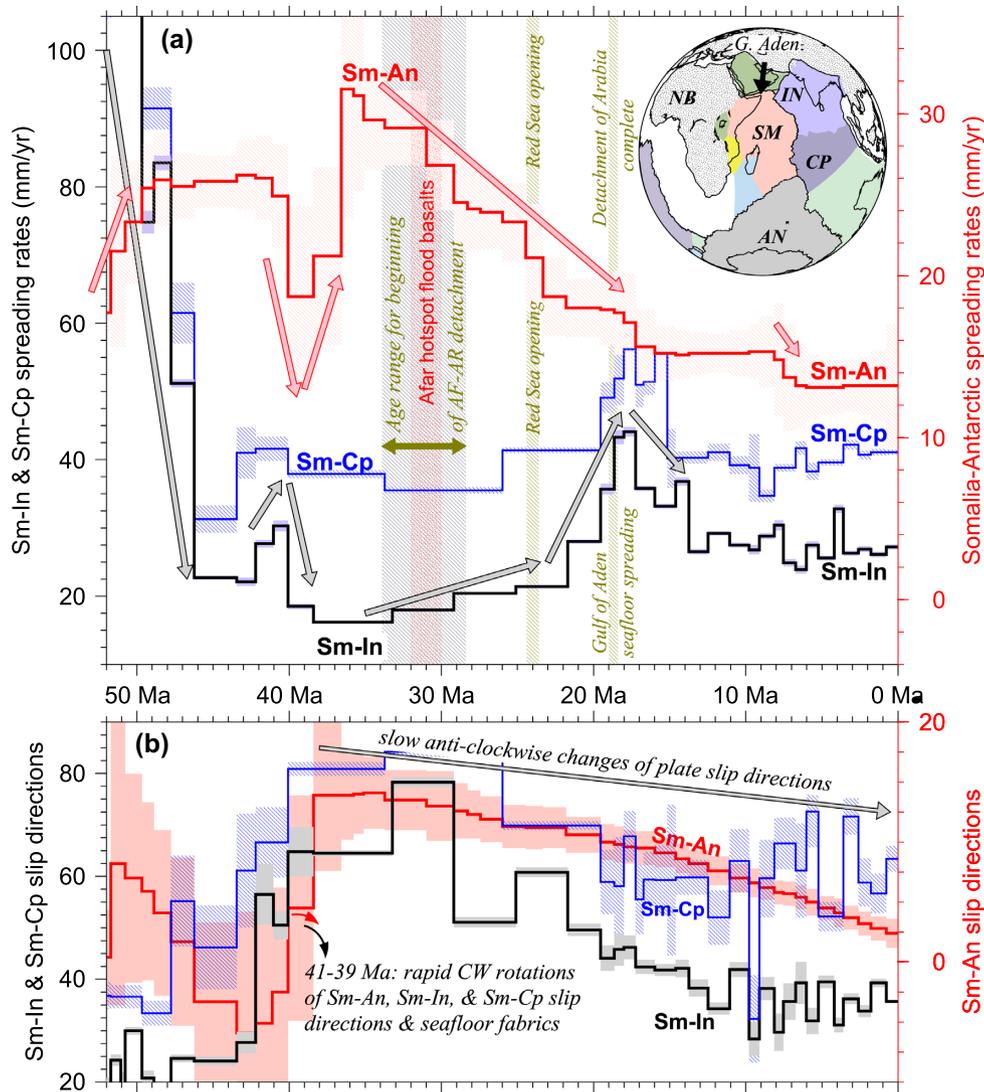
Figure 19. Somalia–Antarctic (Sm-An), Somalia-India (Sm-In) and Somalia–Capricorn (Sm-Cp) seafloor spreading rates (A) and slip directions (b) since 52 Ma. All rates are normalized to reversal ages from GTS20. Velocities are for Somalia Plate flow lines that originate at central locations along the Sm-An, Sm-In and Sm-Cp Plate boundaries. The Sm-In velocities are estimated from angular velocities in Table 3. Angular velocities from table 10 of DeMets *et al.* (2021) and table 2 of Cande & Patriat (2015) are used to estimate the Sm-An velocities for 51.7 Ma to the present and before 51.7 Ma, respectively. The Sm-Cp velocities are estimated with angular velocities derived from finite rotations in Table S4 . The red and grey arrows in (a) highlight significant spreading rate changes. Different vertical axes apply for Sm-An rates (right-hand side) and Sm-In and Sm-Cp rates (left-hand side). The vertical shaded bars denote major events associated with the Arabia Peninsula detachment from Africa, namely the eruption of the Afar hotspot flood basalts at 31 Ma (Hofmann *et al.* 1997), the earliest continental extension bordering the Gulf of Aden (Bosworth *et al.* 2005) and a widespread tectonomagmatic pulse associated with the opening of the Red Sea (Bosworth *et al.* 2005).

Ma and 18 Ma (Fig. 19a). At the same location, $\Delta\omega^{SM\rightarrow HS}_{31\rightarrow 18Ma}$ predicts a ∼50° anticlockwise rotation of Somalia Plate motion over the mantle during this period. The anticlockwise change is consistent with the sense of the observed change in the India–Somalia slip direction from 33 to 18 Ma but is a factor of two larger (Fig. 19b).

Along the Central Indian Ridge, $\Delta\omega^{SM\rightarrow HS}_{31\rightarrow 18Ma}$ also predicts a velocity change that is orthogonal to the Capricorn–Somalia spreading direction (Fig. 20c), in disagreement with the observed ≈15 mm yr^{-1} spreading rate speedup (Fig. 19a). $\Delta\omega^{SM\rightarrow HS}_{31\rightarrow 18Ma}$ correctly predicts the sense and magnitude of the observed ∼25–30° anticlockwise rotation of the Capricorn–Somalia slip direction during this period (Fig. 19b).

Along the Southwest Indian Ridge, $\Delta\omega^{SM\rightarrow HS}_{31\rightarrow 18Ma}$ predicts a SSE-directed velocity change that includes a 13 mm yr^{-1} southward

component parallel to the direction of seafloor spreading (Fig. 20c). The Maher *et al.* (2015) rotations correctly predict that eastern Southwest Indian Ridge spreading rates slowed down from 31 to 18 Ma and closely match the observed 14 mm yr^{-1} slowdown magnitude (Fig. 19a). $\Delta\omega^{SM\rightarrow HS}_{31\rightarrow 18Ma}$ predicts that Somalia–Antarctic slip directions rotated clockwise from 31 to 18 Ma, opposite that observed (Fig. 19b).

Given the consistency of the 31–18 Ma velocity changes that we estimate for the India–Somalia, Capricorn–Somalia and Antarctic–Somalia Plate pairs (Fig. 20b), it seems unlikely that errors in the well-constrained relative plate motion rotations are the cause of the disagreements with the 31–18 Ma velocity changes that are based on the Maher *et al.* (2015) Somalia-hotspot rotations. Instead, some combination of errors in the Maher *et al.*
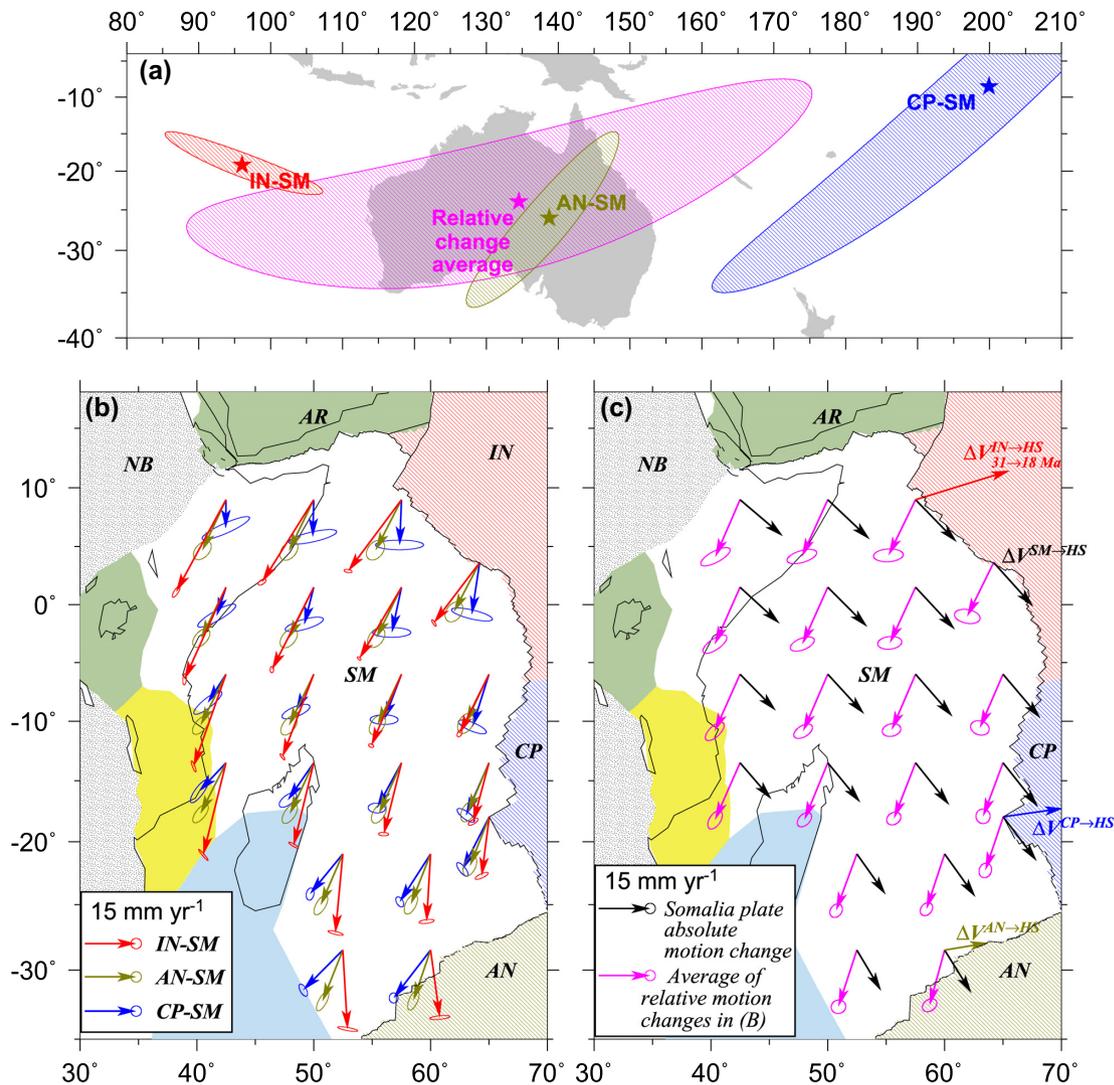
Figure 20. Kinematic evidence for a ∼15 mm yr⁻¹ speedup of the Somalia Plate's absolute motion toward the S–SSW between ∼31 and 18 Ma, which spans the ∼33–31 Ma onset of slow continental extension in the proto-Gulf of Aden and initiation at 18 ± 1 Ma of full seafloor spreading in the Gulf of Aden. Panel (a) shows three ∼31-to-18-Ma poles estimated from Antarctic–Somalia (AN-SM), India–Somalia (IN-SM) and Capricorn–Somalia (CP-SM) rotations and the average pole for the three plate pairs (purple). A 33-to-18-Ma absolute motion change pole we estimated from Maher *et al.* (2015) Table S2 rotations that reconstruct Africa Plate hotspot tracks is located south of the map at 38°S, 347°E. Panel (b) shows ∼31-to-18-Ma changes in the velocity of the Somalia Plate relative to the adjacent IN, CP and AN plates estimated using methods described in the text. Panel (c) compares the ∼33-to-18-Ma Somalia absolute velocity change estimated with Maher *et al.* (2015) rotations to the three-plate relative average change (see text) and plate-specific absolute motion changes (see text) at selected near-ridge locations (ΔV labels are colour coded per the panel b legend). All ellipses show the 2-D 1σ uncertainties propagated from the angular velocity covariances. The colour coding remains consistent through all three figure panels. Other abbreviations: AR, Arabia; HS, hotspot; NB, Nubia.

(2015) absolute motion rotations and changes in the absolute motions of the Antarctic, Capricorn and/or India plates between 31 and 18 Ma may be responsible. We consider both possibilities below.

One source of uncertainty in the Maher *et al.* (2015) Africa-hot spot rotations is their absence of any constraints from Reunion hotspot seamount ages with dates between 31.5 and 7.5 Ma, the period when our rotations suggest a significant slowdown in the Somalia Plate's absolute motion. Future age dates of Reunion hot spot seamounts in this age range would permit a strong test of a possible link between the spreading rate changes and a change in Somalia Plate absolute motion. A second likely source of error in the Maher *et al.* (2015) rotations is their approximation of Africa as a single plate rather than as distinct Nubia and Somalia plates.

Rotations that are derived solely from hotspot data from the Somalia Plate are clearly needed.

As is clear from eqs (1) to (3), any changes in the absolute motions of the Antarctic, Capricorn and/or India plates between 31 and 18 Ma would also account for some of the differences between the 31 and 18 Ma relative motion and absolute motion velocity changes that are depicted in Fig. 20(c). The dark green, blue and red velocity arrows in Fig. 20(c), which were estimated by subtracting the average of the relative motion changes that are shown in Fig. 20(b) from the Somalia Plate absolute motion changes estimated with $\Delta\omega^{SM \to HS}_{31 \to 18Ma}$, show the Antarctic, Capricorn and India Plate absolute velocity changes that would be necessary to resolve the mismatches. For all three plates, eastward increases in the plate motions relative to the mantle from 31 to 18 Ma are indicated, including 12, 17 and

27 mm yr^{-1} changes in the respective absolute velocities of the Antarctic, Capricorn and India plates near the midpoints of their respective boundaries with India.

Given that the IndoCapricorn Plate's motion relative to the mantle before ≈30 Ma was dominantly northward (O'Neill *et al.* 2003), any increase in the plate's east-directed component of absolute motion after 30 Ma would have caused a clockwise change in the direction of the IndoCapricorn Plate's movement relative to the mantle. Some evidence supports such a change. On the southern India/Capricorn Plate, the features that are mostly likely to approximate the plate's direction relative to the mantle since ∼20 Ma are the NE–SW-trending Amsterdam-Saint Paul Plateau and the similarly trending Chain of the Dead Poets >10-Myr-old seamount chain between the Plateau and southern Ninetyeast Ridge (Janin *et al.* 2011; Maia *et al.* 2011). The approximate northeast-to-southwest alignment of both features is 30° or more clockwise from the IndoCapricorn Plate's north-dominated direction of absolute motion before 40 Ma (O'Neill *et al.* 2003). This agrees with our inference of a post-30-Ma clockwise shift in the direction of the IndoCapricorn Plate's absolute motion. Due to the Antarctic Plate's near fixity over the mantle, we are unaware of any Antarctic Plate hot spot track that can be used to test for a post-30-Myr change in the plate's absolute motion.

5.2 Comparisons to previous results

We next compare our new results to previous results, with an emphasis on the differences and similarities in the fracture zone flow lines and seafloor opening rates estimated with our own and previous rotations. Our new and previous India–Somalia poles are compared in Section S4 of the Supporting Information.

5.2.1 Fracture zone flow lines

Spanning the past 43.4 Ma (Chron 20 to the present), India-Somalia flow lines that we estimated with rotations from Seton *et al.* (2012) deviate from the observed and our estimated fracture zone traces by up to 50 km (Fig. 9). The largest differences in the reconstructed flow lines occur for portions of the flow lines with ages older than ≈20 Ma (Chron 6), which we attribute to likely differences in our respective interpretations of fracture zone traces for seafloor older than 20 Ma.

For times before 43.4 Ma, the flow lines that we estimated with the new and previous India–Somalia rotations differ widely (Figs 10 and 21). At the western end of the Carlsberg Ridge, the flow lines we estimated with previous rotations deviate from the two Chain fracture zone strands by up to ≈250 km (Fig. 21a). None of the flow lines, including our own, closely match the Chain fracture zone strands (Fig. 21a), although the flow line estimated with the Cande & Patriat (2015) rotations always lies within 50 km of the fracture zone. The flow line we estimated from the Seton *et al.* (2012) C20-to-C26 rotations (red dashed line in Fig. 21a) follows the trajectory of the nearby Chain Ridge instead of the Chain fracture zone, possibly indicating a different flow line choice by those authors.

Along the Rudra and Maldive fracture zones at the eastern end of the Carlsberg Ridge, the C20-to-C26 flow lines that we estimated with previously published rotations also deviate significantly from the interpreted fracture zone traces (Figs 21b and d). The flow line estimated with the Cande & Patriat (2015) rotations once again matches the fracture zones more closely than any previous rotations.

A flow line comparison for the Boussole Fracture Zone west of the southern Central Indian Ridge (located in Fig. 17) is instructive. The Yatheesh *et al.* (2019) rotations, which were estimated from data that included the Boussole fracture zone, fit this fracture zone well (Fig. 21c), as might be expected. In contrast, the flow line estimated with our Table 2 rotations fits the fracture zone poorly and exhibits sudden deviations. These deviations, which are an artefact of sudden stage pole shifts whose effects are amplified at large distances from the pole, are due to significant fitting tradeoffs in our inversion between the magnetic reversal and fracture zone crossings. Applying smoothing during the data inversion to better optimize the data versus model variance tradeoff is warranted.

None of the rotation sequences, including our own, closely matches all the fracture zones in our comparison. The best over-all flow line fit is for the rotations from Cande & Patriat (2015) rotations (blue dashed lines in Fig. 21), for which the flow lines rarely deviate by more than 50 km from their corresponding fracture zones. The good fit of the Cande & Patriat rotations is surprising given that no data from the Carlsberg or Central Indian ridges were used to estimate their rotations, which they instead estimated by summing India–Antarctic and Antarctic–Africa rotations that best fit data from Southeast Indian and Southwest Indian ridges. We interpret their good fits as strong evidence that the accuracies of C26-to-C20 Africa–India rotations are significantly improved by enforcing closure of the Africa–India–Antarctic Plate circuit during inversions of data from this three plate circuit.

5.2.2 Spreading rates and directions

Spanning the past 20 Myr, seafloor spreading rates and directions that were estimated from our previous high resolution reconstructions of many of the same Carlsberg Ridge data (Merkouriev & DeMets 2006; DeMets *et al.* 2020) differ insignificantly from those estimated herein. In contrast, seafloor spreading rates and directions estimated with India-Somalia rotations from Seton *et al.* (2012) differ significantly from those estimated with our higher resolution rotations (Fig. 13) and clearly undersample the post-20-Ma kinematics of this plate pair.

For the period from 60 to 42 Ma (C26 to C20), the only two previous studies that have estimated India-Somalia rotations solely from Carlsberg Ridge magnetic lineations are those of Royer *et al.* (2002) and Eagles & Hoang (2014). From their finite rotations, we estimated angular velocities and then spreading rates and directions along a western Carlsberg Ridge flow line, where the velocities are the best constrained by the data (Fig. 22). For completeness, we also include spreading rates from Chaubey *et al.* (2002) (green line in Fig. 22a), who used a manual procedure to estimate Carlsberg Ridge spreading rates at a resolution equal to ours. In order to facilitate the comparison of our and previous results, all the spreading rates are normalized to GTS20 reversal ages and we estimated angular velocities from our closely spaced rotations that span the same intervals as in the Royer *et al.* (2002) and Eagles & Hoang (2014) studies.

To first order the spreading rates estimated for the different studies all define the dramatic spreading rate slowdown between 52 and 45 Ma. The 53.5–52.8 Ma spreading rate pulse that is defined by our rotations (Sections 4.2.2 and 4.3.1) also appears in the Chaubey *et al.* (2002) and Royer *et al.* (2002) spreading histories, albeit with lower peak rates than ours (Fig. 22a). Our rotations and the rates estimated by Chaubey *et al.* (2002) both indicate that the post-52-Ma spreading rate slowdown concluded at 46 Ma, ≈1.5 Myr later than the time
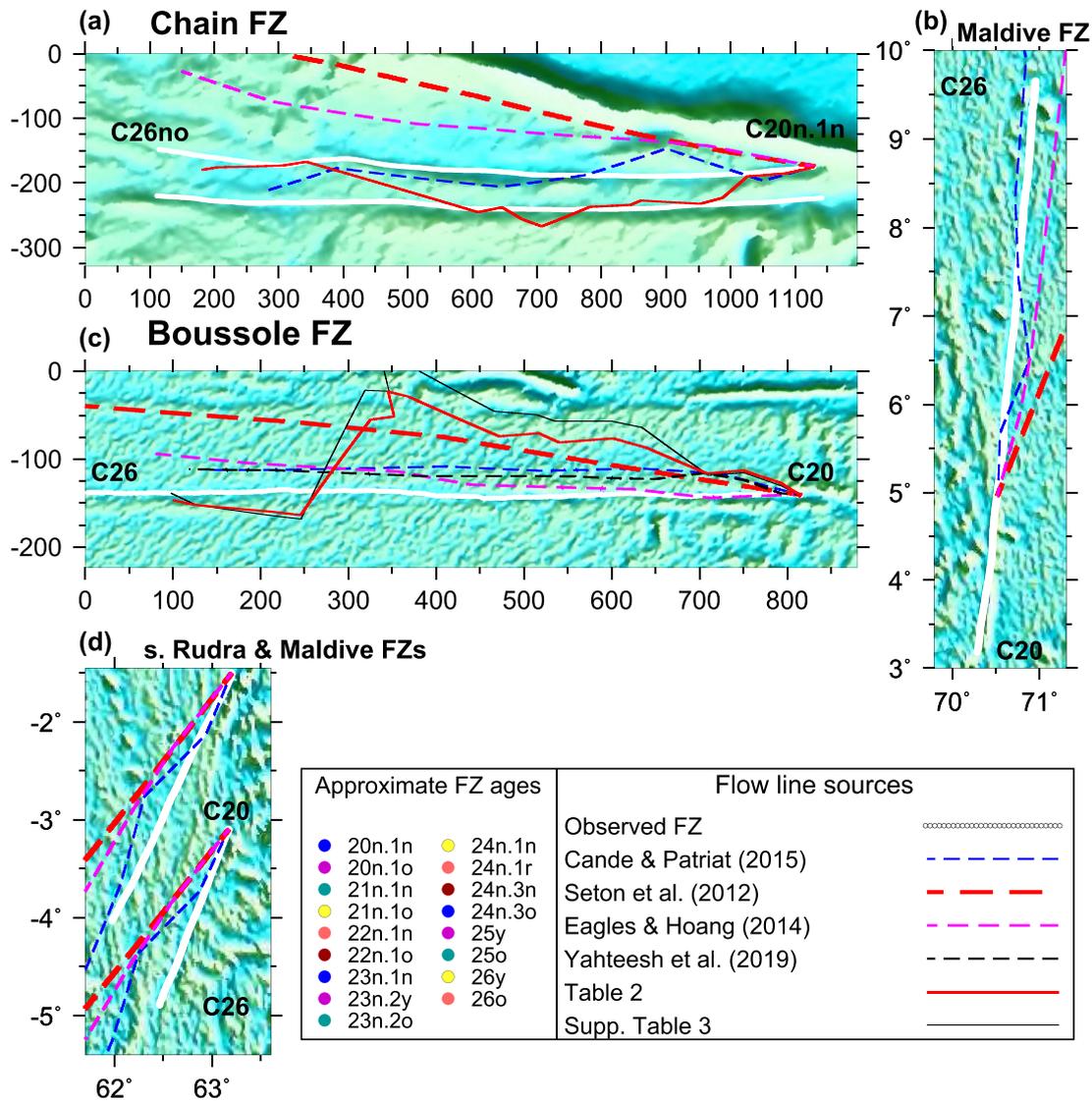
Figure 21. Fracture zone (FZ) flow lines estimated from sources given in the legend for C20n.1n (42.3 Ma) to C26no (59.2 Ma), as follows: (a) Chain FZ strands. (b) Maldive FZ on the India Plate. (c) Boussole FZ on the Somalia Plate. The red and black flow lines are predicted by our Table 2 rotations and rotations in Table S3, respectively. (d) Maldive and Rudra FZs on the Somalia Plate. Fits of our Table 2 rotations to the Chain, Rudra and Maldive fracture zones are displayed in Fig. 10. A flow line estimated with the Capricorn-Somalia rotations of Yahteesh *et al.* (2019) is shown only for Boussole FZ. Panels (a) and (c) are oblique Mercator projections that are, respectively, centred on the C5n.2 India–Somalia pole and on a pole orthogonal to the Boussole FZ. The axes in (a) and (c) are in units of kilometres. The fracture zones are labelled and located in Figs 4, 5(a) and 17. The grids show seafloor gravity (Fig. 5).

indicated by the Eagles & Hoang (2014) rotations (Fig. 22a), but ≈2 Myr earlier than the time indicated by the Seton *et al.* (2012) rotations (Fig. 13a). The Carlsberg Ridge thus transitioned to much slower spreading rates several Myr before the reconfiguration of the palaeospreading centre at ~42 Ma (C20). The rapid clockwise rotation of the India–Somalia slip direction after 42 Ma (Fig. 22b) may instead have triggered the plate boundary reconfiguration.

5.3 India–Eurasia implications: updated plate velocities and Tibetan deformation pulses

Reconstructing India–Eurasia Plate motion is challenging due to the random errors that accumulate around the extended plate circuit that links the two plates (inset to Fig. 24) and temporal artefacts that may be introduced via interpolations between rotations that reconstruct plate motions at significantly different times. Fortunately, rotations

that are spaced at ~1-Myr intervals are now available for 20 Ma to the present for all the plate pairs in the global circuit, nearly obviating the need for rotation interpolations during this period (DeMets *et al.* 2020). For times earlier than 20 Ma, closely spaced rotations are now available for the India–Somalia, Somalia–Antarctic and Antarctic–Nubia Plate pairs for most of the past 60 Myr, although some rotations for the Nubia–North America and Eurasia–North America Plate pairs are still spaced by intervals as long as 14 Myr (Fig. S9).

We estimated updated India–Eurasia rotations back to 60 Ma (Table 4) from the India–Somalia rotations in Table 2 and other published rotations whose sources are given in the Table 4 footnotes and Fig. S9. Each plate circuit rotation that is used in this part of the analysis satisfies the criteria that its data, fits, and covariances are provided in its originating study.
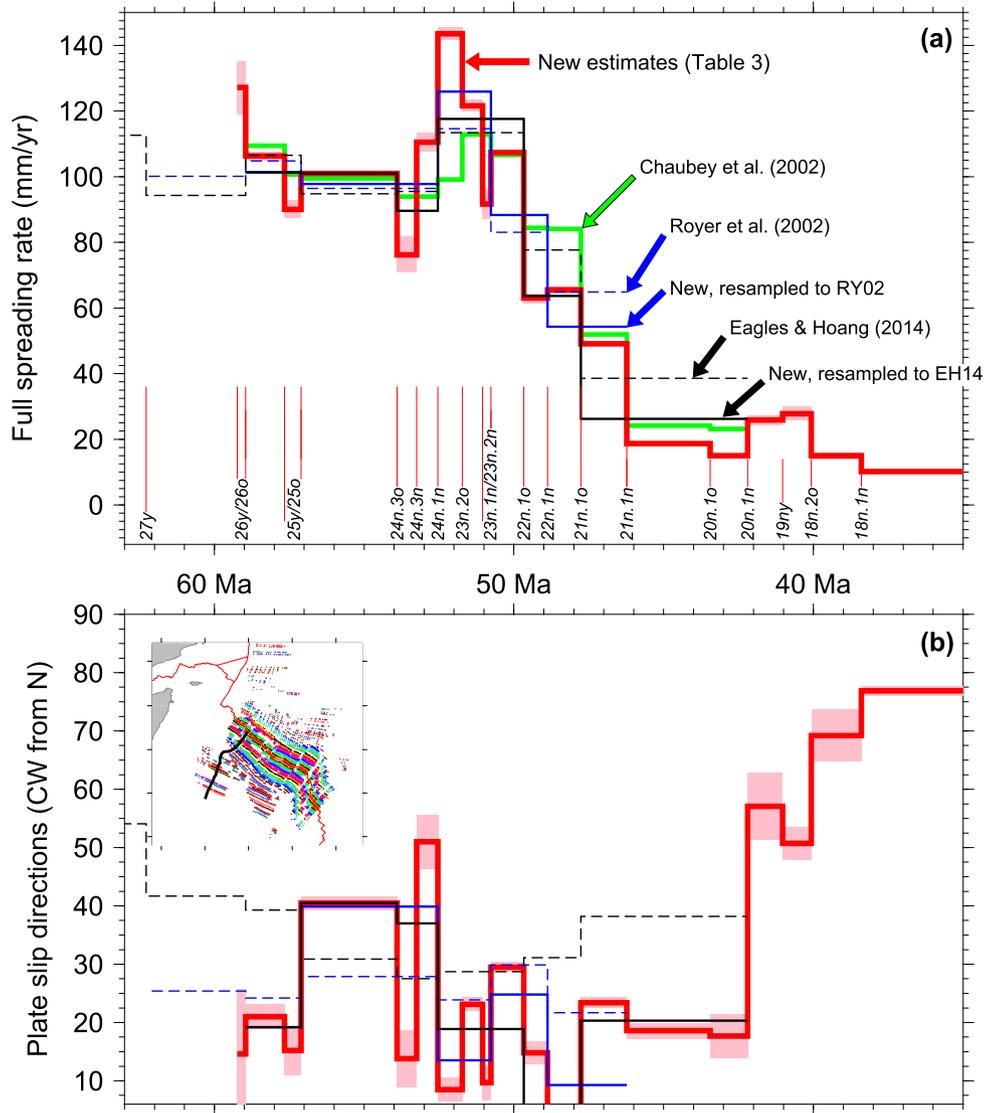
Figure 22. Comparison of India-relative-to-Somalia stage rates (a) and directions (b) estimated along a Somalia Plate flow line that traverses the midpoint of the well-defined Anomaly 26 through A18 sequence that flanks the northwestern third of the Carlsberg Ridge (black line in the inset map). The plate velocities were estimated as follows: (1) Table 3 angular velocities (bold red line). (2) Angular velocities based on Royer *et al.* (2002) C27-to-C21 finite rotations (blue dashed line). (3) Manually-derived rates (green line) from Chaubey *et al.* (2002). (4) Angular velocities based on Eagles & Hoang (2014) C26-to-C20 finite rotations (black dashed line). (5) Angular velocities that sample our Table 2 finite rotations using the same intervals as for Royer *et al.* (2002) rotations (blue line labeled RY02). (6) The same as (5), but using sampling intervals that match those for the Eagles & Hoang (2014) rotations (black line labeled EH14). All the rates were calculated using GTS2020 reversal age estimates unless otherwise noted.

For each plate pair in the global circuit, we first sampled its rotation sequence onto the same 45 ages that are represented in our Table 2 India–Somalia rotations. Fig. S9 graphically displays any interpolations that were needed for each plate pair. We estimated new India-Eurasia finite rotations from the uniformly sampled plate circuit rotation sequences as follows:

$$\hat{A}_{IN\to EU} = (\hat{A}_{NA\to EU})(\hat{A}_{NB\to NA})(\hat{A}_{AN\to NB})$$
$$\times (\hat{A}_{SM\to AN})(\hat{A}_{IN\to SM}), \qquad (4)$$

where for example the rotation $\hat{A}_{IN\to SM}$ moves the India Plate onto the Somalia Plate. Covariances for each India–Eurasia rotation (Table 4) were estimated by propagating the covariances for the individual plate circuit rotations via eq. (2) of DeMets *et al.* (2020). The plate circuit in (4) explicitly accounts for the movement between Nubia and Somalia (e.g. $\hat{A}_{AN\to NB}$ $\hat{A}_{SM\to AN}$). The net displacement

between Nubia and Somalia since 60 Ma is small (<10 per cent) compared to the net displacements for the other three plate pairs. Consequently, changes in India–Eurasia relative motion will mostly reflect changes in the relative motions for the other three faster moving plate pairs.

In order to reconstruct the India–Eurasia convergence velocity history, we estimated India–Eurasia angular velocities (Table S5) from the new India–Eurasia finite rotations. Due to reversal age uncertainties and the rotation errors that accumulate around the global circuit, the uncertainties in the India–Eurasia angular velocities can be large. We averaged down the noise by estimating angular velocities that span time intervals of at least 0.6 Myr (Table S5). This occasionally required us to overlap the time windows that are spanned by some of the angular velocities. Consequently, the stage velocity history presented below is inherently smoothed. Notably,

Table 4. India–Eurasia finite rotations and covariances.

Chron	Age	Lat.	Long.	Ω	Covariances					
	(Myr)	(°N)	(°E)	(°)	a	b	c	d	e	f
					Best-fitting					
1n	0.773	27.24	22.25	−0.376	10.3	−2.9	7.3	10.7	−6.7	9.3
2n	1.775	28.80	23.53	−0.858	12.0	−3.7	8.0	11.7	−7.9	10.9
2An.1	2.595	29.08	22.96	−1.250	13.8	−4.5	8.7	12.6	−9.2	12.5
2An.3	3.596	27.62	27.39	−1.863	17.0	−5.3	9.8	15.1	−11.4	15.4
3n.1	4.187	29.76	21.26	−1.996	18.9	−6.2	10.7	15.9	−13.0	17.6
3n.4	5.235	28.39	24.78	−2.576	21.2	−7.3	12.3	18.5	−15.6	21.1
3An.1	6.023	28.99	21.78	−2.809	24.5	−6.5	13.8	24.7	−17.9	24.8
3An.2	6.727	28.05	23.83	−3.190	26.6	−8.3	15.0	25.0	−20.0	27.5
4n.1	7.537	28.01	23.17	−3.504	28.5	−7.2	15.9	28.7	−19.9	28.3
4n.2	8.125	27.42	23.32	−3.821	28.7	−8.1	16.2	26.1	−19.5	27.9
4A	9.105	27.93	21.63	−4.182	29.3	−7.4	16.1	23.8	−18.1	27.9
5n.1	9.786	27.24	22.16	−4.525	32.2	−5.7	16.8	25.1	−17.9	29.4
5n.2	11.056	27.41	22.25	−5.090	37.6	−5.1	18.0	25.3	−19.7	34.9
5An.2	12.474	27.94	20.39	−5.604	45.3	−3.1	19.1	29.9	−23.8	43.2
5AC	13.739	27.21	23.20	−6.439	58.3	−2.0	24.4	38.8	−28.5	51.9
5AD	14.609	28.52	20.70	−6.701	66.4	−1.7	27.7	35.4	−26.3	50.8
5Cn.1	15.974	28.87	20.37	−7.436	73.9	−4.5	28.4	34.3	−25.3	46.5
5D	17.235	28.56	21.34	−8.314	80.9	−10.1	27.3	34.8	−28.8	46.3
5E	18.007	28.68	20.90	−8.820	88.9	−10.2	26.7	44.1	−32.6	50.3
6ny	18.636	28.14	21.47	−9.362	100.6	−9.5	31.2	57.7	−36.4	57.0
6no	19.535	27.50	20.45	−9.844	111.6	−21.1	36.7	64.5	−50.6	71.0
6AAr.2n	21.691	28.83	20.47	−10.565	258.7	−49.3	−12.1	93.4	−6.3	12.7
8n.1n	25.099	30.87	17.64	−12.496	159.2	−8.4	1.3	72.1	−21.1	32.3
11n.1n	29.183	28.79	22.75	−16.113	112.7	29.0	10.1	52.2	−28.3	46.5
13ny	33.214	30.17	22.84	−18.643	237.3	10.2	−37.0	101.1	−41.1	56.6
18n.1n	38.398	29.02	26.83	−22.336	139.6	73.4	−42.4	196.0	−59.4	106.1
18n.2o	40.073	29.21	26.71	−23.281	139.8	36.3	−64.0	118.8	−75.2	115.1
19ny	41.030	29.40	26.06	−23.851	385.1	118.3	−109.1	292.1	−84.2	115.1
20n.1n	42.196	29.67	25.25	−24.478	150.7	46.1	−81.5	122.6	−92.7	134.6
20n.1o	43.450	28.97	25.40	−25.603	164.4	56.7	−98.8	132.8	−109.4	156.6
21n.1n	46.235	26.64	24.82	−27.652	115.1	46.7	−72.8	100.4	−82.1	121.2
21n.1o	47.760	24.78	24.27	−28.714	123.6	29.1	−69.4	90.4	−68.2	107.4
22n.1n	48.878	22.52	26.02	−31.418	92.4	11.7	−34.6	79.0	−29.7	65.9
22n.1o	49.666	21.82	26.22	−32.699	73.4	−2.7	−18.5	56.9	−13.1	41.6
23n.1n	50.767	21.80	24.80	−33.853	55.5	−7.2	−5.4	45.7	3.6	21.8
23n.2y	51.047	21.32	25.24	−34.704	89.4	−8.2	−17.6	58.6	6.0	20.3
23n.2o	51.724	21.10	24.50	−35.629	55.4	−5.6	−4.4	49.2	7.1	21.4
24n.1n	52.540	19.31	26.22	−39.069	240.0	340.5	117.1	682.9	236.4	102.4
24n.1r	52.930	19.43	26.01	−39.424	268.1	381.5	126.8	745.6	279.3	120.4
24n.3n	53.250	20.31	24.33	−38.270	160.5	160.3	42.2	363.7	125.8	57.1
24n.3o	53.900	20.07	24.11	−38.698	134.9	181.1	63.1	406.5	145.3	66.7
25y	57.101	23.12	15.77	−36.907	56.1	79.6	16.2	215.5	15.9	57.0
25o	57.656	23.68	14.36	−38.813	542.5	−91.4	40.9	324.1	73.7	75.2
26y	58.959	23.06	14.33	−40.927	573.1	−25.1	32.8	445.5	85.6	91.7
26o	59.237	22.75	14.60	−41.627	611.1	24.8	95.1	542.5	219.0	147.5

Notes: These rotations reconstruct past positions of the India Plate relative to a stationary Eurasia. The rotations were determined by combining the best-fitting India–Somalia rotations in Table S1 with the following rotations: Eurasia–North America: C1n–C6no—DeMets *et al.* (2015b); C13ny, C18n.1o, C21n.1o, C22n.1o, C24n.3o, C25y and C31y—Gaina *et al.* (2002); Nubia–North America: C1n–C6no—DeMets *et al.* (2015b); C6Bn.1, C8n.1n and C13ny—Schettino & Macchiavelli (2016); C18n.1n, C21n.1n, C24n.1n, C25y and C30y—Muller *et al.* (1999); Nubia–Antarctic: C1n–C23o—DeMets *et al.* (2021); C24n.3o, C26y and C28y—Cande & Patriat (2015); Somalia-Antarctic: C1n–C23o—DeMets *et al.* (2021); C24n.3o, C26y and C28y—Cande & Patriat (2015). Fig. S9, which displays much of this same information, indicates the interpolations that were done for each plate pair in order to prepare their rotation sequences for the combination that yielded the 45 India–Eurasia rotations in this table. The rotation angles Ω are positive anticlockwise. The covariances, which have units of 10^{-8} rad^2 and are described in the caption of Table 2, quantify the uncertainties in the reconstructed India Plate positions relative to Eurasia.

the use of overlapping angular velocity time windows eliminates an important source of amplified noise in stage spreading rate histories, namely, the anticorrelated error that is introduced between two consecutive stage rates $V^{t_3 \to t_2}$ and $V^{t_2 \to t_1}$ when there is an error in the age of their intermediate shared reversal t_2.

Along a Carlsberg Ridge flow line, where India-Somalia and India-Eurasia stage velocities are the best determined due to their

proximity to the abundant Carlsberg Ridge data, India–Eurasia Plate velocities that are estimated with our new angular velocities change in tandem with our newly estimated India–Somalia Plate velocities (Fig. 23). For example, a steep decline in India–Eurasia convergence rates from 58 to 54 Ma, rapid recovery from 54 to 52 Ma, further slowdown from 52 to 47 Ma, and a smaller-magnitude speedup and slowdown from 43 to 38 Ma all mirror similar changes in
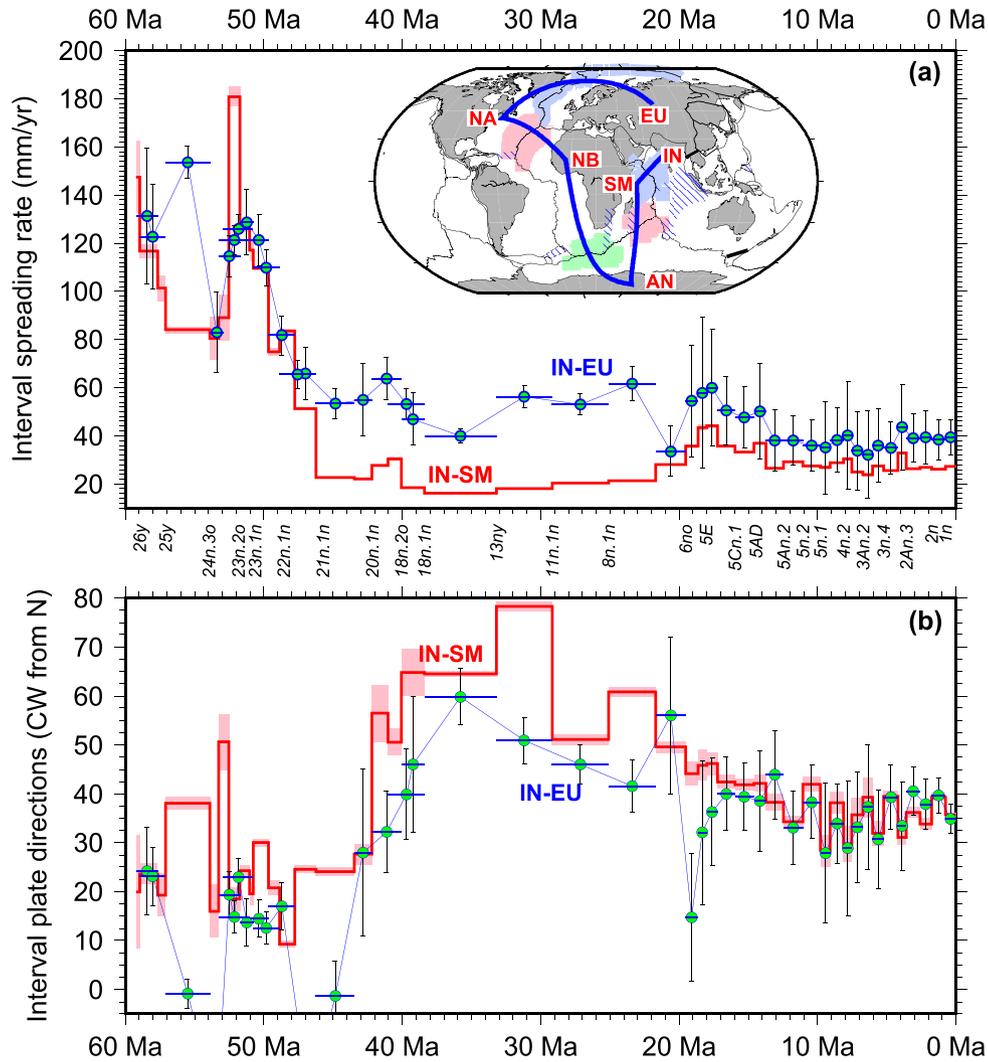
Figure 23. Post-60 Ma India relative to Eurasia (blue/green circles) and India relative to Somalia (red) stage velocities along a flow line that tracks the India Plate's southern boundary with Somalia back to 60 Ma (shown in the Fig. 13 inset map). The velocities for the two plate pairs can be compared directly since they are both determined for a common flow line. The India–Somalia stage velocities are from Fig. 13. Each India–Eurasia rate and direction (blue/green circle) is positioned at the midpoint of its associated stage interval, which is indicated by the horizontal blue line. Reversal ages are normalized to GTS20 and 1σ uncertainties are propagated from the rotation covariances. The blue lines in the inset map trace the plate circuit that we used to estimate the India-Eurasia finite rotations and stage angular velocities. The blue-, green- and pink-shaded areas identify the five plate boundaries from which plate kinematic data were used to estimate India–Eurasia Plate motion. Selected (but not all) magnetic reversals are listed to assist in interpreting the results. Plate name abbreviations are as follows: AN, Antarctic; EU, Eurasia; IN, India; NA, North America; NB, Nubia; SM, Somalia.

India–Somalia seafloor spreading rates (Fig. 23). The changes in the relative motion directions are also similar, including 30–50° clockwise rotations from 47 to 42 Ma and slow anticlockwise rotations for both plate pairs after 35 Ma (Fig. 23b).

For a flow line that originates along the Himalayan frontal thrust (Fig. 24), our new rotations reveal kinematic details that were not obvious in previous lower resolution reconstructions (Molnar & Stock 2009; van Hinsbergen *et al.* 2011; White & Lister 2012). Based on previous work, India–Eurasia convergence rates are predicted to have declined gradually after 60 Ma and remained slow since ~40 Ma (24a). Our angular velocities instead predict larger variations in the convergence rate between 60 and 45 Ma, including more rapid convergence rates from ~53 to 50 Ma and a larger magnitude slowdown in convergence rates after 50 Ma.

India–Eurasia convergence directions that are estimated with our angular velocities and based on previous work are noisy (Fig. 24b),

reflecting the often erratic changes in the reconstructed trajectories of the India Plate since 60 Ma (inset map in Fig. 24a). The reconstructed India Plate trajectory estimated by White & Lister (2012) (red line in the Fig. 24a) inset) is located more than 300 km east of the trajectories reconstructed with our Table 4 rotations and with rotations from Molnar & Stock (2009) and van Hinsbergen *et al.* (2011). The ≈N15°W recent convergence direction that is estimated by White & Lister (2012) (red line in Fig. 24b) is rotated 30° anticlockwise from and is thus highly inconsistent with the N14.5°E–N19°E directions that are estimated with our new and previous angular velocities (Fig. 24b) and with a recently estimated GPS-based angular velocity (DeMets *et al.* 2020).

For times before 20 Ma, the most robust change in the convergence directions that are predicted by our angular velocities is a 20–40° clockwise change at 50–40 Ma. This change mirrors the
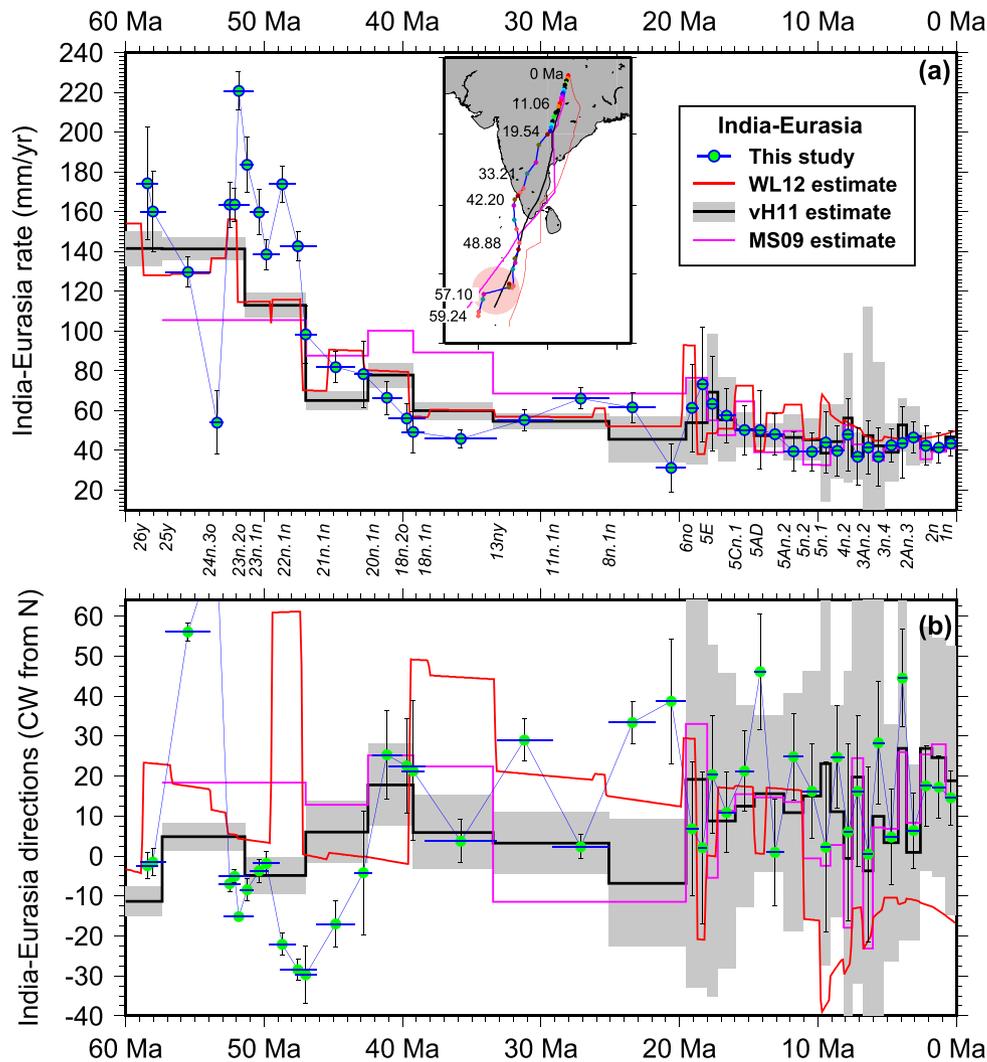
Figure 24. Post-60 Ma reconstructed India relative to Eurasia velocities and flow lines that originates at 28.0°N, 83°E. The coloured lines in the inset map are India Plate flow lines reconstructed with information from Molnar & Stock (2009), van Hinsbergen *et al.* (2011), and White & Lister (2012). The flow line depicted with the coloured circles was reconstructed with C1n–C26o India-Eurasia rotations from Table 4. The stage velocities (green/blue circles), which were calculated at the flow line origin for all stage intervals, were estimated with India-Eurasia angular velocities from Table S5 of this study. The convergence rates are normalized to GTS20 reversal ages except those from White & Lister (2012). The horizontal blue lines indicate the interval that is spanned by each stage velocity. The pink circle in the flow-line map encompasses a possible flow-line artefact that we discuss in the text. WL12, White & Lister (2012); MS09, Molnar & Stock (2009); vH11, van Hinsbergen *et al.* (2011).

clockwise rotation in India–Somalia slip directions during this period (Fig. 24b). Sudden changes at 57.1 and 53–52 Ma in the trajectory that we reconstructed with our rotations (highlighted within the large pink circle in the Fig. 24 a inset map) are artefacts of improbable sudden shifts in our India–Somalia stage poles between 57 and 52.5 Ma (Table 3). More reliable constraints from Carlsberg Ridge and/or Central Indian Ridge flow lines for times before Chron 24 might resolve this problem.

As a test, we updated evidence presented by Li *et al.* (2020) that an abrupt decline at 51 Ma in India–Asia convergence rates coincided with 52–48 Ma changes in palaeomagnetic declinations and enhanced sediment accumulation rates in the Gonjo Basin sedimentary basin of eastern central Tibet (Figs 25b and c). Fig. 25(a) shows that the 53 and 52 Ma Carlsberg Ridge spreading rate pulse estimated with our new India–Somalia angular velocities corresponded closely with a period of more rapid India–Eurasia convergence rates and with enhanced sediment accumulation rates and magnetic declination changes documented by Li *et al.* (2020). In particular, the

rapid decline in India–Somalia spreading rates from 52 to 49.5 Ma coincided closely with the period of rapid clockwise rotations in Gonjo Basin magnetic declinations (Fig. 25b). Our new reconstructions thus strengthen the apparent correlation between deformation pulses in Tibet and plate motion changes. The close agreement between the land-based measurements and offshore seafloor spreading history also suggests that changes in India–Somalia Plate motion are a useful and possibly superior proxy for India–Eurasia Plate motion changes given that the former rotations are immune to plate circuit errors and artefacts related to rotation interpolations.

5.4 Carlsberg and Central Indian Ridge data misfits: Intraplate deformation or rotation errors?

Estimates of India–Eurasia Plate motions during the past 65 Myr depend partly on whether the Africa or India Plate deformed internally before the former IndoCapricorn Plate fragmented into
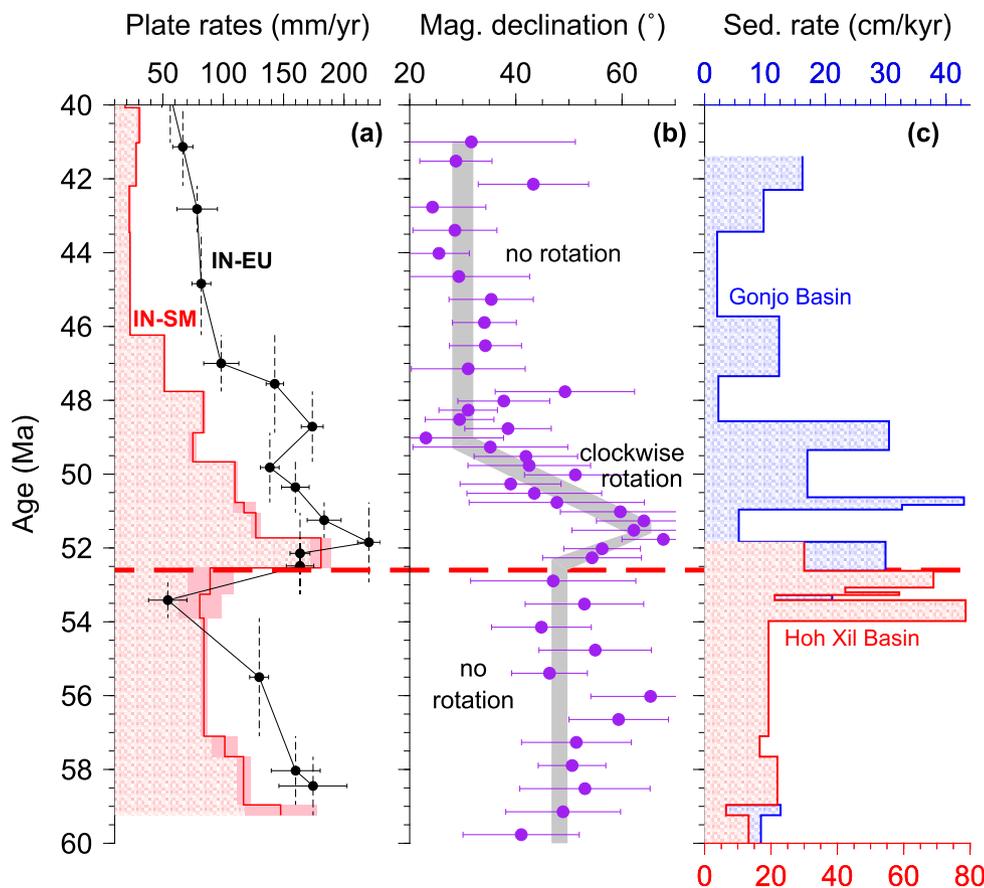
Figure 25. Update of Li *et al.* (2020) test for correlation between pulsed Tibetan deformation and India–Eurasia Plate rate changes, 60–40 Ma. (a) India–Somalia (IN-SM) seafloor spreading rates (red line) and India–Eurasia (IN-EU) convergence rates (black circles), respectively from Figs 13(a) and 24(a). (b) Gonjo Basin vertical axis rotations from Li *et al.* (2020). (c) Gonjo Basin and Hoh Xil Basin sediment accumulation rates (Li *et al.* 2020). The angular velocities that were used to compute the rates in this figure were all calibrated to reversal ages from GTS20.

separate plates at 16 Ma. If neither plate deformed before 16 Ma, then the Carlsberg Ridge and Central Indian Ridge magnetic lineations and fracture zones for a given time should be well fit by a single rotation after removing the estimated post-16-Ma movement between the Capricorn and India plates.

Previous studies are inconclusive about this topic. Cande *et al.* (2010) report that Carlsberg Ridge magnetic lineations older than Chron 23 (51 Ma) are significantly underrotated by Capricorn-Africa rotations once suitable adjustments are made for the movement between the Capricorn and India plates. Based on those misfits, they postulate that convergence may have occurred within the Somalia or India plates before C22o (49.7 Ma). More recently, Cande & Patriat (2015) estimated Capricorn-Africa rotations for C20 and older times by summing Africa–Antarctic and Antarctic–Capricorn rotations they derived from Southwest Indian Ridge and Southeast Indian Ridge data. After correcting their updated Capricorn–Somalia rotations for India–Capricorn Plate motion, they report smaller discrepancies with India–Somalia rotations from Cande *et al.* (2010) and interpret this as evidence that any deformation within the India and/or Somalia plates occurred earlier than C25y.

We revisit whether deformation within the India or Africa plates may have occurred before 16 Ma using our new India-Somalia data and reversal identifications made by Yahteesh *et al.* (2019) for their analysis of C20 and older magnetic lineations from the southern Central Indian Ridge. Specifically, we tested in two stages whether

the Carlsberg Ridge magnetic lineations for C20 to C26 are consistent with the C20-C26 magnetic lineations along the Central Indian Ridge after correcting for the post-16 Ma movement between the Capricorn and India plates. For the test, we use crossings of C20n.1n through C26o that are described in Section 2.2 and displayed in Fig. 17. These numerous data strongly constrain C20 to C26 plate motions along the Africa-IndoCapricorn palaeospreading centre. Preceding each of the tests that are described below, we restored the C20-to-C26 magnetic lineations on the present Capricorn Plate to their equivalent India Plate positions using the C5Cn.1 (16.0 Ma) Capricorn–India rotation from Bull *et al.* (2010).

For the first stage of our test, we rotated the Capricorn-side magnetic lineations for C26–C20 onto the Somalia Plate with our Table 2 India–Somalia rotations (Fig. 26). Encouragingly, our rotations restore the reversal crossings for C20n.1n, C20n.1o and C21n.1n directly onto their Somalia Plate counterparts, with average differences no greater than 5 km (Fig. 26). For comparison, the Cande & Patriat (2015) and Yahteesh *et al.* (2019) Capricorn–Somalia C20 and C21 rotations misalign the C20 and C21 magnetic lineations from the Carlsberg Ridge by distances of 15–110 km after correcting those rotations for Capricorn–India movement (Figs S10b and S12b). The Table 2 rotations for C20n.1n, C20n.1o and C21n.1n are thus more accurate for estimating Africa–India Plate motions at those times than are previous estimates.

For the reversals older than C21n.1n, the mismatches (mostly overrotations) of the reversal crossings that are reconstructed with
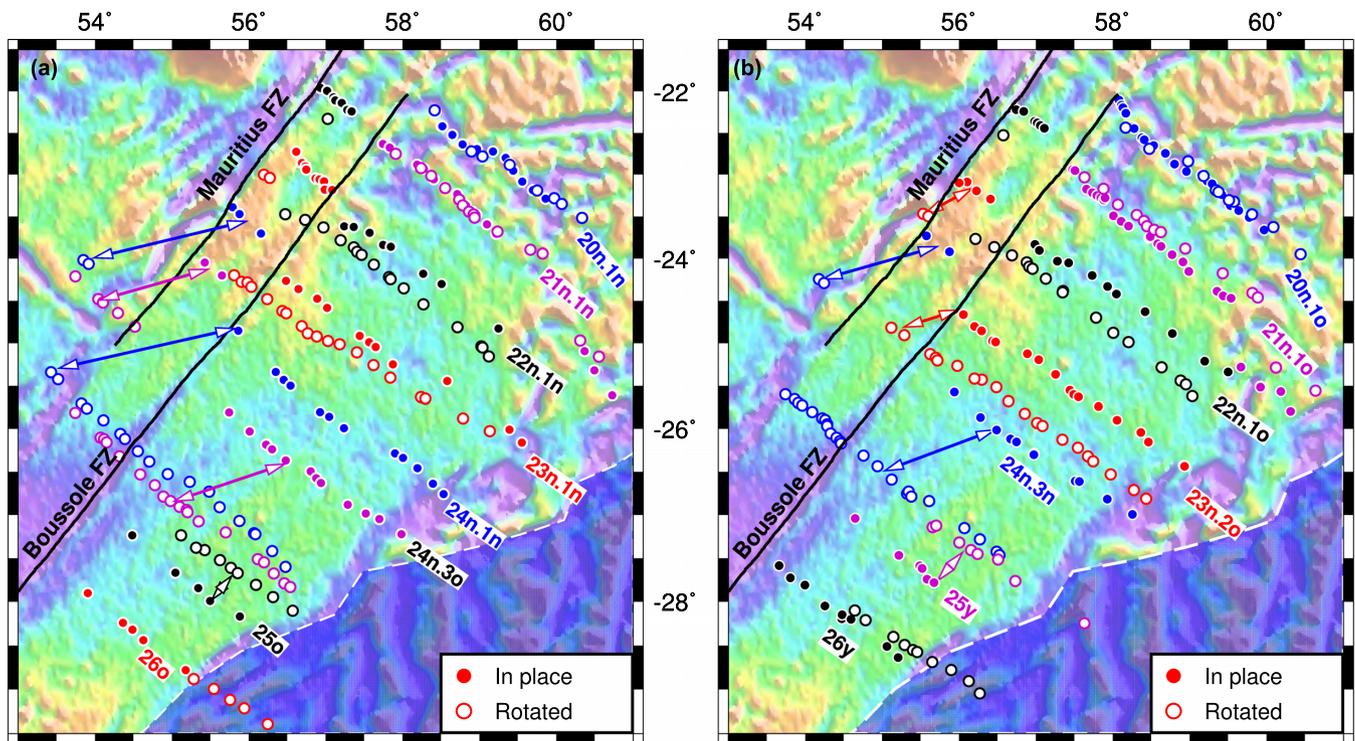
Figure 26. Reconstructions of C20–C26 reversal crossings and fracture zone segments onto the Somalia Plate from their Capricorn Plate locations east of the Central Indian Ridge (Fig. 17) with our Table 2 $\hat{A}^{India \rightarrow Somalia}$ rotations corrected for all Capricorn–India Plate motion since 16 Ma (see the Fig. 18 caption). (a) Reconstructed crossings of the young edges of chrons 20n.1, 21n.1, 22n.1, 23n.1 and 24n.1 and the old edges of chrons 24n.3, 25 and 26. (b) Reconstructed crossings of the old edges of chrons 20n.1, 21n.1, 22n.1, 23n.1 and 24n.1 and young edges of chrons 24n.3, 25 and 26. The C26–C20 reversal crossings are from the Yatheesh *et al.* (2019) supplemental file complemented by additional crossings from sources referenced in the text and Fig. 18. The rotated and in-place reversal crossings are shown by the open and solid circles, respectively. The grids show seafloor gravity (Fig. 5).

our Table 2 rotations increase gradually with reversal age from a few tens of km for C22n.1n to 150–250 km for C24n.1n, C24n.3n and C24n.3o. The magnitude of the overrotations increases suddenly between C23n.1n and C23n.2o (Fig. 26a). The misfits for C22n.1n through C24n.3o also include an along-strike component, whereby the Capricorn-side reversal crossings are restored to locations on the Somalia Plate that are on the wrong side (northwest) of their neighbouring fracture zone. The Table 2 India–Somalia rotations thus violate the pre-Chron 21 flow line constraints that are indicated by the Boussole and Mauritius fracture zones. Oddly, the fits improve progressively for the reversals older than C24n.3o. The C25y, C25o and C26y reconstructed reversal crossings are modestly underrotated and the C26o reconstructed crossings are closely aligned with their in-place counterparts (Fig. 26a).

For the second stage of our test, we simultaneously inverted the C26-to-C20 reversal and fracture zone crossings from the Carlsberg Ridge, northern Central Indian Ridge data and southern Central Indian Ridge to determine whether a single rotation sequence can satisfactorily fit all the data. Based on this and several other exploratory inversions, we could not identify a single set of rotations that satisfied all the data. We instead observe the following:

(1) The C20, C21, C22 and C23n.1n reversal crossings and associated flow line segments were generally well fit everywhere along the Carlsberg and Central Indian Ridges, with misfits that were comparable to the Table 2 WRMS misfits at some locations and only modestly worse (1–2 km) at others. Misfits this small suggest that any deformation within the Africa or IndoCapricorn plates between C23n.1n (50.8 Ma) and 16 Ma was small. More work is needed to quantify an upper bound on any such deformation.

(2) The C23n.1n (50.8 Ma) and more recent India–Somalia seafloor spreading rates and slip directions that are estimated with the angular velocities derived from the joint data inversion versus angular velocities that are estimated solely from Carlsberg Ridge and northern Central Indian Ridge data (Table 3) differ insignificantly from each other. Estimating India–Somalia finite rotations from Carlsberg Ridge data and southern Central Indian Ridge data suitably corrected for the post-16 Ma movement between the Capricorn and India plates thus only marginally affects the resulting India–Somalia Plate motion estimates back to C23n.1n. Nonetheless, the C23-to-C20 rotations that we derived using the additional Central Indian Ridge data have covariances ∼50 per cent smaller than the Table 2 rotation covariances due to the much greater geographical span of the combined data from the entire palaeoplate boundary.

(3) Chrons 23n.2o to C24n.3o are fit poorly in our joint inversion. Exploratory inversions in which we increased the weights of these magnetic lineations to encourage better fits degraded the fits to the fracture zone flow lines, and vice versa. This fitting tradeoff may reflect an inconsistency between the two data types, possibly due to an unrecognized misinterpretation of the fracture zone flow lines and/or magnetic anomalies for these ages. Alternatively, deformation within the Africa or IndoCapricorn Plate before C22 might explain why we cannot simultaneously fit the C23n.2o, C24n.1n, C24n.3n and C24n.3o reversal and flow line data from everywhere along the palaeoplate boundary.

More work is needed to evaluate whether a single set of rotations can satisfactorily fit all the magnetic lineation and fracture zone data back to Chron 26. Although the good fits of the Cande & Patriat

(2015) rotations to flow lines everywhere along the plate boundary suggests this may be possible (Fig. 21 and Section 5.2.1), we show in Section 5 of our Supporting Information that the Cande & Patriat (2015) rotations exhibit the same large increase in misfit for C24 that we observe with our own rotations. In Section S5, we compare the fits of three previous Capricorn–Somalia rotation sequences to the Carlsberg Ridge C26–C20 magnetic lineations after correcting those rotations for Capricorn–India Plate motion (Patriat & Segoufin 1988; Cande & Patriat 2015; Yahteesh *et al.* 2019). None of the previous rotations satisfactorily realign the Carlsberg Ridge magnetic lineations for C20 and older times; however, the Cande & Patriat (2015) rotations realign the C20 and C21 Carlsberg Ridge conjugate magnetic lineations to within 15–25 km (Fig. S10b). Given the differing approaches and data that were used in our study and previous studies (in particular Cande & Patriat 2015), the similar patterns in our misfits are encouraging and reinforce our results.

6 CONCLUSIONS

A new sequence of 45 rotations that describes India–Somalia Plate motion across the Carlsberg and northern Central Indian Ridges since 60 Ma is estimated from ∼9000 identifications of magnetic reversals 1n to 26no and thousands of additional fracture zone and transform fault crossings from a variety of marine bathymetric observations. From these detailed new rotations, we find the following:

(1) Evidence that a ∼50 per cent spreading rate decline from 57 to 52.7 Ma was terminated by a spreading rate acceleration that may have doubled the spreading rate by ∼52 Ma depending on uncertainties in the ages of Chrons 23 and 24. A sustained slowdown after 51.7 Ma reduced the plate motion by as much as ∼90 per cent by 46.7 Ma.

(2) A brief upward pulse in India–Somalia spreading rates from 42 to 40 Ma overlapped a similar-magnitude decline from 41 to 37 Ma in eastern Southwest Indian Ridge spreading rates. These opposite-sense spreading rate changes on opposing sides of the Somalia Plate may be evidence for a change in the Somalia Plate's absolute motion during this period.

(3) India–Somalia seafloor spreading rates during the little studied period between Chron 18 (40 Ma) and Chron 6 (20 Ma) were as slow as 10 ± 1 mm yr^{-1} along the western Carlsberg Ridge from 38.6 to 33.2 Ma but gradually doubled by 17 Ma. During the same period, spreading rates along the eastern Southwest Indian Ridge declined by ∼50 per cent, consistent with the hypothesis that both changes were caused by a change in the Somalia Plate's absolute motion from 37 to 18 Ma. The anticorrelated changes in Carlsberg Ridge and Southwest Indian Ridge spreading rates that began after 40 Ma both ceased at 18 ± 1 Ma, when seafloor spreading initiated in the central and western Gulf of Aden.

(4) India–Somalia spreading rates declined by nearly 50 per cent from 18 to 13 Ma and have remained steady to within a few per cent (± 1 mm yr^{-1}) since 13.7 Ma, in accord with previous high-resolution studies of this plate pair.

(5) Comparisons of the azimuths of Carlsberg Ridge abyssal hills and fracture zones in 40–16-Myr-old Central Indian Ridge seafloor to plate slip directions and fracture zone flow lines that are predicted with our new India–Somalia rotations suggest that the new rotations are accurate at all ages since 48 Ma. The new rotations may also explain unusually broad gravity lows along many Central Indian Ridge fracture zone valleys.

(6) Along the southern Central Indian Ridge, the new India–Somalia rotations accurately reconstruct crossings of Chrons 13 to 21n.1n and pre-C13 fracture segments on the Capricorn Plate onto their conjugates on the Somalia Plate when the rotations are corrected for the movement of the Capricorn Plate relative to India since 16.0 Ma. The close fits confirm that India–Capricorn Plate motion began at ∼16 Ma, that the Bull *et al.* (2010) correction for India–Capricorn motion is accurate, and that our India-Somalia rotations for C21n.1n through C5C are accurate.

(7) We postulate that the southward component of the Somalia Plate's absolute motion increased by 10–25 mm yr^{-1} from 31 to 18 Ma, possibly explaining observed changes in the velocities of the Somalia–India, Somalia–Antarctic and Somalia–Capricorn Plate pairs during this period. A direct test for the existence and magnitude of the proposed southward speedup will require accurate ages for ∼35- to 10-Myr-old Reunion hotspot seamounts.

(8) India–Eurasia rotations estimated with our new India–Somalia rotations and updated rotations elsewhere in the global plate circuit predict ∼30 per cent more rapid convergence rates from 55 to 47 Ma than previous studies and a gradual slowdown after 52 Ma that reduced the convergence rate by ∼75 per cent by 38 Ma. India–Eurasia Plate motion since 43 Ma has included a small convergence pulse from 43 to 38 Ma, an acceleration from 22 to 18 Ma, a 50 per cent convergence slowdown from 18 to 13 Ma, and steady motion since 13 Ma. The accuracies and uncertainties of India–Eurasia rotations for times earlier than ∼50 Ma would benefit from enforcing closure around the Africa–Antarctic–IndoCapricorn Plate circuit and unification of Carlsberg Ridge and Central Indian Ridge data for times back to Chron 27.

(9) A joint inversion of Chron 26–C20 magnetic reversal and fracture zone data from the Carlsberg and Central Indian Ridges satisfactorily fits all the data for C23n.1n (50.7 Ma) to C20. Any deformation that may have occurred within the Africa and/or IndoCapricorn plates between 50.7 Ma and the break-up of the former IndoCapricorn Plate at 16 Ma is thus too small to detect with our data. Large misfits to the data for the times older than C23n.1n may be evidence for significant deformation within the Africa or IndoCapricorn Plate before ∼50 Ma.

DATA AVAILABILITY

The magnetic reversal identifications and fracture zone flow lines used for the analysis are available from the Marine Geoscience Data System (marine-geo.org/tools/search/Files.php?data_set_uid=30268; data DOI 10.26022/IEDA/330268). The Russian magnetic data used for our analysis are archived at the Russian Navy's Central Cartographic Production facility. Inquiries should be directed to Dr Sergey Merkouriev.

REFERENCES

Bosworth, W., Huchon, P. & McClay, K., 2005. The Red Sea and Gulf of Aden Basins, *J. Afr. Earth Sci.,* **43,** 334–378.

Bull, J.M., DeMets, C., Krishna, K.S., Sanderson, D.J. & Merkouriev, S., 2010. Reconciling plate kinematic and seismic estimates of lithospheric convergence in the central Indian Ocean, *Geology,* **38,** 307–310.

Cande, S.C. & Patriat, P., 2015. The anticorrelated velocities of Africa and India in the Late Cretaceous and early Cenozoic, *Geophys. J. Int.,* **200,** 227–243.

Cande, S.C., Patriat, P. & Dyment, J., 2010. Motion between the Indian, Antarctic, and African plates in the early Cenozoic, *Geophys. J. Int.,* **183,** 127–149.

Cande, S.C. & Stegman, D.R., 2011. Indian and African plate motions driven by the push force of the Reunion plume head, *Nature,* **475,** 47–52.

Carbotte, S.M. *et al.*, 2004. New integrated data management system for Ridge2000 and MARGINS research, *EOS,* **85,** 553–559.

Chang, T., 1988. Estimating the relative rotation of two tectonic plates from boundary crossings, *J. Am. Stat. Assoc.,* **83,** 1178–1183.

Charles, C., 2007. Multibeam sonar (Longsberg EM120) data as collected during the cruise KNOX10RR, https://doi.org/10.7284/107436.

Chaubey, A.K., Dyment, J., Bhattacharya, G.C., Royer, J.-Y., Srinivas, K. & Yatheesh, V., 2002. Paleogene magnetic isochrons and palaeo-propagators in the Arabian and Eastern Somali basins, NW Indian Ocean, in *The Tectonic and Climatic Evolution of the Arabian Sea Region, Geol. Soc. London Special Publications,* Vol. **195,** pp. 71–85, eds CLift, P.D., Kroon, D., Gaedicke, C. & Craig, J., Geol. Soc. London.

Chenet, A.-L., Courtillot, V., Fluteau, F., Gerard, M., Quidelleur, X., Khadri, S., Subbarao, K. & Thordarson, T., 2009. Determination of rapid Deccan eruptions across the Cretaceous-Tertiary boundary using paleomagnetic secular variations: 2. Constraints from analysis of eight new sections and synthesis for a 3500-m-thick composite section, *J. geophys. Res.,* **114**(B6),.

Cormier, M.-H. & Sloan, H., 2018. Abyssal hills and abyssal plains, in Submarine Geomorphology, Micallef, A., Krastel, S. & Savini, A., *Springer Geology,* Springer International, 389–408, doi: 10.1007.978-3-319-57852-1_20.

d'Acremont, E., Leroy, S., Maia, M., Patriat, P., Bselier, M.-O., Bellahsen, N., Fournier, M. & Gente, P., 2006. Structure and evolution of the eastern Gulf of Aden: insights from magnetic and gravity data (Encens-Sheba MD117 cruise), *Geophys. J. Int.,* **165,** 786–803.

DeMets, C., Gordon, R.G. & Argus, D.F., 2010. Geologically current plate motions, *Geophys. J. Int.,* **181,** 1–80.

DeMets, C., Gordon, R.G. & Royer, J.-Y., 2005. Motion between the Indian, Capricorn, and Somalian plates since 20 Ma: implications for the timing and magnitude of distributed deformation in the equatorial Indian ocean, *Geophys. J. Int.,* **161,** 445–468.

DeMets, C., Gordon, R.G. & Vogt, P., 1994. Location of the Africa-Australia-India triple junction and motion between the Australian and Indian plates: Results from an aeromagnetic investigation of the Central Indian and Carlsberg ridges, *Geophysical Journal International,* **119,** 893–930.

DeMets, C., Iaffaldano, G. & Merkouriev, S., 2015b. High-resolution Neogene and Quaternary estimates of Nubia-Eurasia-North America plate motion, *Geophys. J. Int.,* **203,** 416–427.

DeMets, C. & Merkouriev, S., 2019. High-resolution reconstructions of South America plate motion relative to Africa, Antarctica, and North America: 34 Ma to present, *Geophys. J. Int.,* **217,** 1821–1853.

DeMets, C., Merkouriev, S. & Jade, S., 2020. High-resolution reconstructions and GPS estimates of India-Eurasia and India-Somalia plate motions: 20 Ma to the present, *Geophys. J. Int.,* **220,** 1149–1171.

DeMets, C., Merkouriev, S. & Sauter, D., 2015a. High-resolution estimates of Southwest Indian Ridge plate motions, 20 Ma to present, *Geophys. J. Int.,* **203,** 1495–1527.

DeMets, C., Merkouriev, S. & Sauter, D., 2021. High resolution reconstructions of the Southwest Indian Ridge, 52 Ma to present: Implications for the breakup and absolute motion of the Africa plate, *Geophys. J. Int.,* **226,** 1461–1497.

DeMets, C. & Wilson, D.S., 2008. Toward a minimum change model for recent plate motions: calibrating seafloor spreading rates for outward displacement, *Geophys. J. Int.,* **174,** 825–841.

Doubrovine, P.V., Steinberger, B. & Torsvik, T.H., 2012. Absolute plate motions in a reference frame defined by moving hot spots in the Pacific, Atlantic, and Indian oceans, *J. geophys. Res.,* **117**(B9),.

Drolia, R.K. & DeMets, C., 2005. Deformation in the diffuse India-Capricorn-Somalia triple junction from a multibeam and magnetic survey of the northern Central Indian ridge, 3°S-10°S, *Geochem., Geophys., Geosys.,* **6,** doi:10.1029/2005GC000950.

Dyment, J., 1998. Evolution of the Carlsberg Ridge between 60 and 45 Ma: ridge propagation, spreading asymmetry, and the Deccan-Reunion hotspot, *J. geophys. Res.,* **103,** 24 067–24 084.

Eagles, G. & Hoang, H.H., 2014. Cretaceous to present kinematics of the Indian, African and Seychelles plates, *Geophys. J. Int.,* **196,** 1–14.

Fisher, R.L., Sclater, J.G. & McKenzie, D.P., 1971. Evolution of the central Indian Ridge, western Indian Ocean, *Geol. Soc. Am. Bull.,* **82,** 553–562.

Fournier, M. *et al.*, 2010. Arabia-Somalia plate kinematics, evolution of the Aden-Owen-Carlsberg triple junction, and opening of the Gulf of Aden, *J. geophys. Res.,* **115,** doi:10.1029/2008JB006257.

Gaina, C., Roest, W.R. & Muller, R.D., 2002. Late Cretaceous-Cenozoic deformation of northeast Asia, *Earth planet. Sci. Lett.,* **197,** 273–286.

George, R., Rogers, N. & Kelley, S., 1998. Earliest magmatism in Ethiopia: evidence for two mantle plumes in one flood basalt province, *Geology,* **26,** 923–926.

Glebovsky, V.Y. *et al.*, 1995. Mid-oceanic ridges and deep ocean basins: AMF structure, in *Anomalous Magnetic Field of the World Ocean,* pp. 67–144, ed. Gorodnitsky, A.M., CRC Press.

Hassan, R., Williams, S.E., Gurnis, M. & Muller, D., 2020. East African topography and volcanism explained by a single, migrating plume, *Geosci. Front.,* **11,** 1669–1680.

Hekinian, R., Bideau, D., Cannat, M., Francheteau, J. & Hebert, R., 1992. Volcanic activity and crust-mantle exposre in the ultrafast Garrett transform fault near 13°28'S in the Pacific, *Earth planet. Sci. Lett.,* **108,** 259–275.

Hellinger, S.J., 1981. The uncertainties of finite rotations in plate tectonics, *J. geophys. Res.,* **86,** 9312–9318.

Hofmann, C., Courtillot, V., Feraud, G., Rochette, P., Yirgu, G., Ketefo, E. & Pik, R., 1997. Timing of the Ethiopian flood basalt event and implications for plume birth and global change, *Nature,* **389,** 838–841.

Iaffaldano, G., Bodin, T. & Sambridge, M., 2013. Slow-downs and speed-ups of India-Eurasia convergence since 20 Ma: data-noise, uncertainteis and dynamic implications, *Earth planet. Sci. Lett.,* **367,** 146–156.

Iaffaldano, G., Davies, D.R. & DeMets, C., 2018. Indian Ocean floor deformation induced by the Reunion plume rather than the Tibetan Plateau, *Nat. Geosci.,* **11,** 362–366.

Janin, M., Hemond, C., Guillou, H., Maia, M., Johnson, K., Bollinger, C., Liorzou, C. & Mudholkar, A., 2011. Hot spot activity and tectonic settings near Amsterdam-St. Paul plateau (Indian Ocean), *J. geophys. Res.,* **116**(B5),.

Kamesh Raju, K.A., Chaubey, A.K., Amarnath, D. & Mudholkar, A., 2008. Morphotectonics of the Carlsberg Ridge between 62°20' and 66°20'E, northwest Indian Ocean, *Mar. Geol.,* **252,** 120–128.

Kamesh Raju, K.A., Samudrala, K., Drolia, R.K., Amarnath, D., Ramachandran, R. & Mudholkar, A., 2012. Segmentation and morphology of the Central Indian Ridge between 3°S and 11°S, Indian Ocean, *Tectonophys.,* **554-557,** 114–126.

Karasik, A.M., Mercuriev, S.A., Mitin, L.I., Sochevanova, N.A. & Yanovsky, V.N., 1986. Peculiarities in the history of opening of the Arabian Sea from systematic magnetic survey data, *Doc. Acad. Sci. U.S.S.R.,* **286,** 933–938.

Li, S., van Hinsbergen, D.J.J., Najman, Y., Liu-Zeng, J., Deng, C. & Zhu, R., 2020. Does pulsed Tibetan deformation correlate with Indian plate motion changes?, *Earth planet. Sci. Lett.,* **536,** doi:10.1016/j.epsl.2020.116144.

Lodolo, E., Coren, F. & Ben-Avraham, Z., 2013. How do long-offset oceanic transform faults adapt to plate motion changes? The example of the western Pacific-Antarctic plate boundary, *J. geophys. Res.,* **118,** 1195–1202.

Maher, S.M., Wessel, P., Muller, R.D., Williams, S.E. & Harada, Y., 2015. Absolute plate motion of Africa around Hawaii-Emperor bend time, *Geophys. J. Int.,* **201,** 1743–1764.

Maia, M. *et al.*, 2011. Building of the Amsterdam-Saint Paul plateau: A 10 Myr history of a ridge-hot spot interaction and variations in the strength of the hot spot source, *J. geophys. Res.,* **116**(B9),.

Maia, M., 2019. Topographic and morphologic evidences of deformation at oceanic transform faults: far-field and local-field stresses, in *Transform Plate Boundaries and Fracture Zones,* pp. 61–87, ed. Duarte, J.C., Elsevier.

Malinverno, A., Quigley, K.W., Staro, A. & Dyment, J., 2020. A Late Cretaceous-Eocene geomagnetic polarity timescale (MQSD20) that steadies spreading rates on multiple mid-ocean ridge flanks, *J. geophys. Res.,* **125**, e2020JB020034,.

McQuarrie, N. & van Hinsbergen, D.J.J., 2013. Retrodeforming the Arabia-Eurasia collision zone: age of collision versus magnitude of continental subduction, *Geology,* **41**, 315–318.

Mercuriev, S., Patriat, P. & Sochevanova, N., 1995. Evolution de la dorsale de Carlsberg: evidence pour une phase d'expansion tres lente entre 40 et 25 Ma (A18 a A7), *Oceanol. Acta,* **19**, 1–13.

Merkouriev, S. & DeMets, C., 2006. Constraints on Indian plate motion since 20 Ma from dense Russian magnetic data: Implications for Indian plate dynamics, *Geochem. Geophys. Geosyst.,* **7**(2), Q02002,.

Merkouriev, S. & DeMets, C., 2014a. High-resolution estimates of Nubia-North America plate motion: 20 Ma to present, *Geophys. J. Int.,* **196**, 1281–1298.

Merkouriev, S. & DeMets, C., 2014b. High-resolution Quaternary and Neogene reconstructions of Eurasia-North America plate motion, *Geophys. J. Int.,* **198**, 366–384.

Merkouriev, S.A. & Sotchevanova, N.A., 2003. Structure and evolution of the Carlsberg Ridge: Evidence for non-stationary spreading on old and modern spreading centers, *Curr. Sci.,* **85**, 334–338.

Molnar, P., Pardo-Casas, F. & Stock, J., 1988. The Cenozoic and Late Cretaceous evolution of the Indian Ocean Basin: uncertainties in the reconstructed positions of the Indian, African and Antarctic plates, *Basin Res.,* **1**, 23–40.

Molnar, P. & Stock, J.M., 2009. Slowing of India's convergence with Eurasia since 20 Ma and its implications for Tibetan mantle dynamics, *Tectonics,* **28**, TC3001.

Muller, R.D., Royer, J.-Y., Cande, S.C., Roest, W.R. & Maschenkov, S., 1999. New constraints on the Late Cretaceous/Tertiary plate tectonic evolution of the Caribbean, in *Caribbean Basins,* **4**, pp. 33–59, Sedimentary Basins of the World, ed. Mann, P., Elsevier Science B. V.

O'Neill, C., Muller, D. & Steinberger, B., 2003. Geodynamic implications of moving Indian Ocean hotspots, *Earth planet. Sci. Lett.,* **215**, 151–168.

Ogg, J.G., 2012. Geomagnetic polarity time scale, in *The Geologic Time Scale 2012,* pp. 85–113, eds Gradstein, F.M., Ogg, J.G., Schmitz, M. & Ogg, G., Elsevier, doi:10.1016/B978-0-444-59425-9.00005-6.

Ogg, J.G., 2020. Chapter 5 - geomagnetic polarity time scale, in *Geologic Time Scale 2020,* pp. 159–192, eds Gradstein, F.M., Ogg, J.G., Schmitz, M.D. & Ogg, G.M., Elsevier.

Patriat, P., 1987. *Reconstitution de l'evolution du syst''eme de dorsales de l'oc'ean Indien par les m'ethodes de la cin'ematique des plaques,* Publ. Territoire des Terres Australes et Antarctiques Francaises.

Patriat, P. & Achache, J., 1984. India-Eurasia collision chronology has implications for crustal shortening and driving mechanism of plates, *Nature,* **311**, 615–621.

Patriat, P. & Segoufin, J., 1988. Reconstruction of the central Indian Ocean, *Tectonophys.,* **155**, 211–234.

Perez-Diaz, L., Eagles, G. & Sigloch, K., 2020. Indo-Atlantic plate accelerations around the Cretaceous-Paleogene boundary: a time-scale error, not a plume-push signal, *Geology,* **48**, 1169–1173.

Pockalny, R.A., Fox, P.J., Fornari, D.J., Macdonald, K.C. & Perfit, M.R., 1997. Tectonic reconstructions of the Clipperton and Siqueiro Fracture Zones: evidence and consequences of plate motion change for the last 3 Myr, *J. geophys. Res.,* **102**, 3167–3181.

Pusok, A.E. & Stegman, D.R., 2020. The convergence history of India-Eurasia records multiple subduction dynamics processes, *Sci. Adv.,* **6**, eaaz8681, doi:10.1126/sciadv.aaz8681.

Royer, J.-Y., Chaubey, A.K., Dyment, J., Bhattacharya, G.C., Srinivas, K., Yatheesh, V. & Ramprasad, T., 2002. Paleogene plate tectonic evolution of the Arabian and Eastern Somali basins, in *The Tectonic and Climatic Evolution of the Arabian Sea Region,* Vol. 195, pp. 7–23, eds CLift, P.D., Kroon, D., Gaedicke, C. & Craig, J., Geological Society, London, Special Publications.

Sandwell, D.T., Muller, R.D., Smith, W.H.F., Garcia, E. & Francis, R., 2014. New global marine gravity model from CryoSat-2 and Jason-1 reveals buried tectonic structure, *Science,* **346**, 65–67.

Schettino, A. & Macchiavelli, C., 2016. Plate kinematics of the central Atlantic during the Oligocene and early Miocene, *Geophys. J. Int.,* **205**, 408–426.

Seton, M. *et al.*, 2012. Global continental and ocean basin reconstructions since 200 Ma, *Earth-Science Rev.,* **113**, 212–270.

Seton, M. *et al.*, 2014. Community infrastructure and repository for marine magnetic identifications, *Geochem. Geophys. Geosys.,* **15**(4), 1629–1641.

Shaw, P.R. & Cande, S.C., 1990. High-resolution inversion for South Atlantic plate kinematics using joint altimeter and magnetic anomaly data, *J. geophys. Res.,* **95**, 2625–2644.

Shuhail, M., Yatheesh, V., Bhattacharya, G.C., Muller, R.D., Raju, K.A.K. & Mahender, K., 2018. Formation and evolution of the Chain-Kairali Escarpment and the Vishnu Fracture Zone in the western Indian Ocean, *J. Asian Earth Sci.,* **164**, 307–321.

van Hinsbergen, D.J.J., Steinberger, B., Doubrovine, P.V. & Gassmoller, R., 2011. Acceleration and deceleration of India-Asia convergence since the Cretaceous: roles of mantle plumes and continental collision, *J. geophys. Res.,* **116**(B6),.

Wessel, P. & Smith, W.H.F., 1991. Free software helps map and display data, *EOS, Trans. Am. Geophys. Un.,* **72**, 441–446.

White, L. & Lister, G., 2012. The collision of India with Asia, *J. Geodyn.,* **56–57**, 7–17.

Yatheesh, V. *et al.*, 2019. Detailed structure and plate reconstructions of the Central Indian Ocean between 83.0 and 42.5 Ma (Chrons 34 and 20), *J. geophys. Res.,* **124**, 4305–4322.

Zhang, T., Gordon, R.G. & Wang, C., 2018. Oblique seafloor spreading across intermediate and superfast spreading centers, *Earth Planet. Sci. Lett.,* **495**, 146–156.

SUPPORTING INFORMATION

Supplementary data are available at *GJI* online.

Figure S1: Location chart for supplemental figures that are maps.m
Figure S2: Along-track magnetic anomaly data used in the analysis overlaid on the vertical derivative of the 1-min gravity field (version 29 available at ftp://topex.ucsd.edu/pub/global_grav_1min; Sandwell *et al.* 2014). Our interpretations and reconstructions of all 45 magnetic reversals and flow lines that are described in the main document are shown in Fig. S4. The sources of the data are indicated by the colour and shading of each track, as follows: Red tracks and pink shading identify ship data available through the National Geophysical Data Center marine geophysical data archive. Blue tracks and shading identify Diego Garcia aeromagnetic data that are available through the same archive. The black tracks and grey shading show the Russian shipboard data that are described in the main document. Digitized fracture zone flow lines are shown by the aquamarine circles. The best-fitting reconstructed flow lines are shown in Fig. S4.
Figure S3: Reversal correlation points between magnetic anomalies 26n and 6 and magnetic block model used for our study. The synthetic magnetic profile was calculated using a model with half-spreading rates of 15 mm yr^{-1} for 20–42 Ma and 60 mm yr^{-1} for times before 42 Ma, similar to that estimated for our study area.

The synthetic profile further uses a ridge azimuth of N54°W, a 3-km-wide reversal transition zone, and ambient and palaeomagnetic inclinations and declinations for a point near the centre of the Carlsberg Ridge (3.6°N, 64.2°E). The shaded anomalies occurred during periods of normal magnetic field polarity.

Figure S4: (Note to viewer: This graphic is best viewed when magnified 200 per cent or more). Along-track magnetic anomaly data from Fig. S2 with our interpretations and reconstructions of all 45 magnetic reversals and flow lines that are described in the main document. The colours that are used to identify each magnetic reversal are defined in the legend above the figure. The solid and open circles identify the reversal crossings at their original locations and their locations reconstructed with the Table 2 best-fitting rotations. The black and red lines show the great circles that best fit the stationary and rotated reversal crossings for each palaeo-spreading segment. The original (digitized) fracture zone flow lines are shown by the aquamarine circles. The coloured circles that are used to represent the fracture zone flow lines estimated with the Table 2 rotations use the same colour coding found in the legend above the figure. The red flow lines are Chron 20n.1n to Chron 26o flow lines predicted by the rotations from Table S1, which are constrained by the Chain fracture zone strands during C20–C26 time rather than the Maldive and Rudra fracture zones. The blue flow lines along the Chain FZ strands south of the westernmost Carlsberg Ridge are predicted with the Table 2 rotations, which optimize the fits to the Rudra and Maldive FZs at the eastern end of the Carlsberg Ridge. The poor fits of the Table 2 rotations to the Chain FZ and the Table S2 rotations to the Rudra and Maldive FZs illustrate the inconsistency of the FZs at the two ends of the ridge for constraining India-Somalia rotations for times earlier than C21. See the Fig. S2 caption for other information.

Figure S5: Reconstructions of all 45 magnetic reversals, fracture zone flow lines, and transform faults with Table 2 rotations overlaid on a 3-km-resolution bathymetric grid derived from depth measurements along the ship tracks displayed in Fig. 2 of the main document. The reconstructions in this figure focus on the subregion of Fig. S4 with the four transform faults that constrain the C1n rotation and the bathymetric constraints on the transform fault traces. The thick white lines near 3°N, 65.25°E, 0.5°N, 0.3°S and 1.2°S identify the digitized traces of the four transform faults; the red lines that overlay the digitized transform fault traces are the small circles around the best-fitting Chron 1n pole from Table 2. The large black circles along the ridge axis identify the centre of Chron 1 and thus approximate the ridge axis. See the caption for Fig. S4 for other information.

Figure S6: India relative to Somalia spreading rates estimated with angular velocities derived from the Table 2 best-fitting finite rotations and reversal ages from GTS12 (black line), GTS2020 (red line) and Malinverno *et al.* (2020) (MQSD20 label and blue line). The spreading rates are estimated along the Somalia Plate flow line indicated in the inset map All rates are corrected for outward displacement. IN, India; SM, Somalia.

Figure S7: (a) and (b): Best fitting reconstructions of C26–C20 reversal crossings from the Capricorn Plate onto the Somalia Plate corrected for Capricorn–India Plate motion since 16 Ma (see text). The reversal crossings are from sources referenced in the text. The multicoloured and red lines, respectively, show the fit of the best fitting rotations to the Boussole fracture zone, which was used to estimate the rotations, and the Mauritius fracture zone, which was not. C - Comparison of India–Somalia (IN-SM) spreading rates from Fig. 22 a (red line) to Capricorn–Somalia (CP-SM) rates (normalized to GTS20) estimated with Yahteesh *et al.* (2019) rotations

(dashed green line) and rates estimated with the rotations that best fit the data shown in panels (a) and (b) (blue line) for a flow line through the data shown in panels (a) and (b).

Figure S8: (a) Comparison of finite opening poles from this study, Royer *et al.* (2002), Seton *et al.* (2012) and Eagles and Hoang (2014) for Chron 13 and older from reconstructing Carlsberg Ridge (India–Somalia) reversal and fracture zone crossings. The ellipses show the 2-D 95 per cent confidence regions. (b) Comparison of Chron 20 and older finite opening poles from this study (Table 2) to Cande & Patriat (2015) and Yatheesh *et al.* (2019) opening poles that reconstruct southern Central Indian Ridge (Capricorn–Somalia) reversal and fracture zone crossings. In order to compare the latter poles to the India–Somalia poles in Table 2, the Capricorn–Somalia rotations have been corrected for the movement of the Capricorn Plate relative to India since C5Cn.1 (16 Ma) as follows: $\Omega^{\text{Capricorn} \rightarrow \text{India}}\Omega^{\text{Somalia} \rightarrow \text{Capricorn}}$, where the latter rotation accounts for all Capricorn–India Plate motion since the postulated initiation of movement between the two plates at the time of Chron 5Cn.1 (∼16 Ma) (Bull *et al.* 2010). The poles that are shown from Table 2 are limited to poles that were estimated in the studies cited above. Selected poles are labeled to facilitate the comparison.

Figure S9: Plate circuit rotations that constrain the India–Eurasia rotations in Table 4 of the main document. The circles indicate the times for which rotations have been estimated by ourselves or other authors from magnetic reversal and fracture zone reconstructions at the times indicated at the bottom of the figure. The vertical lines indicate the interpolation ages that we used for our India–Eurasia rotations; each interpolation age corresponds to one of the 45 reversals that were reconstructed in this study for the India–Somalia Plate pair (Table 2). All interpolated rotations were estimated from rotations for the next oldest and youngest times. After interpolating the available finite rotations for each plate pair, we combined the interpolated rotation sequences as described in the main document in order to determine India–Eurasia rotations at all 45 times. The sources for the plate pair rotations are specified on the figure.

Figure S10: Fits of Cande & Patriat (2015) (CP15) Capricorn–Somalia rotations to magnetic lineations C23n.2o to C26no along the western Carlsberg Ridge (Panel A) and magnetic lineations C20n.1o to C23n.2o along the eastern Carlsberg Ridge (panel b) after correcting their $\Omega^{\text{Somalia} \rightarrow \text{Capricorn}}$ rotations as follows: $\Omega^{\text{Capricorn} \rightarrow \text{India}}\Omega^{\text{Somalia} \rightarrow \text{Capricorn}}$, where the latter rotation accounts for all Capricorn-India Plate motion since the postulated initiation of movement between the two plates at the time of Chron 5Cn.1 (∼16 Ma) (Bull *et al.* 2010). The double-headed arrows identify the misfits of the Cande & Patriat rotations. The Somalia Plate reversal crossings in both panels are rotated onto the India Plate. The red and black lines are the great circle segments that best fit the reversal crossings reconstructed with our best-fitting rotations.

Figure S11: (a) Comparisons of Table 2 rotation fits to Cande & Patriat (2015) Somalia-Capricorn rotation fits for C20n.1o to C23n.2o after correcting their $\Omega^{\text{Capricorn} \rightarrow \text{Somalia}}$ rotations as follows: $\Omega^{\text{Capricorn} \rightarrow \text{Somalia}}\Omega^{\text{India} \rightarrow \text{Capricorn}}$. The latter rotation accounts for all Capricorn–India Plate motion since the postulated initiation of movement between the two plates at the time of Chron 5Cn.1 (∼16 Ma, Bull *et al.* 2010). The Cande & Patriat rotations were estimated from Capricorn–Africa–Antarctic data. Fig. 16 from the main document shows the location of this area. (b) Same as panel (a) but with the $\Omega^{\text{Somalia} \rightarrow \text{Capricorn}}$ rotations from Yatheesh *et al.* (2019). In both panels, India Plate reversal crossings are rotated onto the Somalia Plate. The coloured lines are the great circle segments that best fit the reversal crossings reconstructed with our best-fitting Table 2 rotations. The reversals that are displayed in each panel

are limited to the subset of reversals that were reconstructed by Cande & Patriat (2015) and Yakteesh *et al.* (2019). CIR, Central Indian Ridge; CP2015, Cande & Patriat (2015); Y19, Yakteesh *et al.* (2019).

Figure S12: Fits of Yatheesh *et al.* (2019) (Y19) Capricorn–Somalia rotations to magnetic lineations C23n.2o to C26no along the western Carlsberg Ridge (panel a) and magnetic lineations C20n.1o to C23n.2o along the eastern Carlsberg Ridge (panel b) after correcting their $\Omega^{\text{Somalia} \rightarrow \text{Capricorn}}$ rotations as follows: $\Omega^{\text{Capricorn} \rightarrow \text{India}} \Omega^{\text{Somalia} \rightarrow \text{Capricorn}}$, where the latter rotation accounts for all Capricorn-India Plate motion since the postulated initiation of movement between the two plates at the time of Chron 5Cn.1 (~16 Ma) (Bull *et al.* 2010). The red and black lines are the great circle segments that best fit the reversal crossings reconstructed with our best-fitting Table 2 rotations. The double-headed arrows identify the misfits of the Yatheesh *et al.* rotations. The Somalia Plate reversal crossings in both panels are rotated onto the India Plate.

Figure S13: Fits of Patriat & Segoufin (1988) (PS88) Capricorn–Somalia rotations to magnetic lineations C23n.2o to C26no along the western Carlsberg Ridge (panel a) and magnetic lineations C20n.1o to C23n.2o along the eastern Carlsberg Ridge (panel b) after correcting their $\Omega^{\text{Somalia} \rightarrow \text{Capricorn}}$ rotations as follows: $\Omega^{\text{Capricorn} \rightarrow \text{India}} \Omega^{\text{Somalia} \rightarrow \text{Capricorn}}$, where the latter rotation accounts for all Capricorn–India Plate motion since the postulated initiation of movement between the two plates at the time of Chron 5Cn.1 (~16 Ma, Bull *et al.* 2010). The double-headed arrows identify the misfits of the rotations from PS88. The Somalia Plate reversal crossings in both panels are rotated onto the India Plate.

Table S1: Somalia–India finite rotations.

Table S2: Somalia–India stage angular velocities.

Table S3: India–Somalia finite rotations.

Table S4: Capricorn–Somalia finite rotations.

Table S5: India–Eurasia stage angular velocities.

Please note: Oxford University Press is not responsible for the content or functionality of any supporting materials supplied by the authors. Any queries (other than missing material) should be directed to the corresponding author for the paper.